1 APRIL 1976

VOLUME IIA (1)

FOCAL PLANE CAMERA FINAL REPORT

SQT

# SPACE TELESCOPE OPTICAL TELESCOPE ASSEMBLY/SCIENTIFIC INSTRUMENTS PHASE B PRELIMINARY DESIGN AND PROGRAM DEFINITION STUDY

Prepared for
GEORGE C MARSHALL SPACE FLIGHT CENTER
NATIONAL AERONAUTICS AND SPACE ADMINISTRATION
MARSHALL SPACE FLIGHT CENTER, ALABAMA

Under contract NAS8-29949

GODDARD SPACE FLIGHT CENTER
NATIONAL AERONAUTICS AND SPACE ADMINISTRATION
GREENBELT, MARYLAND

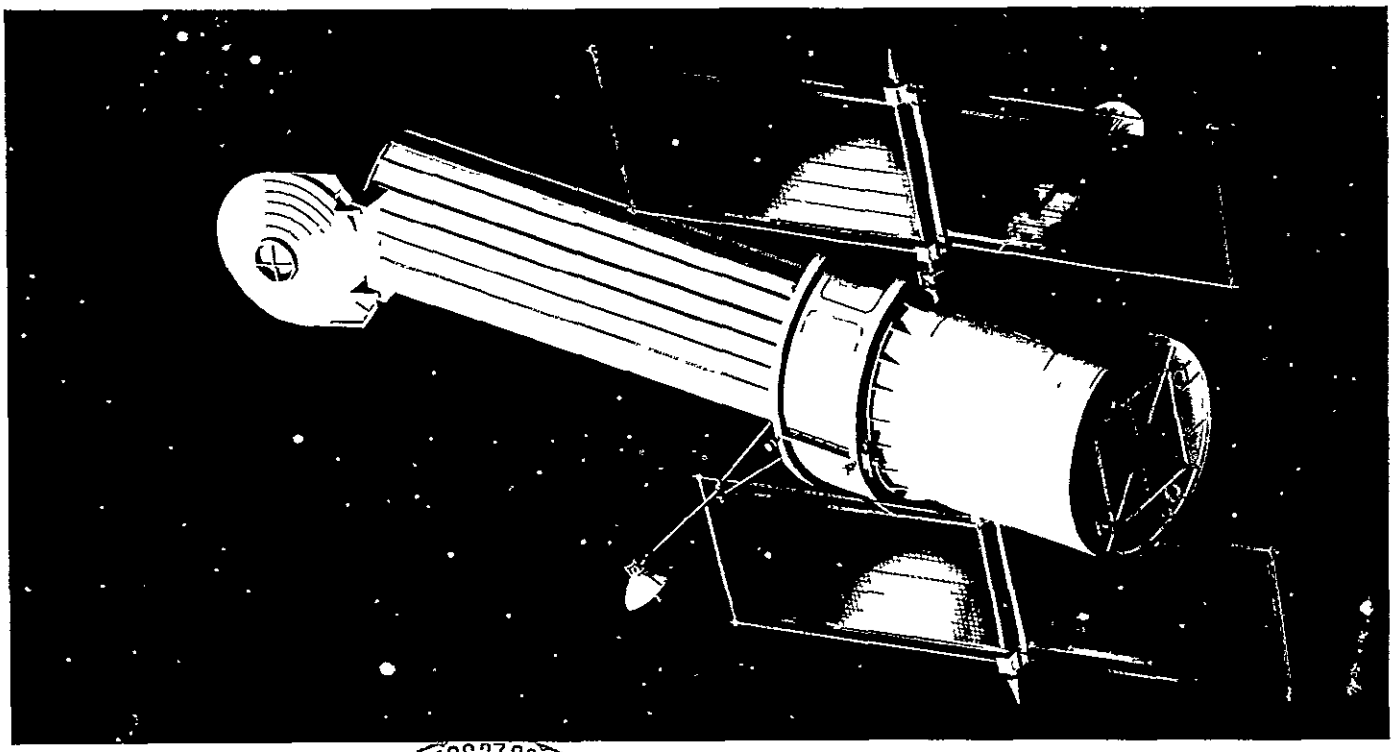



Itek
Optical Systems
A Division of Itek Corporation
10 Maguire Road
Lexington, Massachusetts 02173

Bendix
Aerospace
Systems Division

MARTIN MARIETTA
DENVER DIVISION

Lockheed
MISSILES
& SPACE
COMPANY,
INC.

TABLE OF CONTENTS

TABLE OF CONTENTS
(Continued)

LIST OF FIGURES

LIST OF FIGURES
(Continued)

LIST OF TABLES

# INTRODUCTION

This report describes the preliminary design of a radial bay Focal Plane Camera for the 2.4 meter Space Telescope.

The trade studies that lead to the selection of the on-axis pick-off mirror configuration are documented in Section 1. The resulting design is detailed in Section 2.

FIGURE 1.1-1

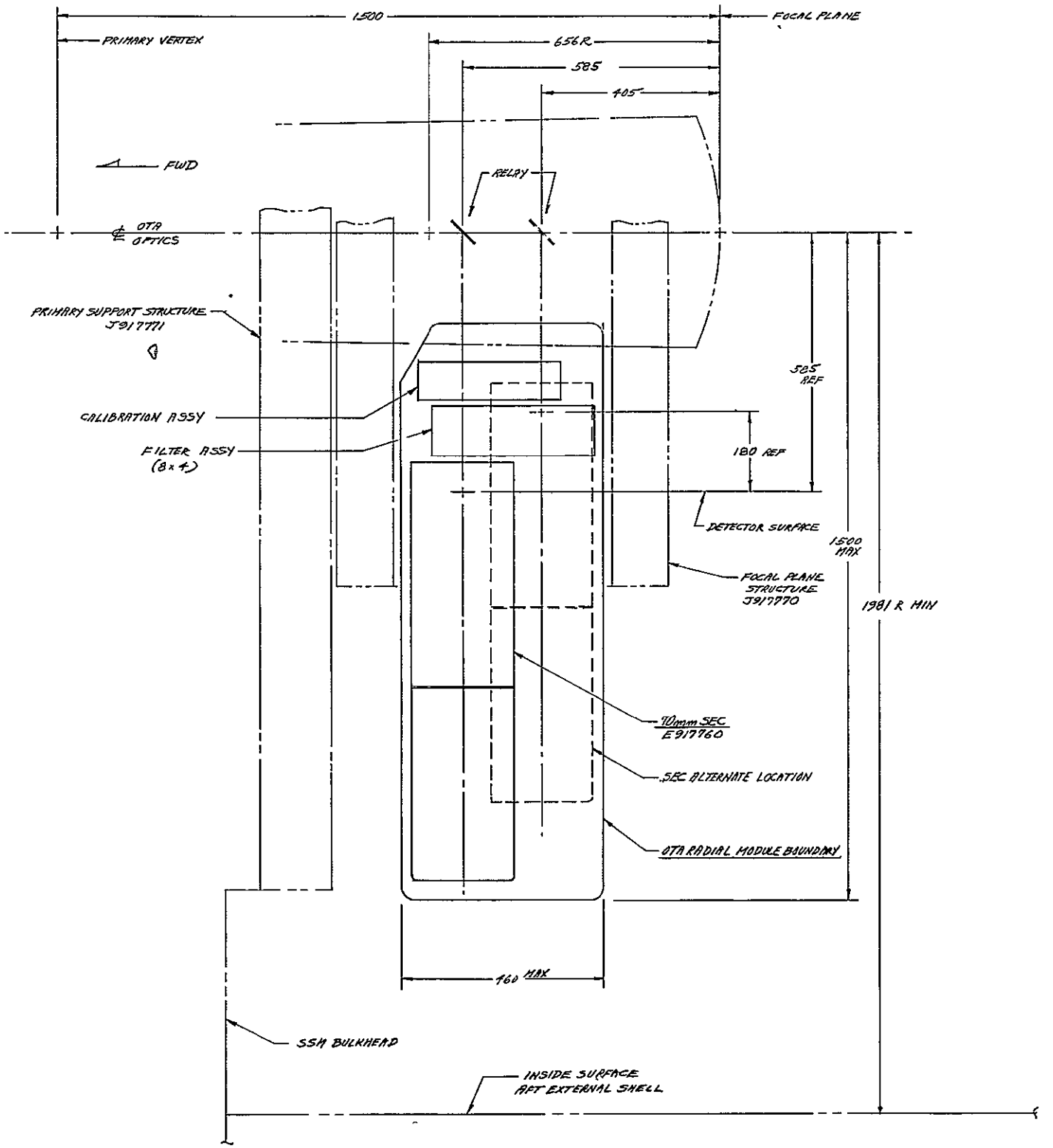


FOCAL PLANE CAMERA STUDY
ON-AXIS PICKOFF, ST.D. SECO

ALL DIMENSIONS IN MM

FIGURE 1.1-2

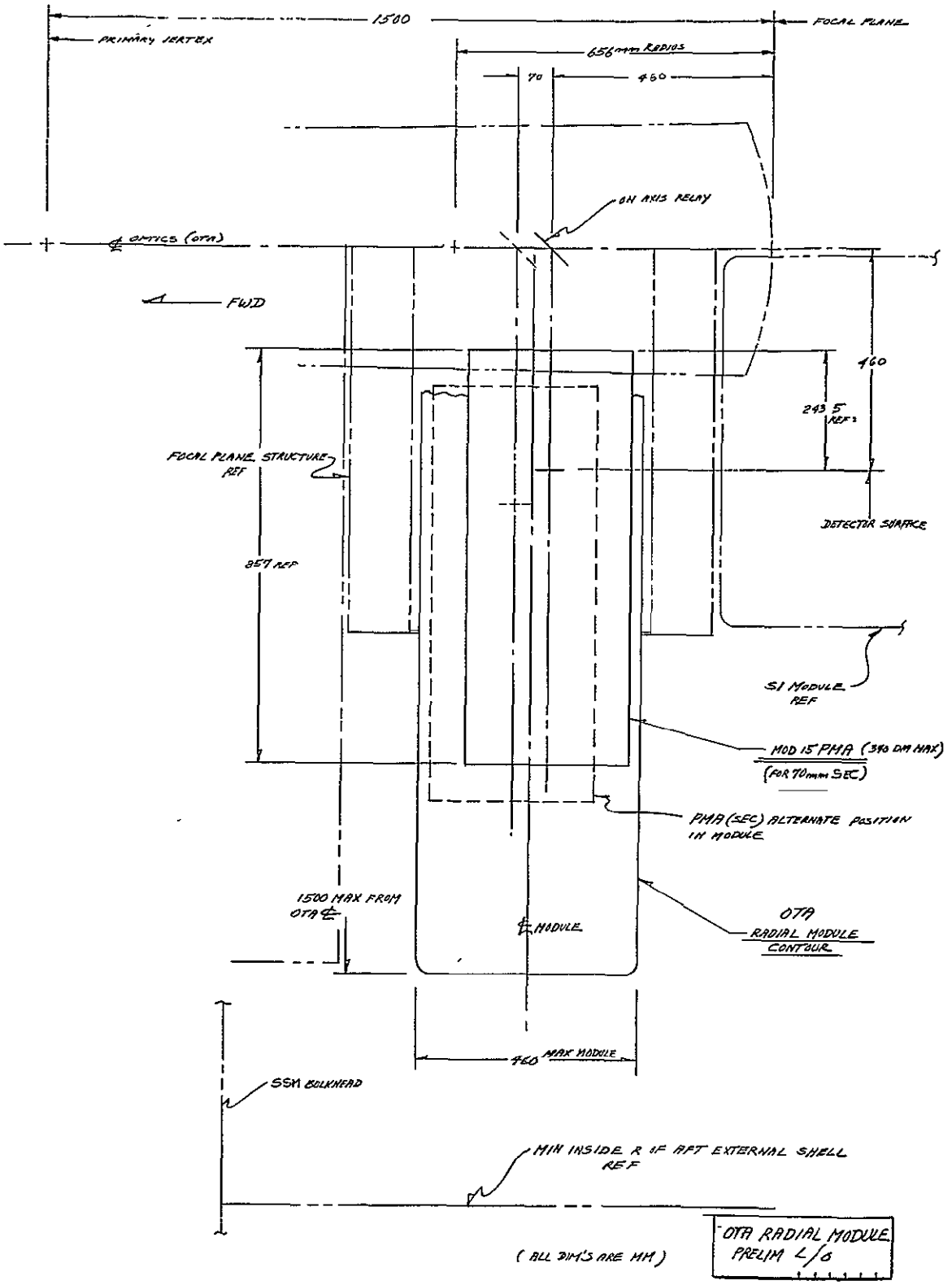


FOCAL PLANE CAMERA STUDY
ON-AXIS PICKOFF, P.M. SECO

FIGURE 1.1-3

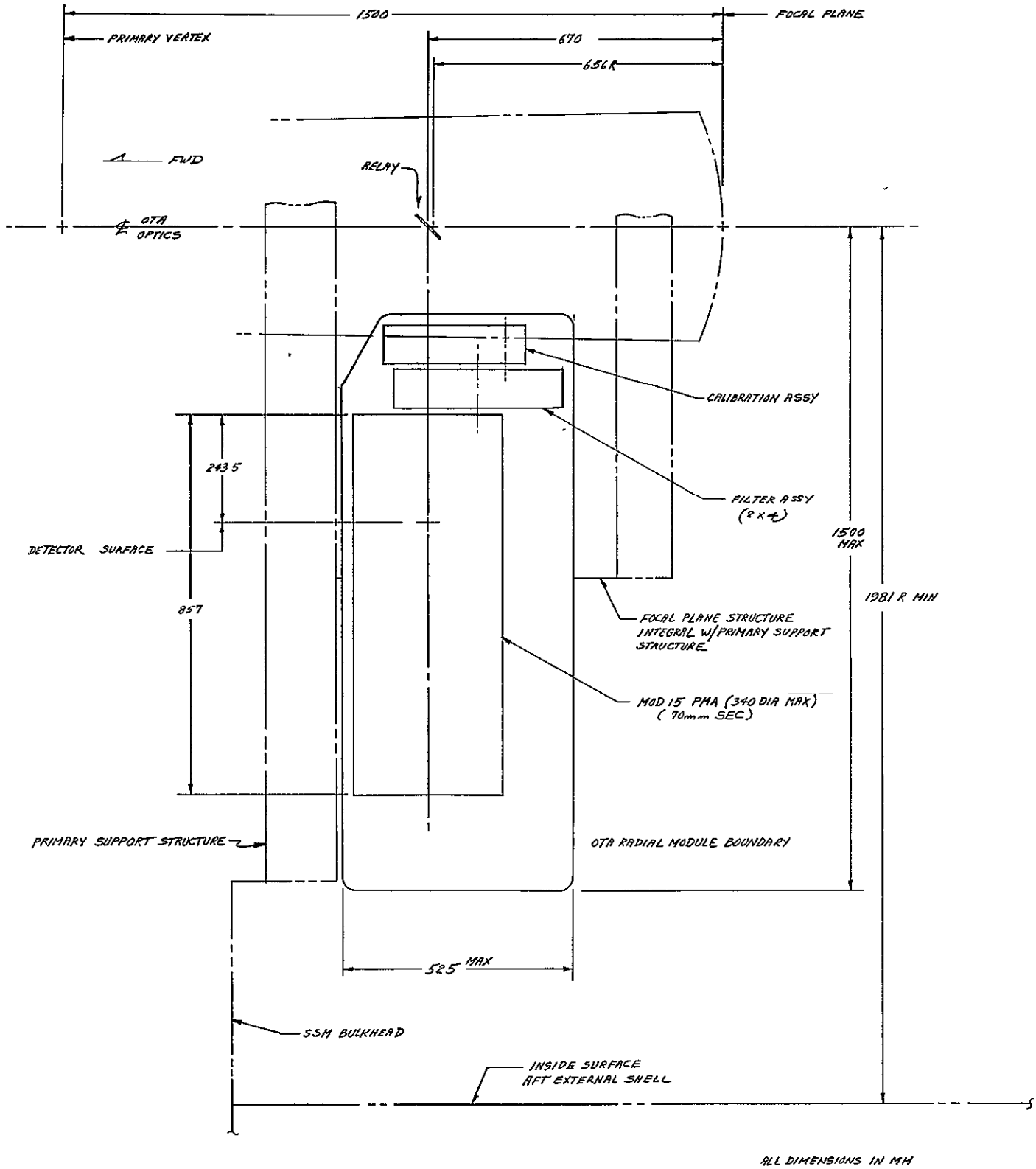


FOCAL PLANE CAMERA STUDY
MODIFIED STRUCT., P.M. SECO

FIGURE 1.1-4

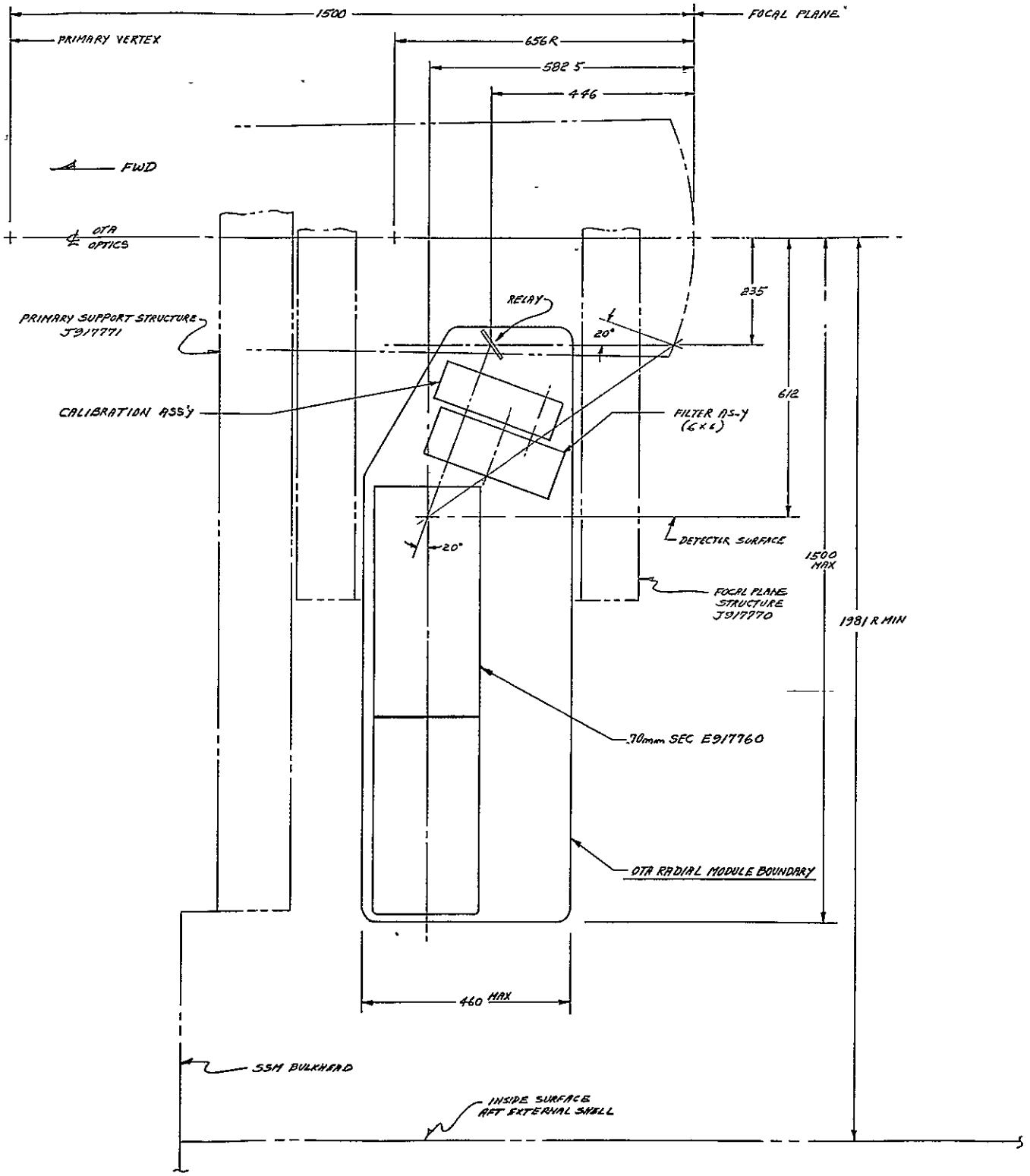


FOCAL PLANE CAMERA STUDY
OFF-AXIS PICKOFF, STD. SECO

ALL DIMENSIONS IN MM

In this configuration, which includes the pick-off mirror within the module, orbital maintainability is provided since the module can be removed in the same manner as the first concept above (Figure 1.1-1).

Since in the off-axis configuration the light rays are not normal to the SECO faceplate, the long permanent magnet assembly of the PM SECO is incompatible since the magnet assembly would block the incoming rays.

## 1.2 Heat Dissipation From the Radial Module

To ensure the ability of the radial module to dissipate the heat generated within it, the OTA thermal model was updated to include the radial module within it. A radial module average heat dissipation of 110 watts and a worst case dissipation of 140 watts was assumed. Table 1.2-1 lists the heat inputs in the SI area in the four cases run. Figures 1.2-1 through 1.2-4 show the temperature distributions in the four cases. Figure 1.2-1 shows the cold case with all SI's off. Figure 1.2-2 shows a case with only the focal plane camera on, dissipating 110 watts. Figure 1.2-3 shows a nominal case with the focal plane camera on, dissipating 110 watts, and an axial SI on, dissipating 200 watts. Figure 1.2-4 shows the hot case, with the focal plane camera at a maximum of 140 watts, axial SI's running at 300 watts, and all three fine guidance sensors on.

The thermal analysis indicates that in the nominal case, the radial module wall runs at about 6°C, while in the hot case, the wall runs at about 14°C. These are average wall temperatures and in all cases, are low enough that the required amount of heat can be dissipated from the camera components at acceptable temperature levels. The thermal design is detailed in Sections 2.3.3 and 2.4.2.

## 1.3 Focal Plane Obscuration

Focal plane obscuration by the pick-off mirror and supporting structure has been determined for the on-axis pick-off, an edge-of-field pick-off, and an intermediate pick-off. The obscuration is shown in Figures 1.3-1, 1.3-2, and 1.3-3. Figure 1.3-1 shows the obscuration of the on-axis pick-off for the camera using the standard SECO. A radius of 50 mm around the optical axis of the telescope is obscured, which means that the closest location for an axial instrument aperture relative to the optical axis is 50 mm. Also shown on the figure are the aperture positions for the instruments as of August 1975. The FOS redesign is being conducted with the slit 60 mm off-axis.

If the pick-off mirror is part of the OTA and is suspended by a spider, then some obscuration along the edges of the fields will occur as shown. If the mirror is part of the focal plane camera, then the obscuration by the structure will occur only in the space between two of the axial instrument areas (the lower area of the picture).

Table 1.2-1

HEAT INPUTS FOR THERMAL ANALYSIS

| Case | Heat Inputs, Watts | | | |
|---|---|---|---|---|
| | Cold | Focal Plane Camera Only | Nominal | Hot |
| OTA | | | | |
| Thermal Control Electronics | 40 | 40 | 40 | 40 |
| Fine Guidance Sensors | 0 | 0 | 30(2) | 30(3) |
| FGS Electronics | 0 | 0 | 120 | 120 |
| Figure Sensor | 0 | 0 | 0 | 0 |
| Performance Control Electronics | 0 | 0 | 0 | 0 |
| Instrumentation Electronics | 0 | 0 | 41 | 0 |
| Rate Gyros | 0 | 0 | 18(2) | 18(3) |
| Star Trackers | 0 | 0 | 5(2) | 5(2) |
| Primary Mirror Heaters | 119 | 115 | 102 | 98 |
| Secondary Mirror Heaters | 5 | 5 | 4 | 5 |
| Focal Plane Assembly Heaters | 198 | 172 | 116 | 91 |
| SI | | | | |
| Focal Plane Camera | 0 | 110 | 110 | 140 |
| Axial SI | 0 | 0 | 200(1) | 300(1) |

Figure 1.2-1 TEMPERATURE DISTRIBUTION - COLD CASE

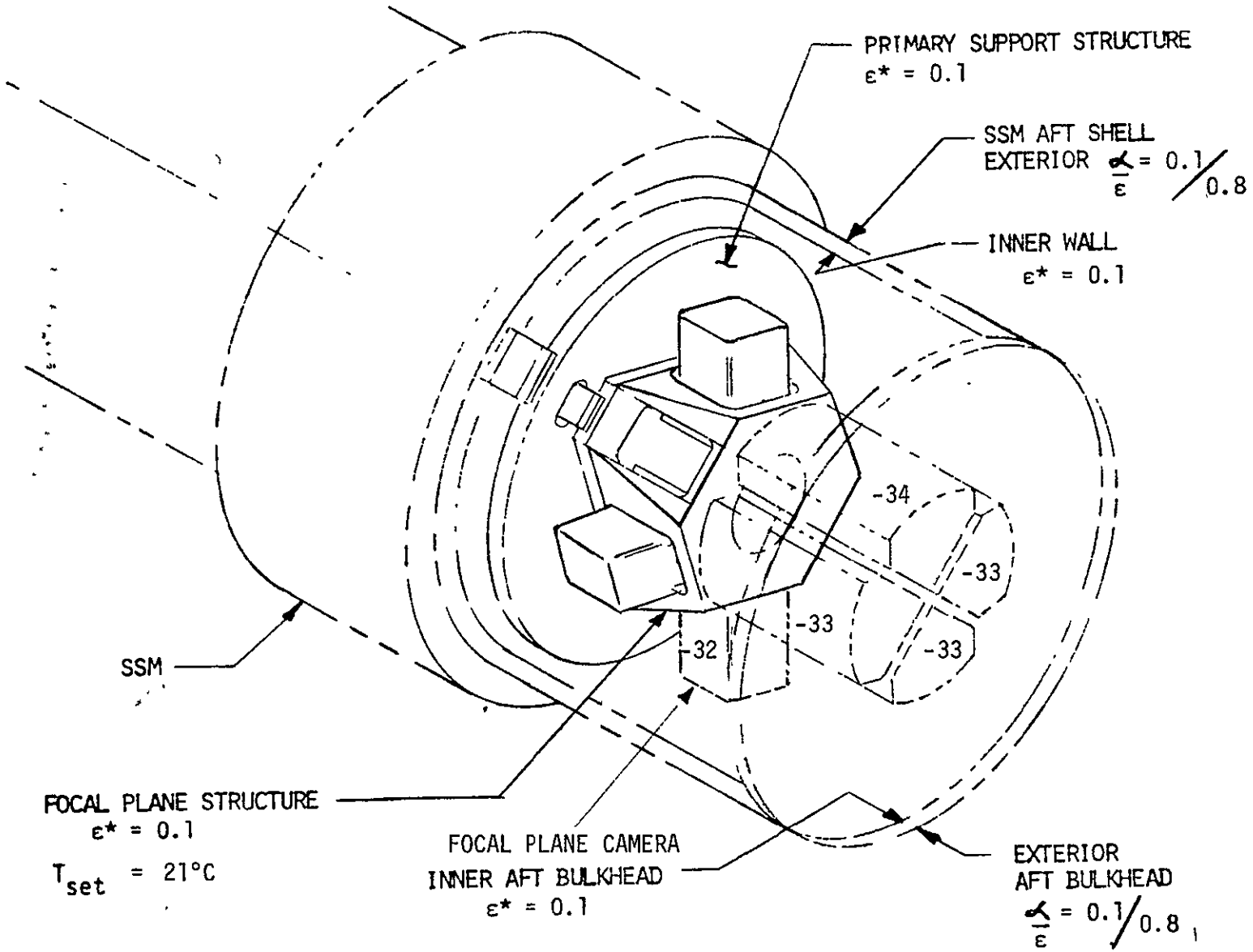

Figure 1.2-2 TEMPERATURE DISTRIBUTION - FOCAL PLANE CAMERA ONLY

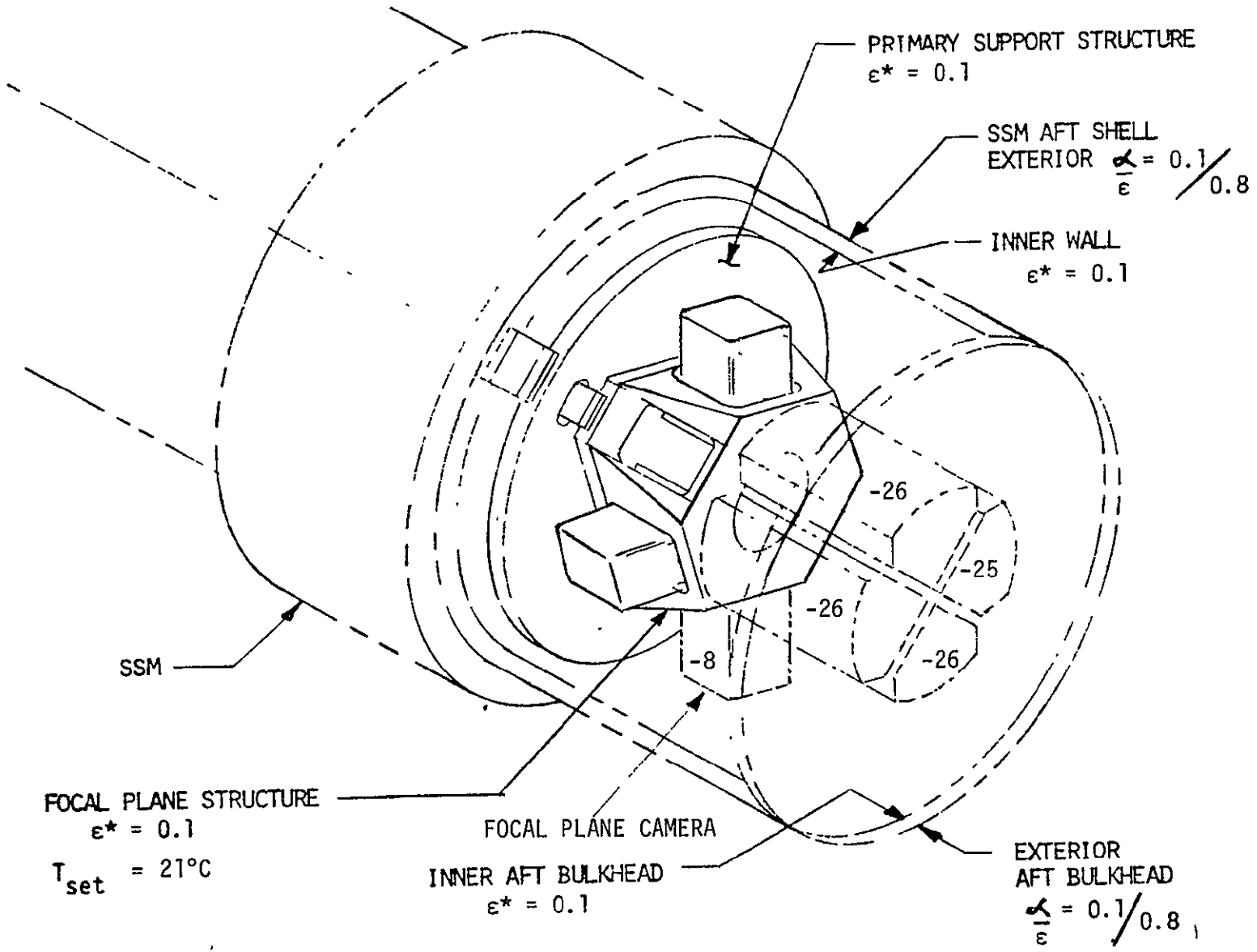

Figure 1.2-3 TEMPERATURE DISTRIBUTION - NOMINAL CASE

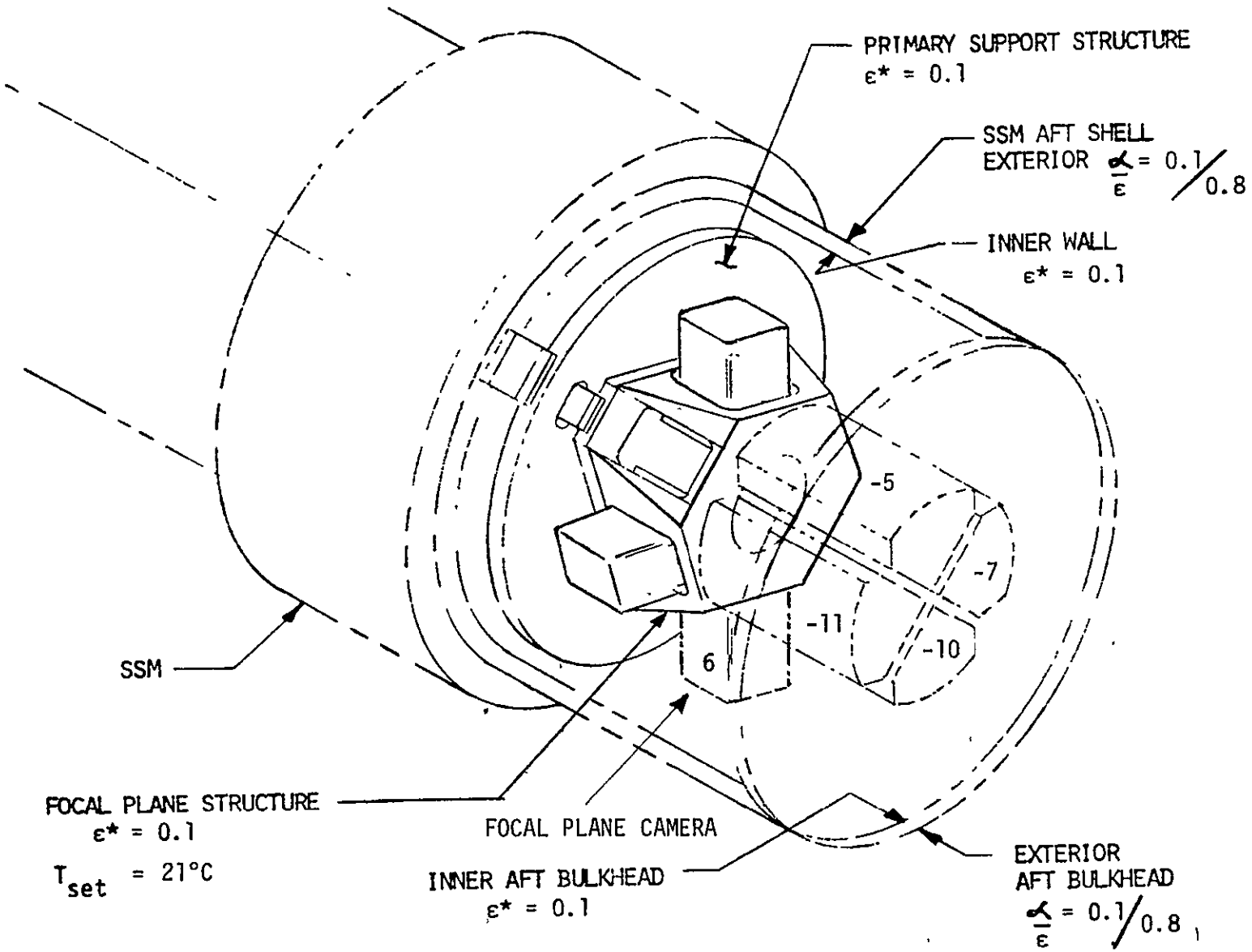

Figure 1.2-4 TEMPERATURE DISTRIBUTION - HOT CASE

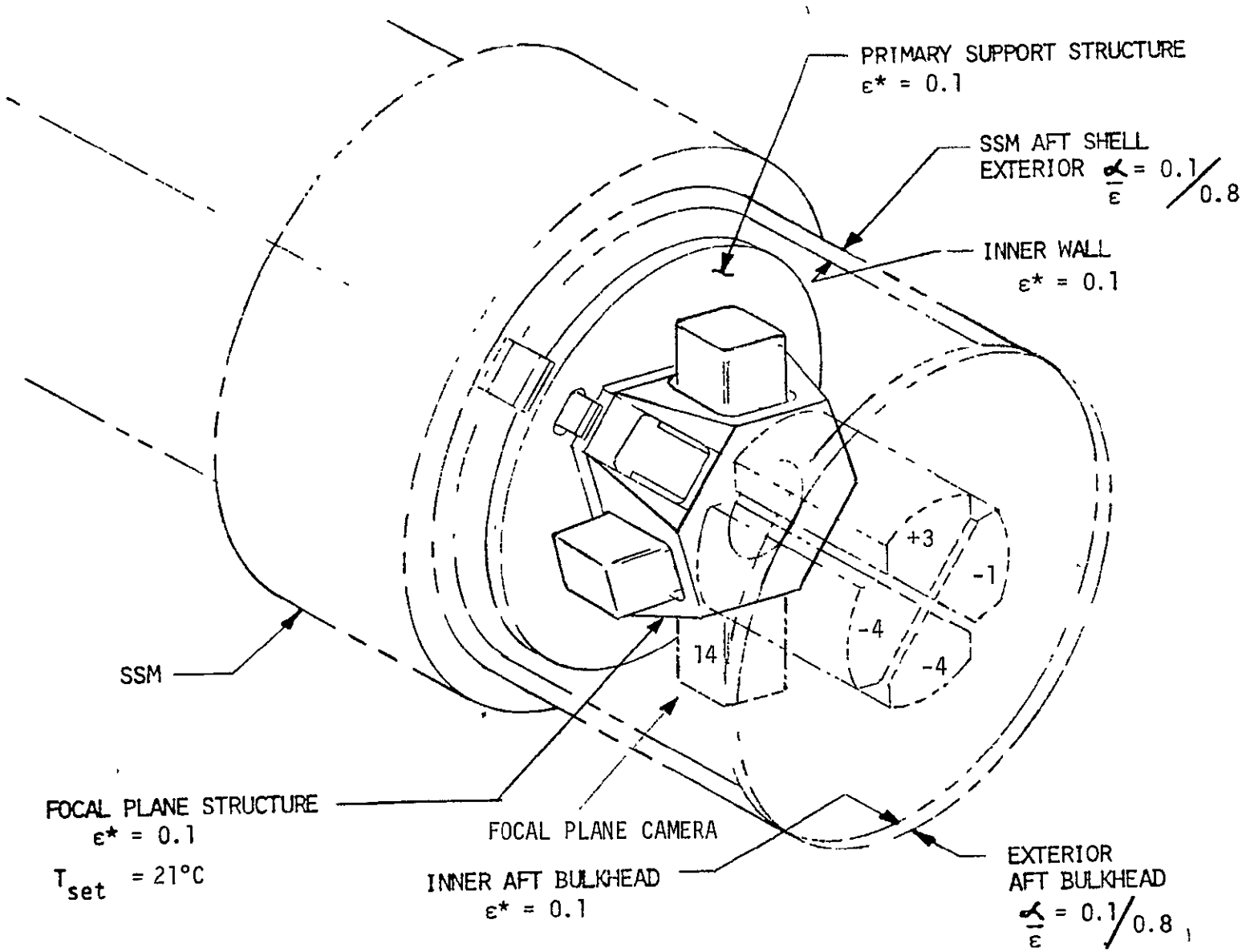

FIGURE 1.3-1
VIGNETTING AT FOCAL PLANE BY CENTER PICK-OFF MIRROR

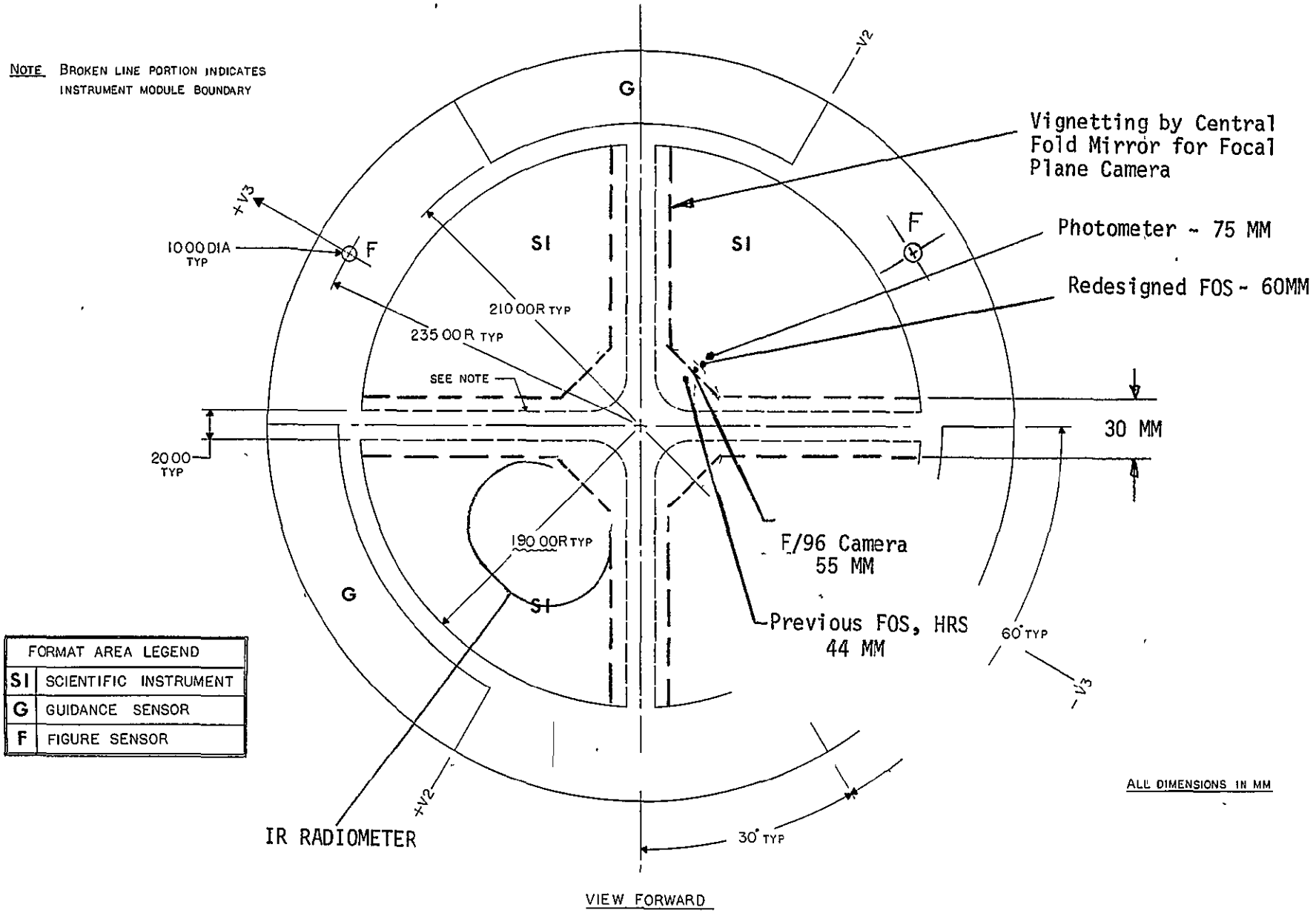


ST FOCAL PLANE FORMAT

Figure 1.3-2 VIGNETTING AT FOCAL PLANE EDGE-OF-FIELD PICK-OFF

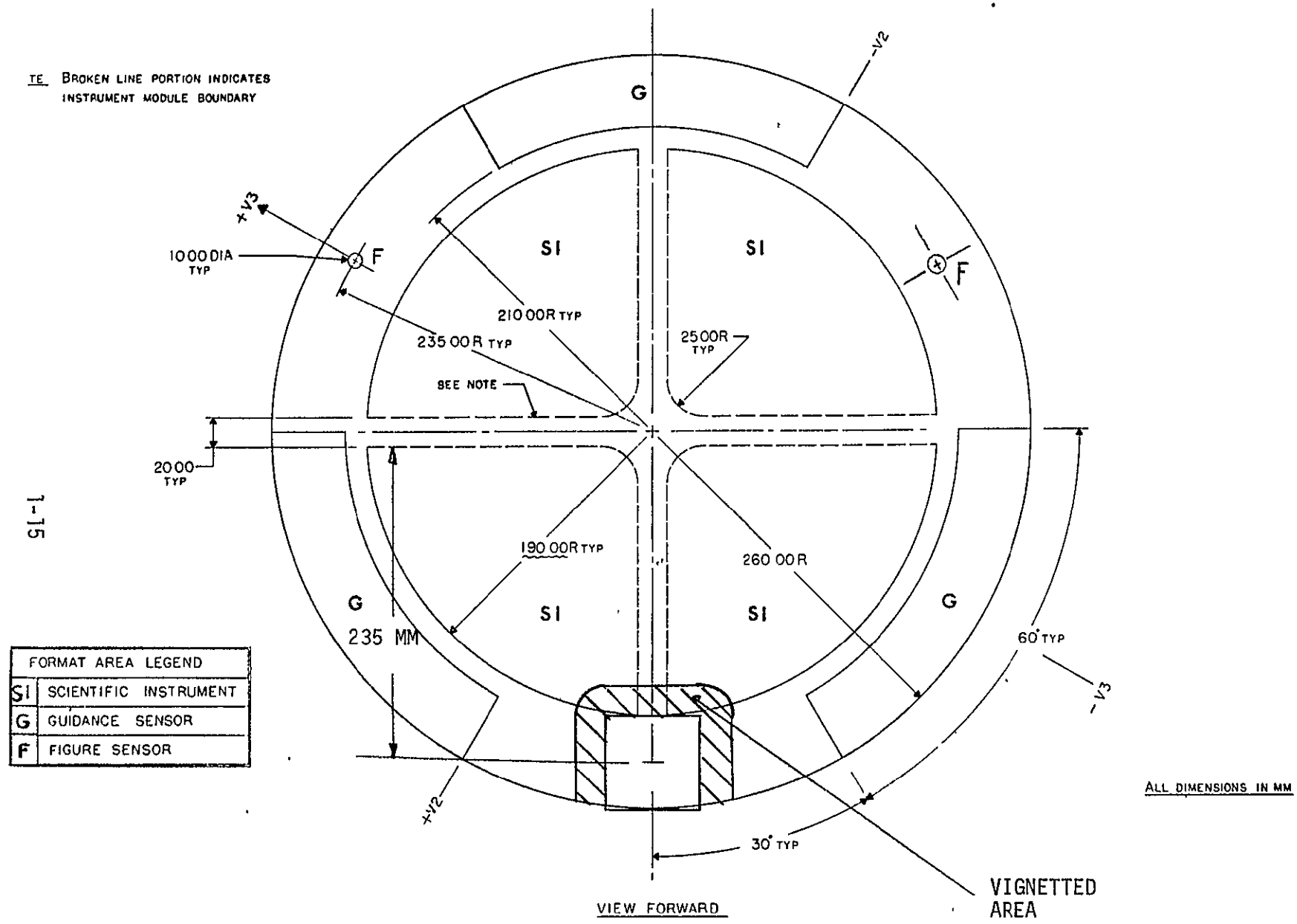


ST FOCAL PLANE FORMAT

VIGNETTING AT FOCAL PLANE BY INTERMEDIATE PICK-OFF MIRROR

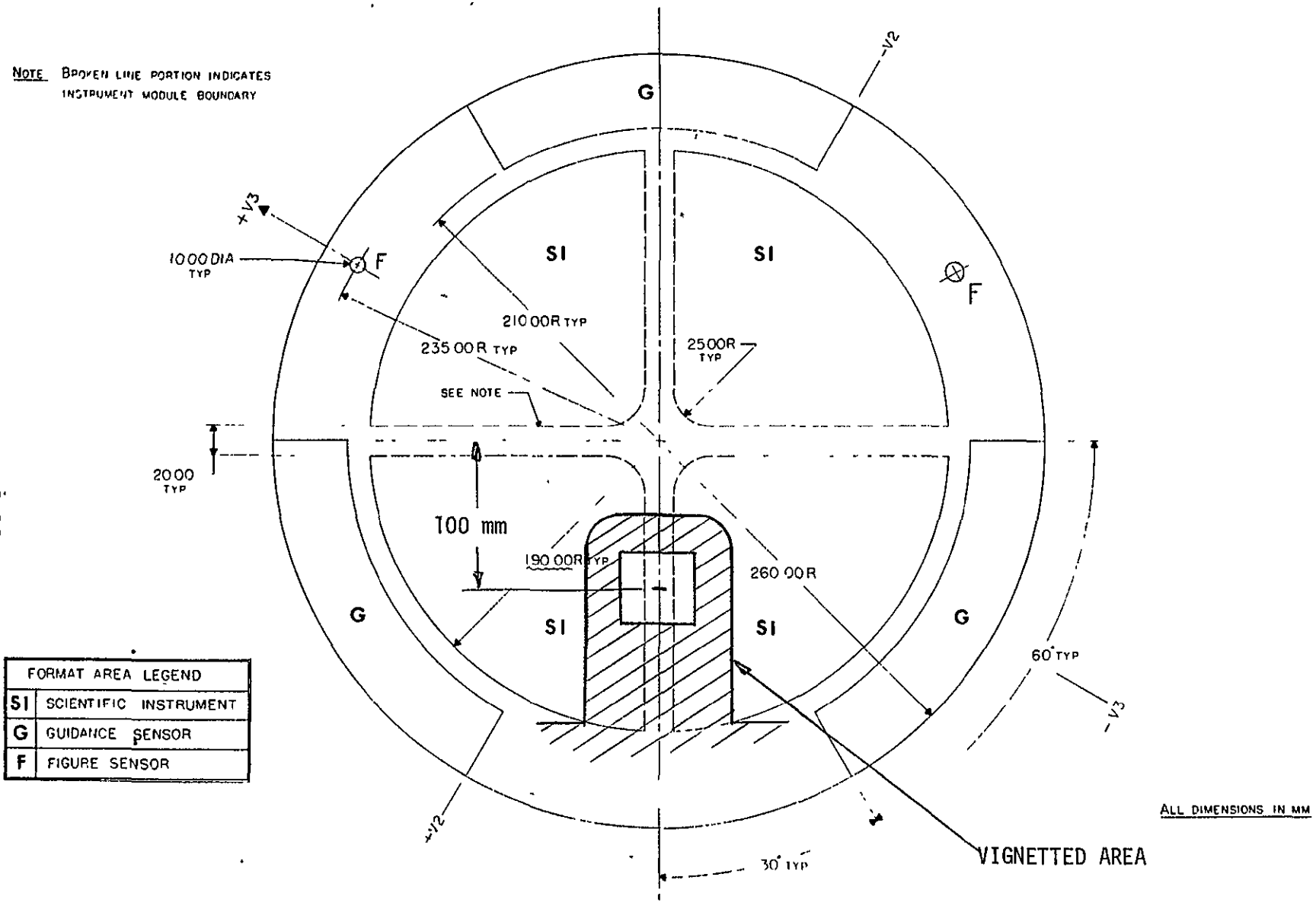


| FORMAT AREA LEGEND | |
|---|---|
| SI | SCIENTIFIC INSTRUMENT |
| G | GUIDANCE SENSOR |
| F | FIGURE SENSOR |

ST FOCAL PLANE FORMAT
FIGURE 1.3-3

Figure 1.3-2 shows the area obscured by the pick-off at the edge of the field. The obscuration is minimal, which is the only real advantage of this configuration.

Figure 1.3-3 shows the obscuration of the pick-off mirror in an intermediate position, chosen to allow axial SI's to have their apertures as close as possible to the optical axis, but still have the focal plane camera pick-off reasonably close to the axis.

## 1.4 Optical Design

Optical designs were generated for the camera with edge-of-field, intermediate, and center-of-field pick-off mirrors.

Figure 1.4-1 shows the design for the edge-of-field pick-off. The mirror is centered 235 mm off the optical axis. The mirror is an aspheric fold that corrects the astigmatism in the OTA image so that the image quality is good by the time the rays reach the camera focal plane. The field is also flattened somewhat, so that the radius of curvature of the field is 0.737 meter, as opposed to 0.626 meter for the OTA focal plane on-axis. The rays strike the focal plane at an angle of 23° from normal, which is probably the worst problem with this design since it causes a significant amount of lateral color aberration in the faceplate of the camera (described in Section 1.5).

Figure 1.4-2 shows the 6 locations in the focal plane at which spot diagrams were generated for the design. Figures 1.4-3 a-f show the actual spot diagrams which represent the pattern of rays from all portions of the pupil as they intercept the best-fit spherical focal plane. The box surrounding each spot diagram represents a focal plane size of 20 micrometers, which is close to the 25 micrometer pixel size of the detector. It is evident from the spot diagrams that the image quality is not limited by design aberrations since in each case, the spot pattern is much smaller than the pixel size. Furthermore, the design can be considered near diffraction-limited since the spots are significantly smaller than the airy disc size of the image (19 micrometers at 325 nm, 37 micrometers at 633 nm).

Figures 1.4-4 and 1.4-5 show surface contours for the pick-off mirror. Figure 1.4-4 shows the contours relative to a best-fit spherical surface. The maximum departure from spherical is about 21 micrometers. It is evident from the contours that the mirror contains a considerable amount of cylinder, and so Figure 1.4-5 shows residual contours after cylinder is removed. The maximum residual departure in this case is 5.5 micrometers.

Appendix A, at the end of this report, describes how such a mirror would be tested during manufacturing using Computer Generated Holograms (CGH's) in conjunction with a null lens to perform a null interferometer test. The generation of the holograms is accurate to about 1/8 wave peak-to-peak with

FIGURE 1.4-1 ST WITH EDGE-OF-FIELD PICK-OFF

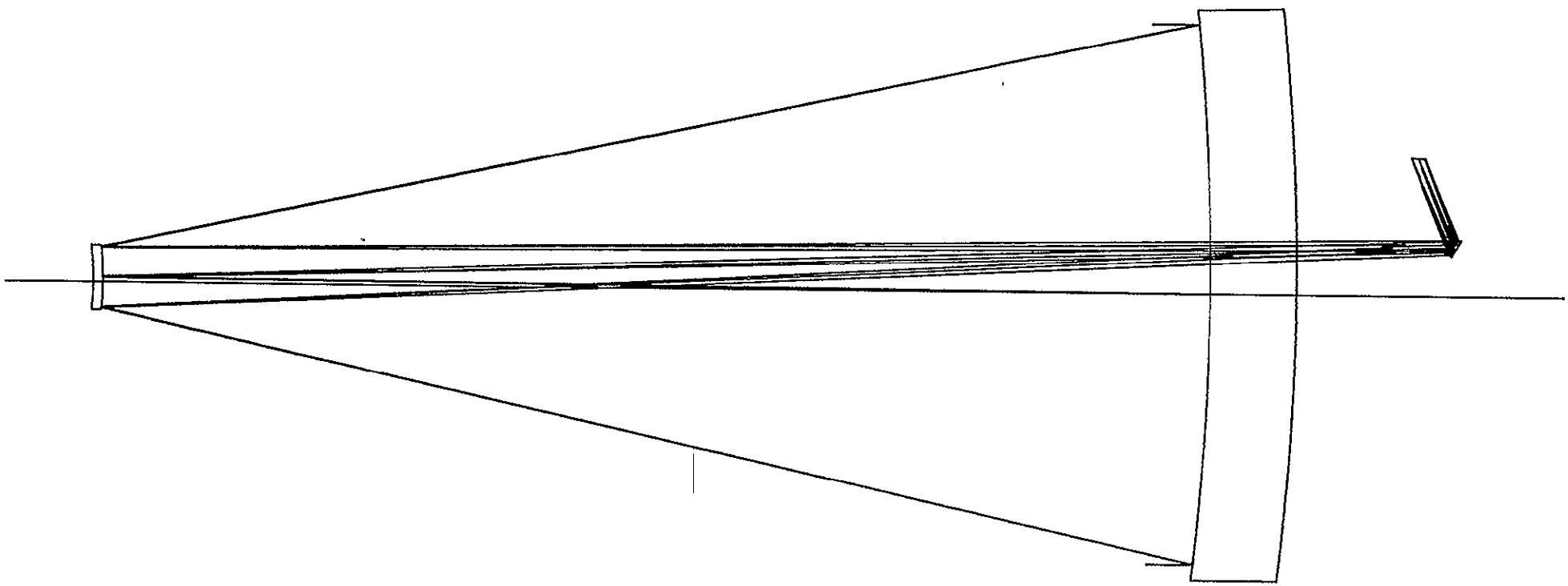

FIGURE 1.4-2

FOCAL PLANE LOCATIONS
EDGE-OF-FIELD SPOT DIAGRAMS

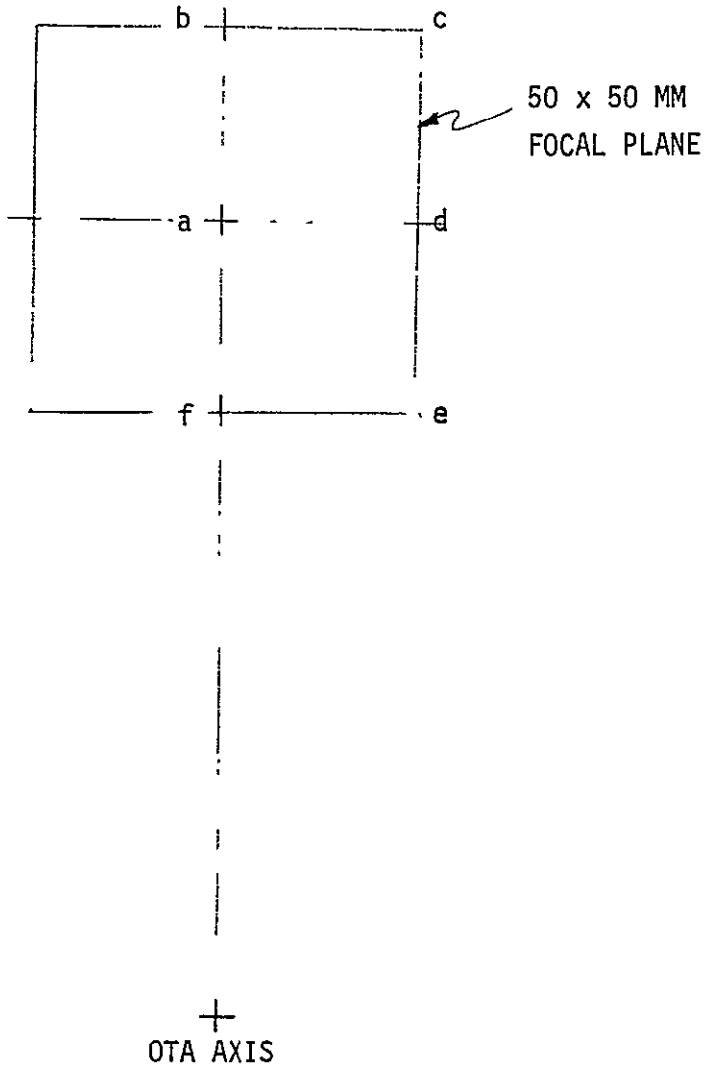

ID LST

FIGURE 1.4-3(a)

HBARX = 0.0 HBARY = 1.000 SCALE= 0.0010

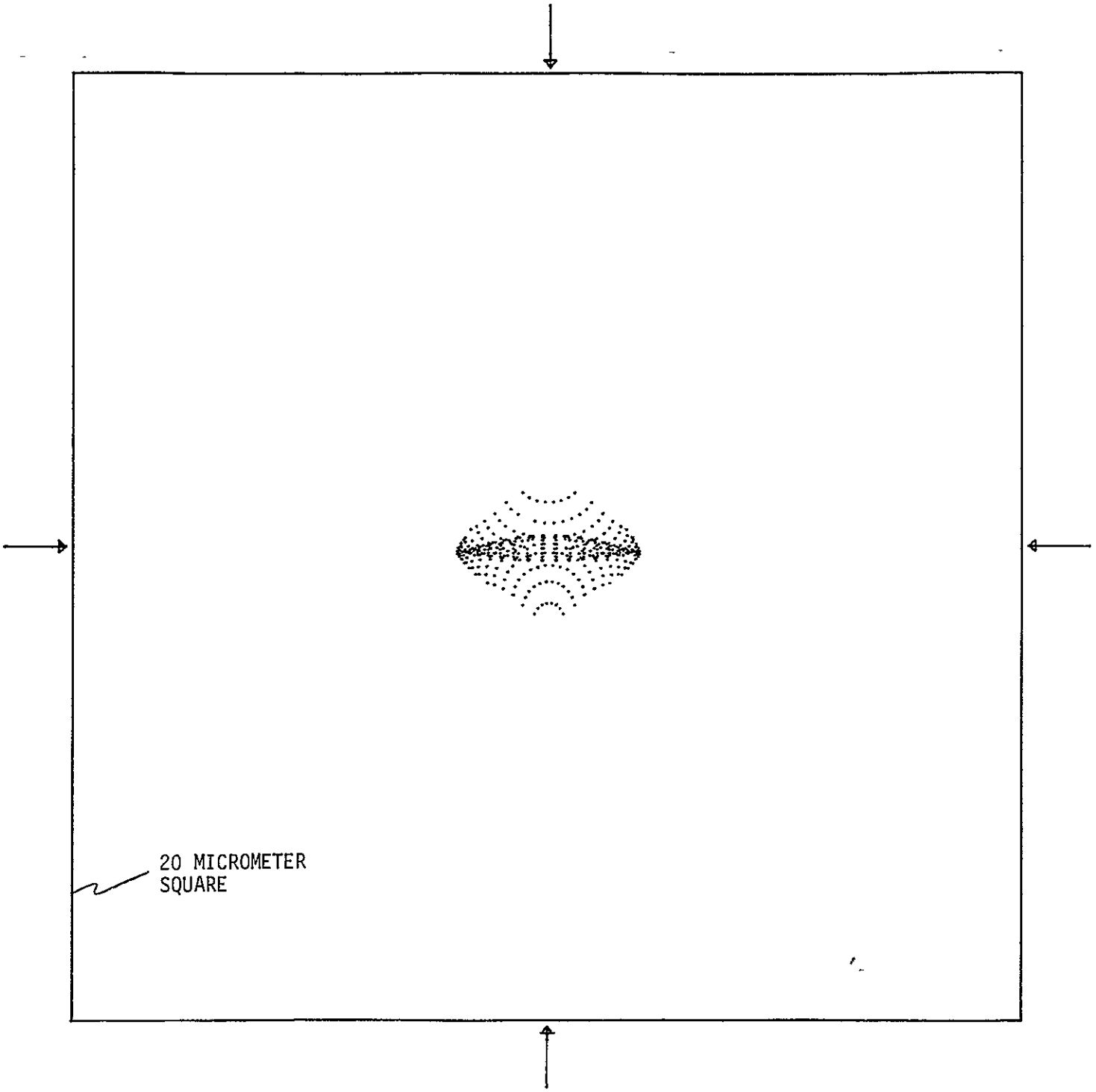


LENS NO. 16 PLOT NO. 2

ID LST

FIGURE 1.4-3(b)

HBARX = 0.0 HBARY = 1.106 SCALE= 0.0010

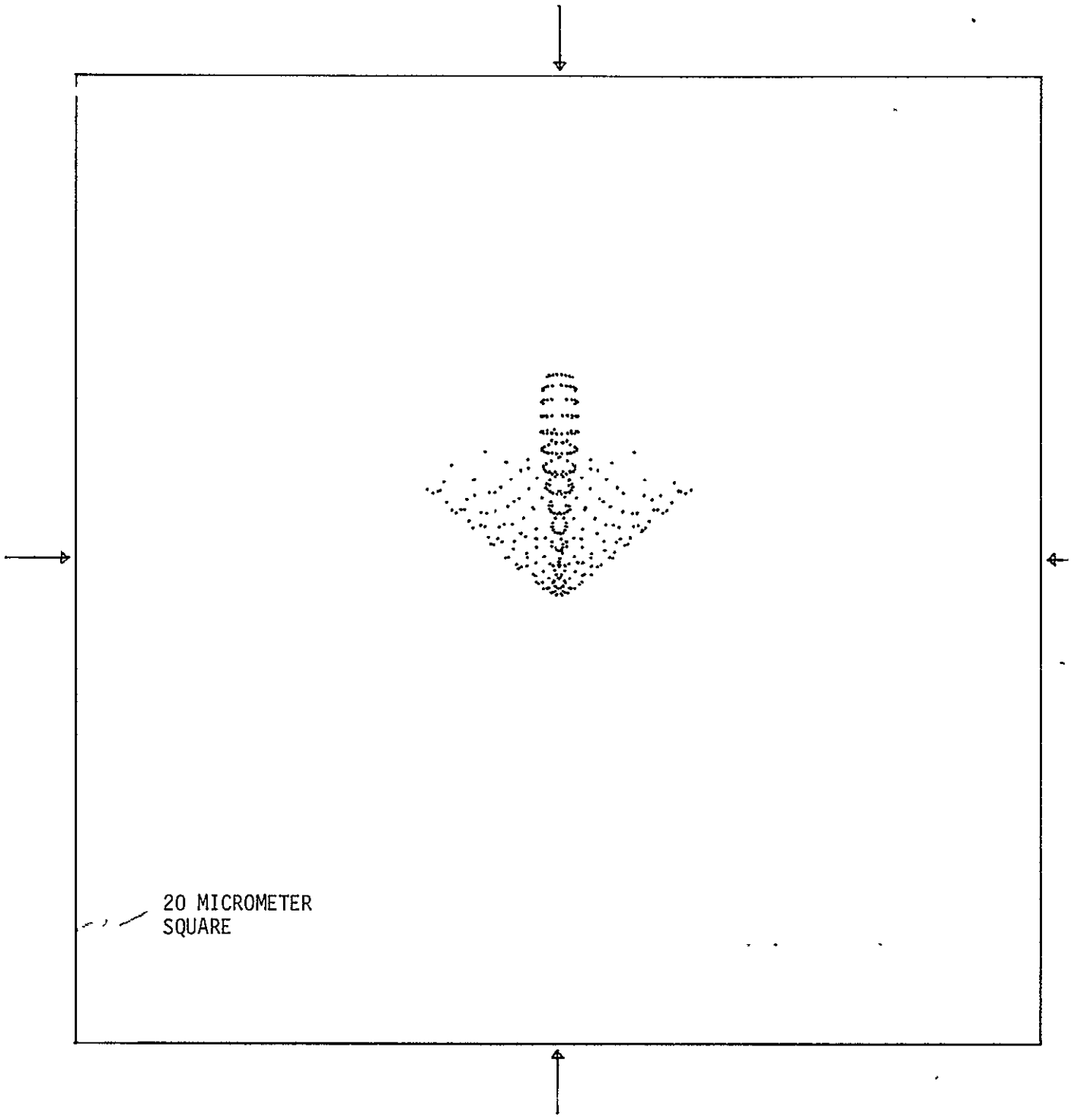


LENS NO. 16 PLOT NO. 3

ID LST

FIGURE 1.4-3(c)

HBARX = 0.106 HBARY = 1.106 SCALE= 0.0010

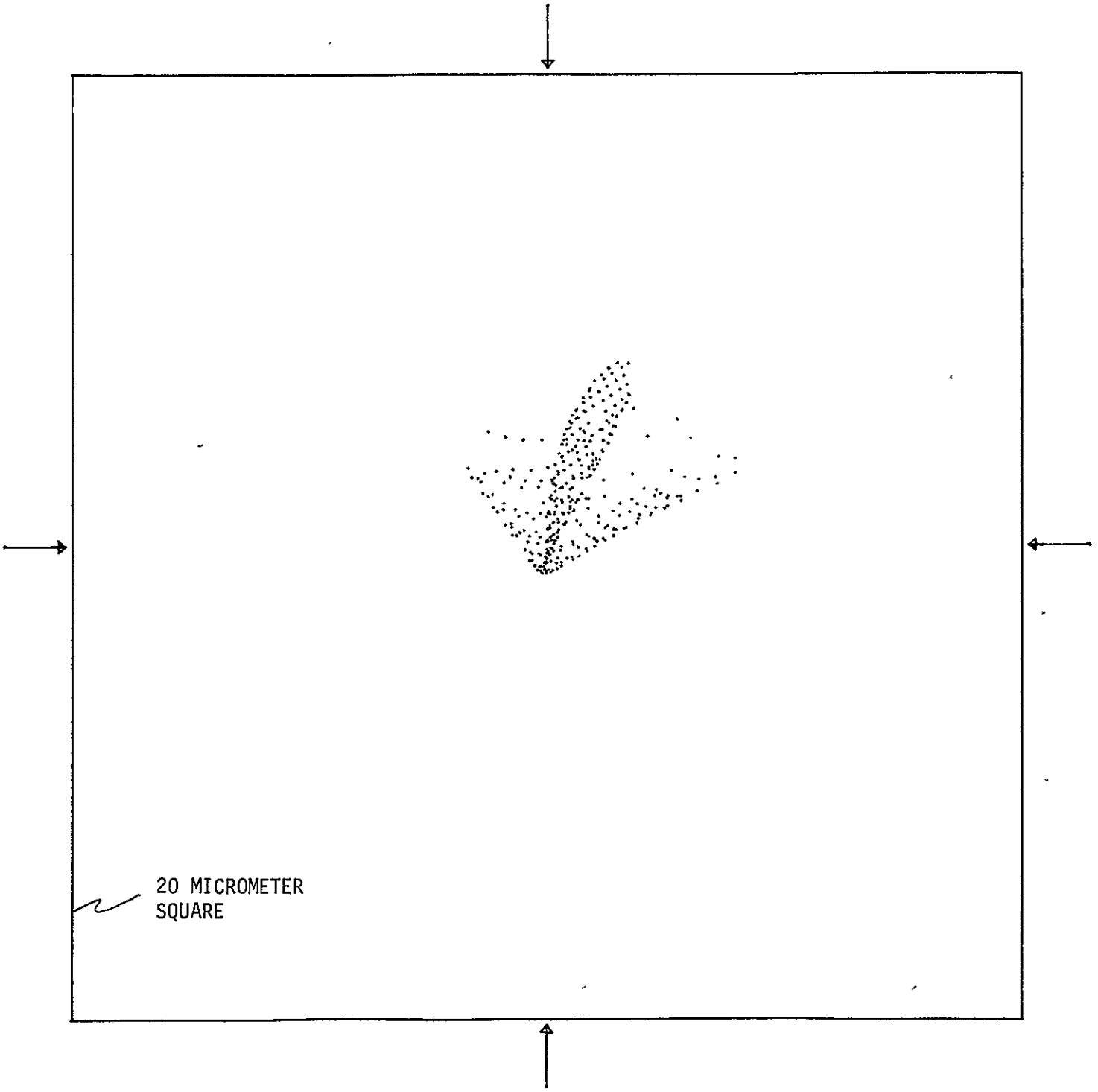


LENS NO. 16 PLOT NO. 3

ID LST

FIGURE 1.4-3(d)

HBARX = 0.106 HBARY = 1.000 SCALE= 0.0010

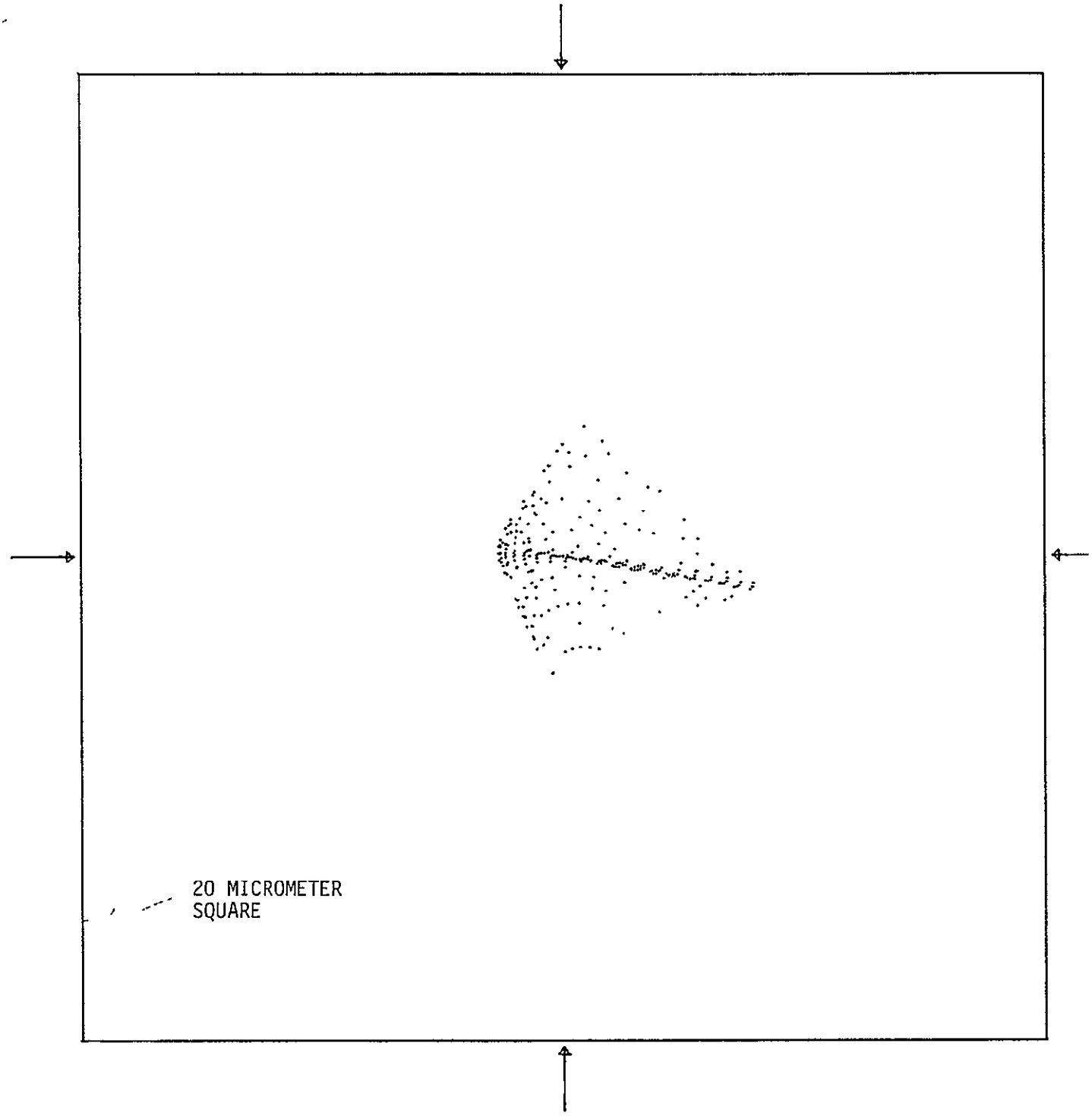

ID LST

FIGURE 1.4-3(e)

HBARX = 0.106 HBARY = 0.894 SCALE= 0.0010

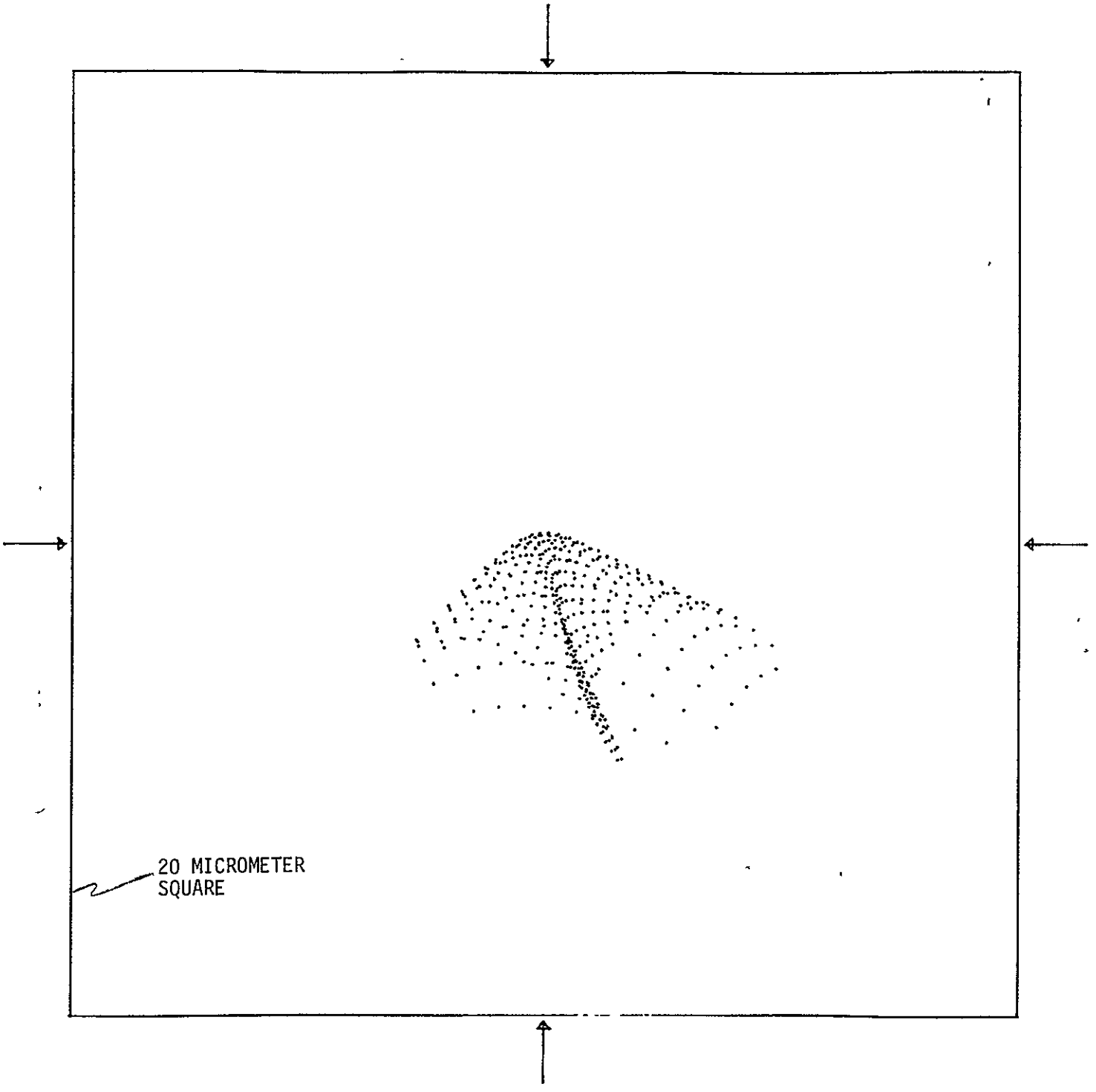


LENS NO. 16 PLOT NO. 1

ID LST

FIGURE 1.4-3(f)

HBARX = 0.0 HBARY = 0.894 SCALE= 0.0010

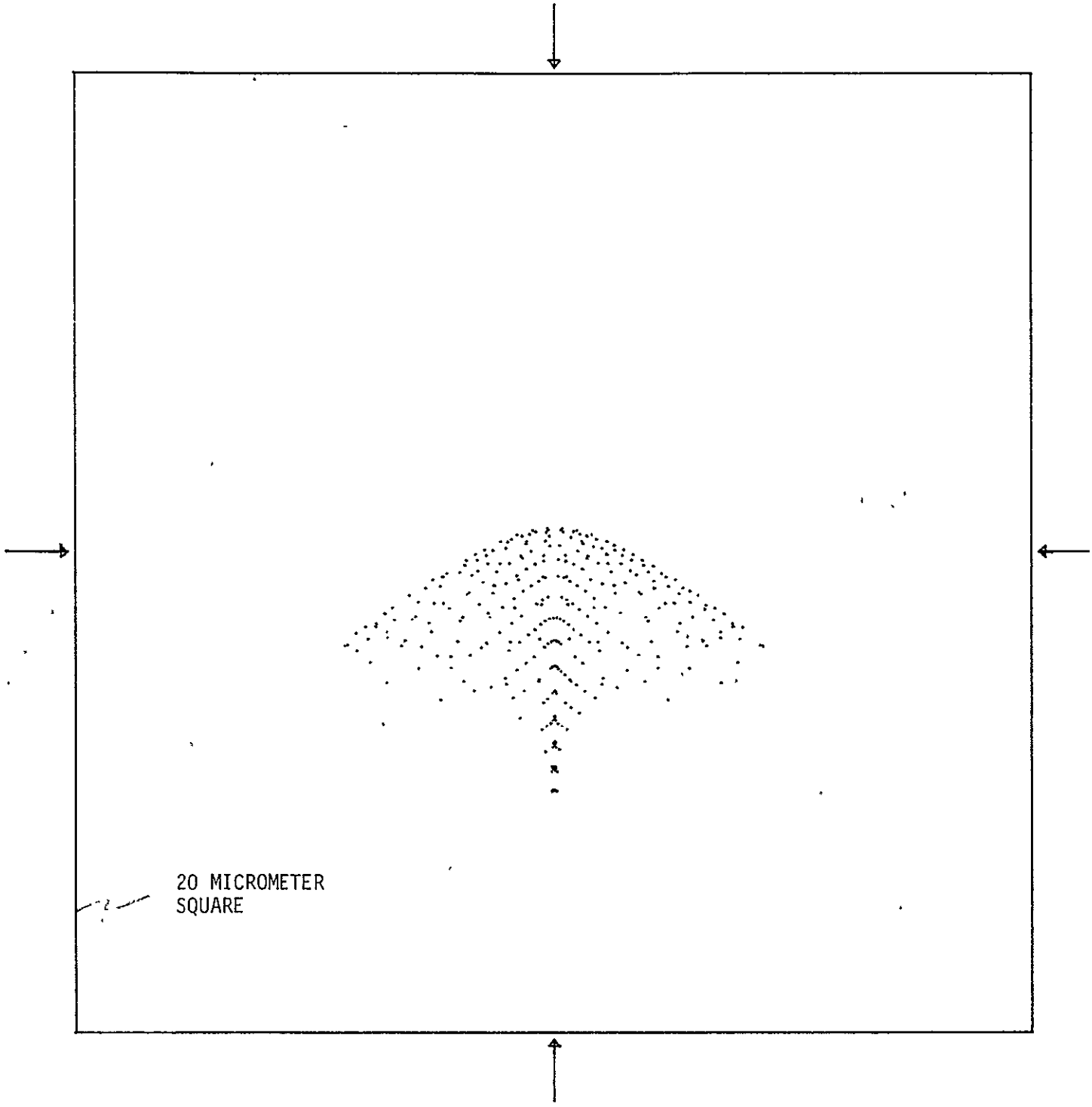

FIGURE 1.4-4 CONTOURS FOR EDGE-OF-FIELD PICK-OFF MIRROR - RELATIVE TO SPHERE

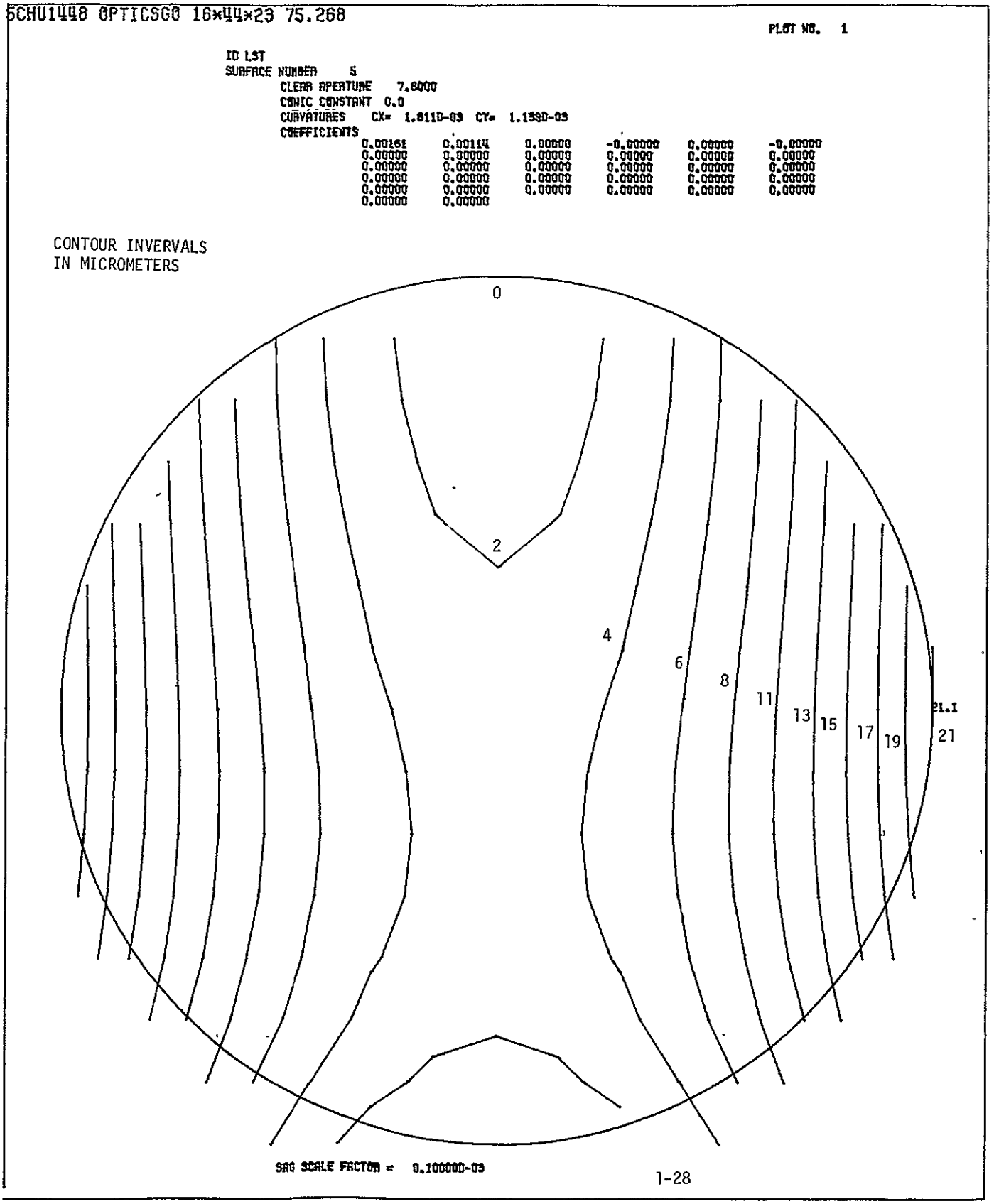

FIGURE 1.4-5 CONTOURS FOR EDGE-OF-FIELD PICK-OFF MIRROR - CYLINDER REMOVED

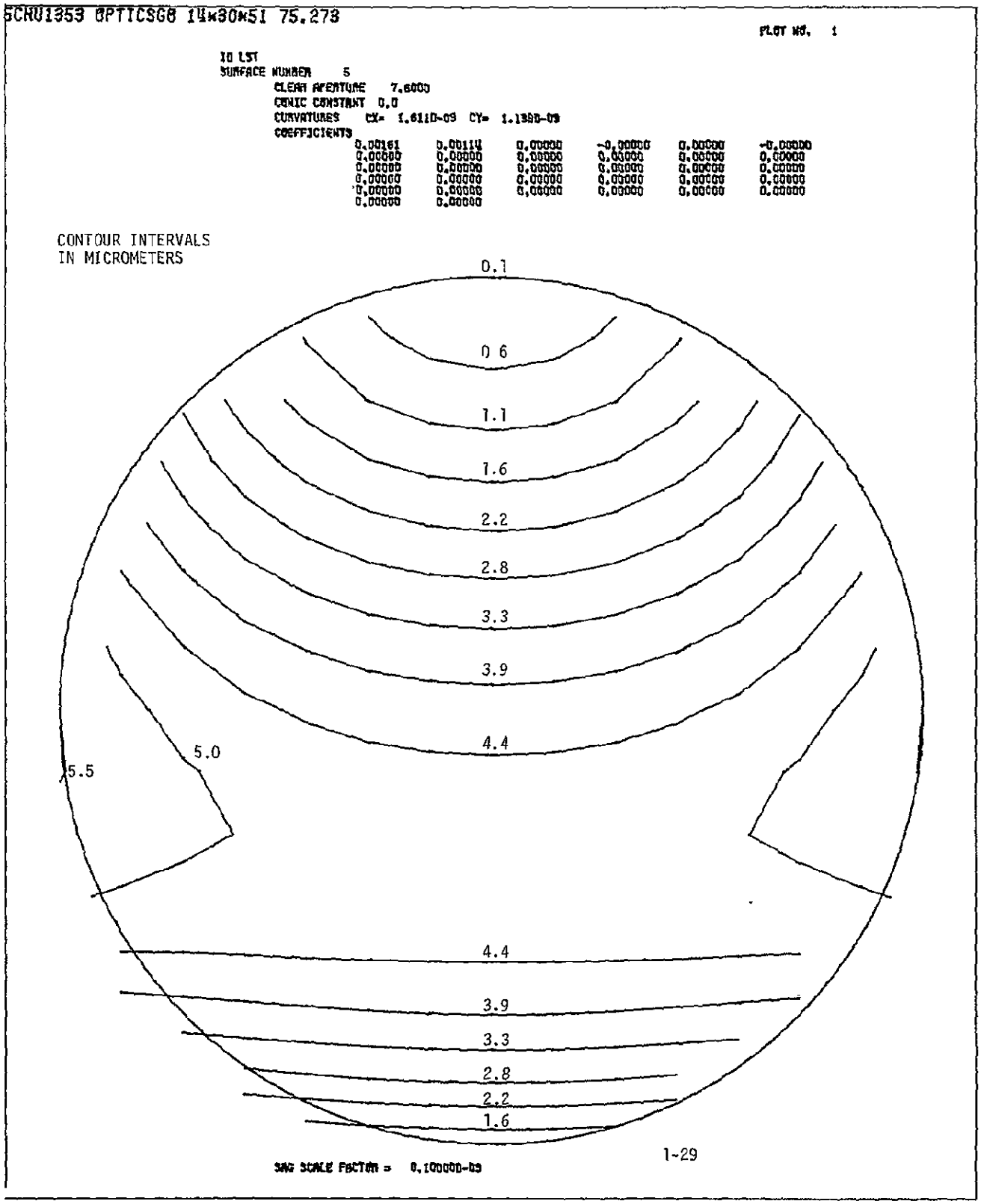

present equipment. Itek's experience with highly aspheric pieces indicates that a figuring error in the range of 1/6 to 1/4 wave peak-to-peak can be expected on the surface. These errors can be converted to rms wavefront error by the 20% rule of thumb (40% of the surface error). From these, a wavefront error of 0.08 to 1.11 wave rms at 633 nm is predicted for the finished mirror.

Figure 1.4-6 shows the design for the intermediate position pick-off mirror for the best-fit spherical focal plane. The mirror is centered 100 mm off the optical axis. In this case, the radius of curvature of the corrected focal plane is 0.656 meter compared to 0.626 meter for the OTA focal plane on axis. The rays strike the focal plane at an angle of 7° from normal, which is considerably better than the 23° of the edge-of-field mirror.

Spot diagrams are shown in Figure 1.4-7. The spot sizes are generally about half those of the edge-of-field mirror, and the design can be considered virtually diffraction-limited.

The mirror surface contours are shown in Figure 1.4-8, relative to a sphere, and 1.4-9 with cylinder removed. The departure from spherical is about 10 microns. With the cylinder removed, the residual is about 1.2 microns. Hence, this mirror is considerably closer to spherical than the edge-of-field mirror, although it is still somewhat more aspheric than the relay first mirror described in the Focal Plane Camera Final Report. One might expect this mirror to come out somewhat better than the edge-of-field mirror, although relating its asphericity to Itek experience still puts it in the range of a 0.08 - 0.11 wave rms mirror at 633 nm.

At the on-axis pick-off position, the image quality from the telescope is excellent, and a flat pick-off mirror, made to very high accuracy, can be used. Also, the rays are normal to the detector faceplate. These are the chief advantages of the on-axis position.

Over the detector field in this position, the worst aberration is that from field curvature (0.626 meter radius). If the system is adjusted so that the corners of the field and the center of the field are equally out of focus, then the image will be in focus at 7/10 of the maximum field radius. The maximum defocus spot diameter, at the corners and the center, will be 20 micrometers. The astigmatism in the image is insignificant compared to the defocus from field curvature. Figure 1.4-10 shows the tangential and sagittal ray fans at the on-axis, 4/10, 7/10, and full field positions of the detector with the field curvature removed. In each plot, the abcissa is the position in the pupil from which the ray comes, and the ordinate is ray intercept at the focal plane with respect to the chief ray for that field position. At the full-field position (corner of the format), the maximum astigmatic spot size is about 4 micrometers.

Common to all configurations is the problem of the chromatic aberration within the detector faceplate because of the extreme spectral range over which the detector must operate. Figure 1.4-11 shows the index of refraction of magnesium fluoride as a function of wavelength. For the on-axis configuration with a 5 mm thick faceplate, as shown in Figure 1.4-12, rays were traced at five wavelengths, 185, 200, 405, 589, and 706 nanometers, and the

FIGURE 1.4-6

STH WITH INTERMEDIATE PICK-OFF

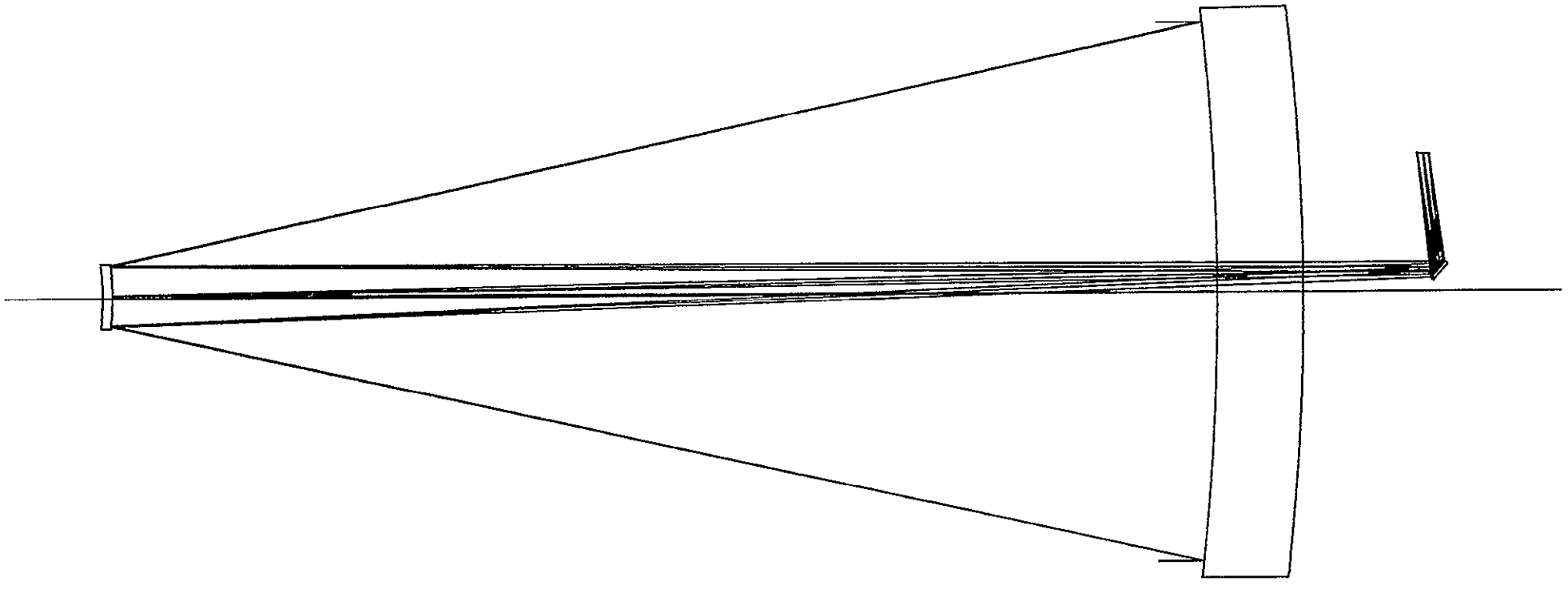

FIGURE 1.4-7

FOCAL PLANE LOCATIONS
INTERMEDIATE SPOT DIAGRAMS

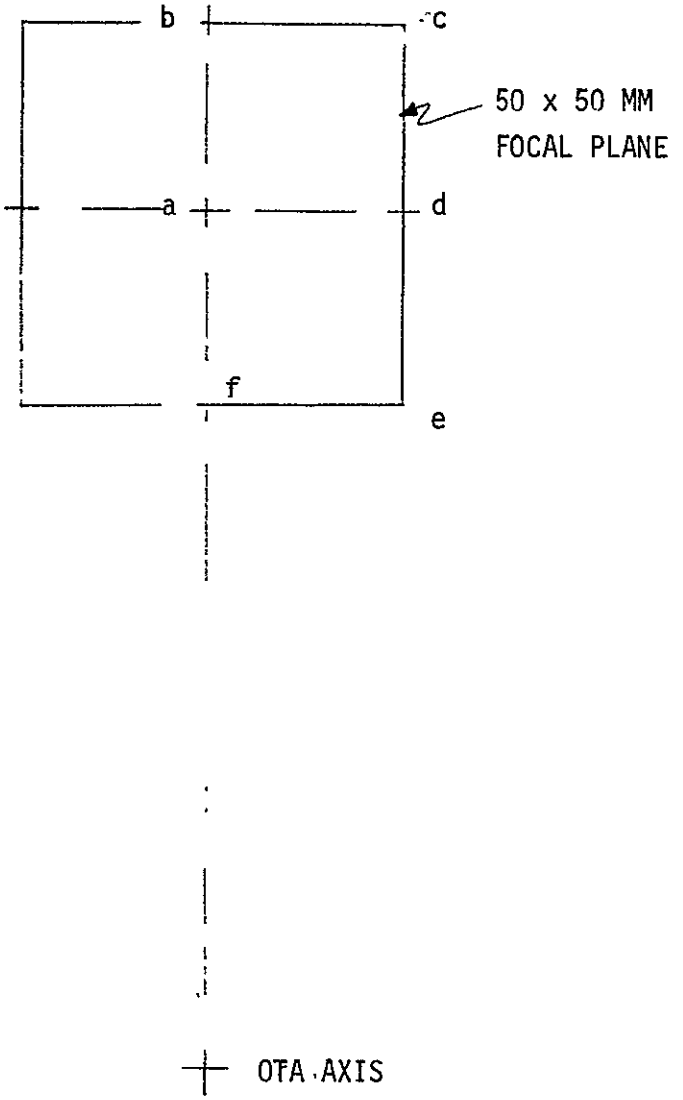

ID LST

FIGURE 1.4-7(a)

HBARX = 0.0 HBARY = 1.000 SCALE= 0.0010

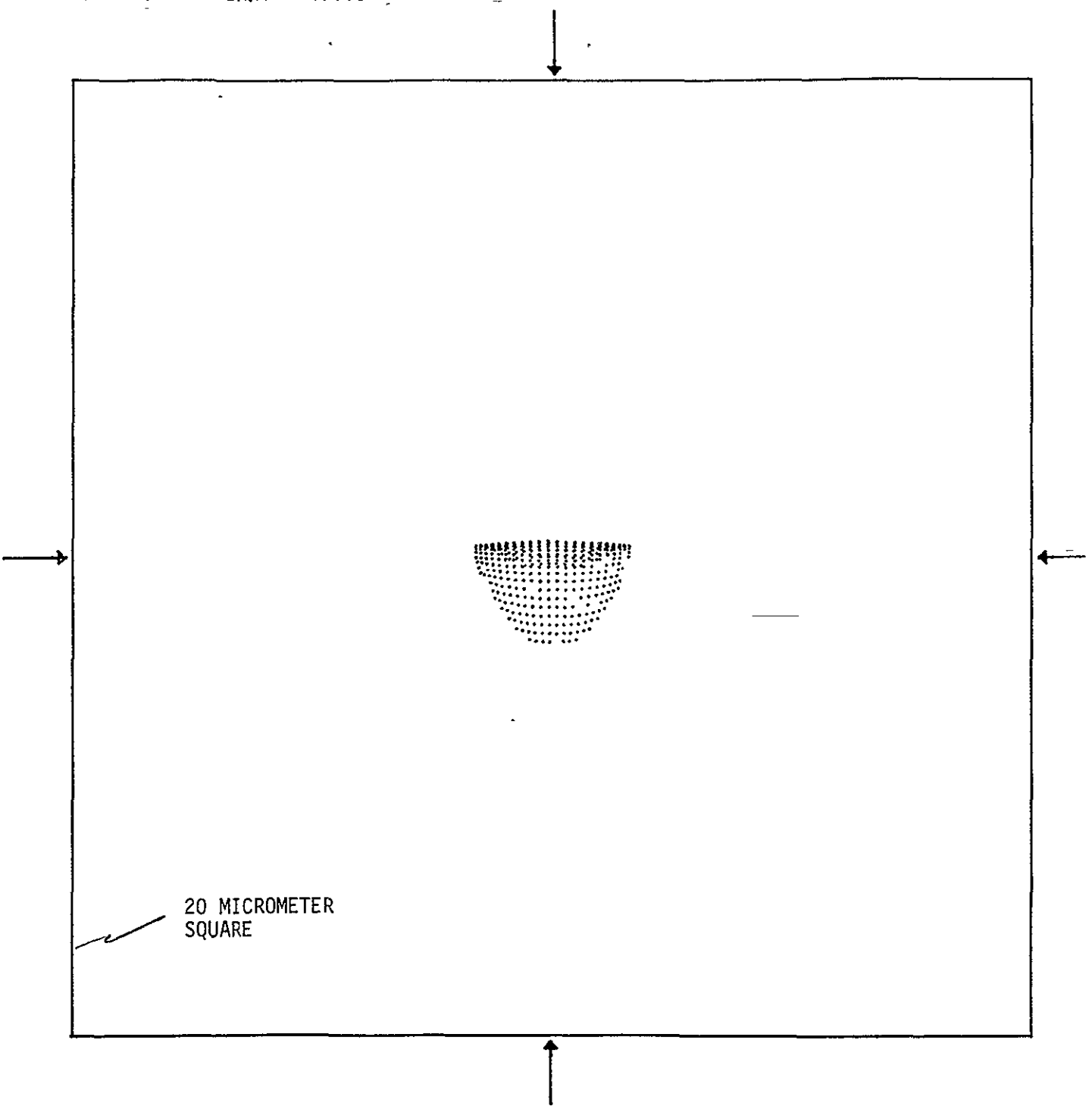

ID LST

FIGURE 1.4-7(b)

HBARX = 0.0 HBARY = 1.250 SCALE= 0.0010

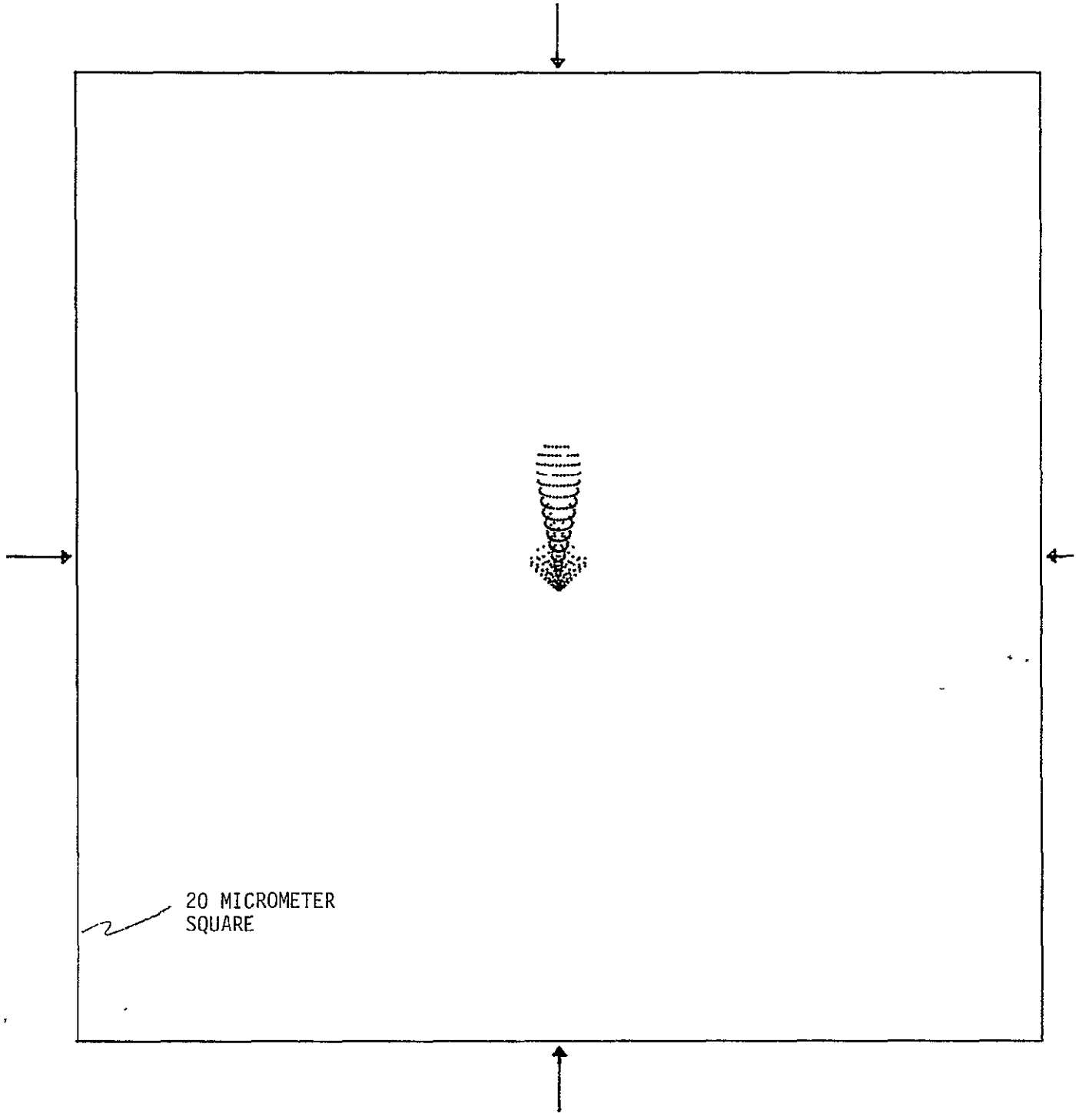

ID LST

FIGURE 1.4-7(c)

HBARX = 0.250 HBARY = 1.250

SCALE= 0.0010

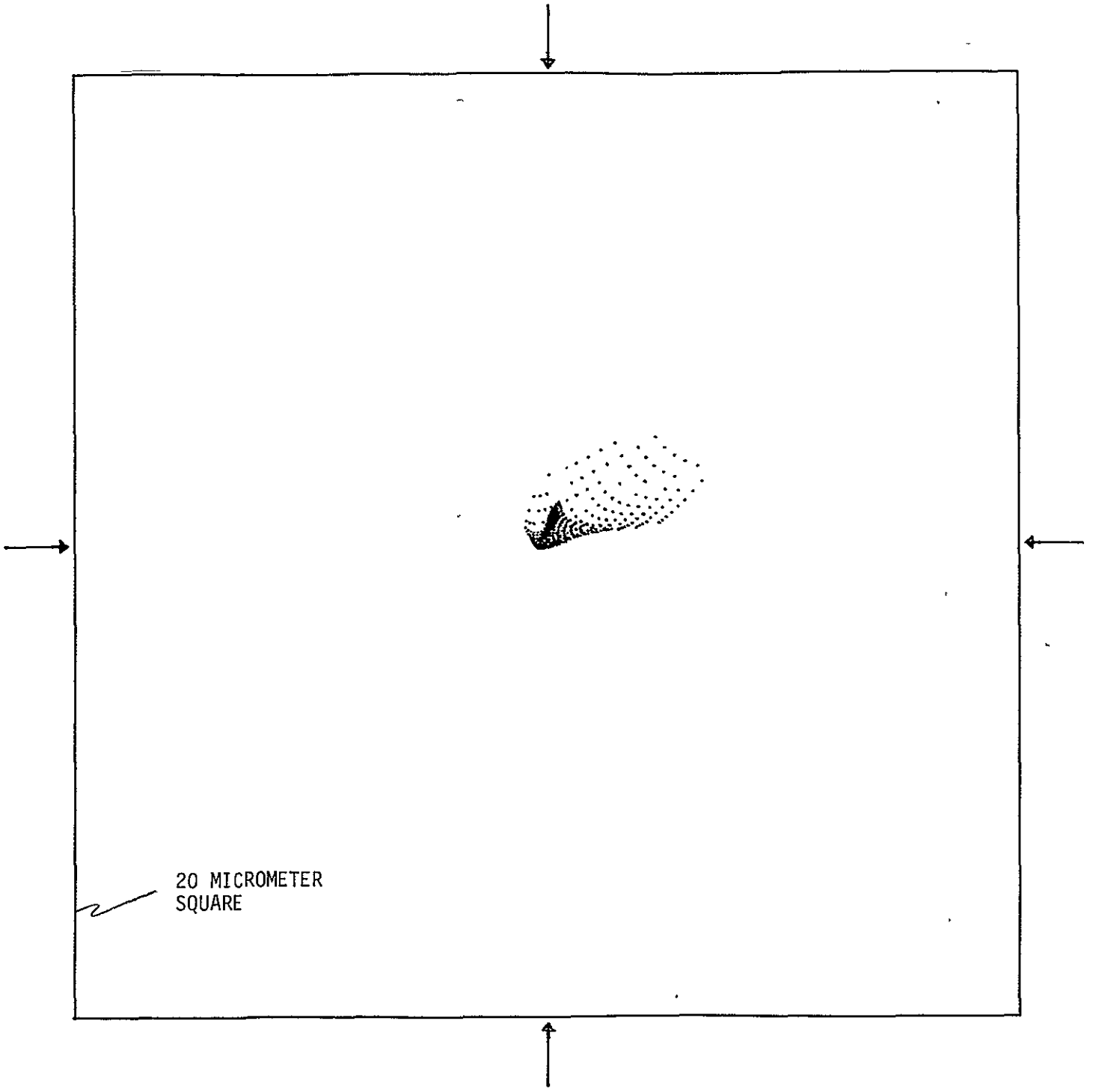


LENS NO. 15 PLOT NO. 6

ID LST

FIGURE 1.4-7(a)

HBARX = 0.250 HBARY = 1.000 SCALE= 0.0010

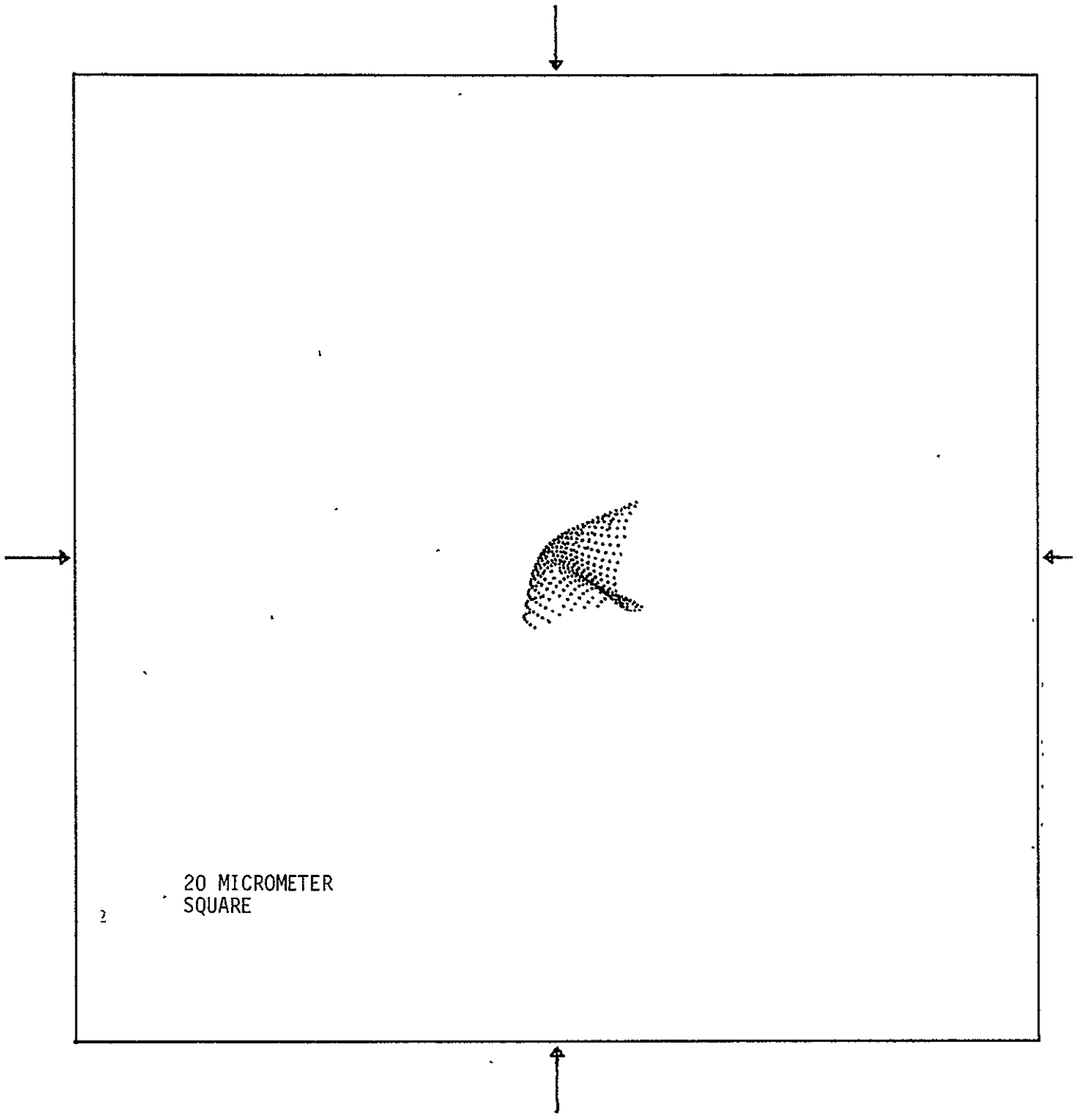


LENS NO. 15 PLOT NO. 5

ID LST

FIGURE 1.4-7(e)

HBARX = 0.250 HBARY = 0.750

SCALE= 0.0010

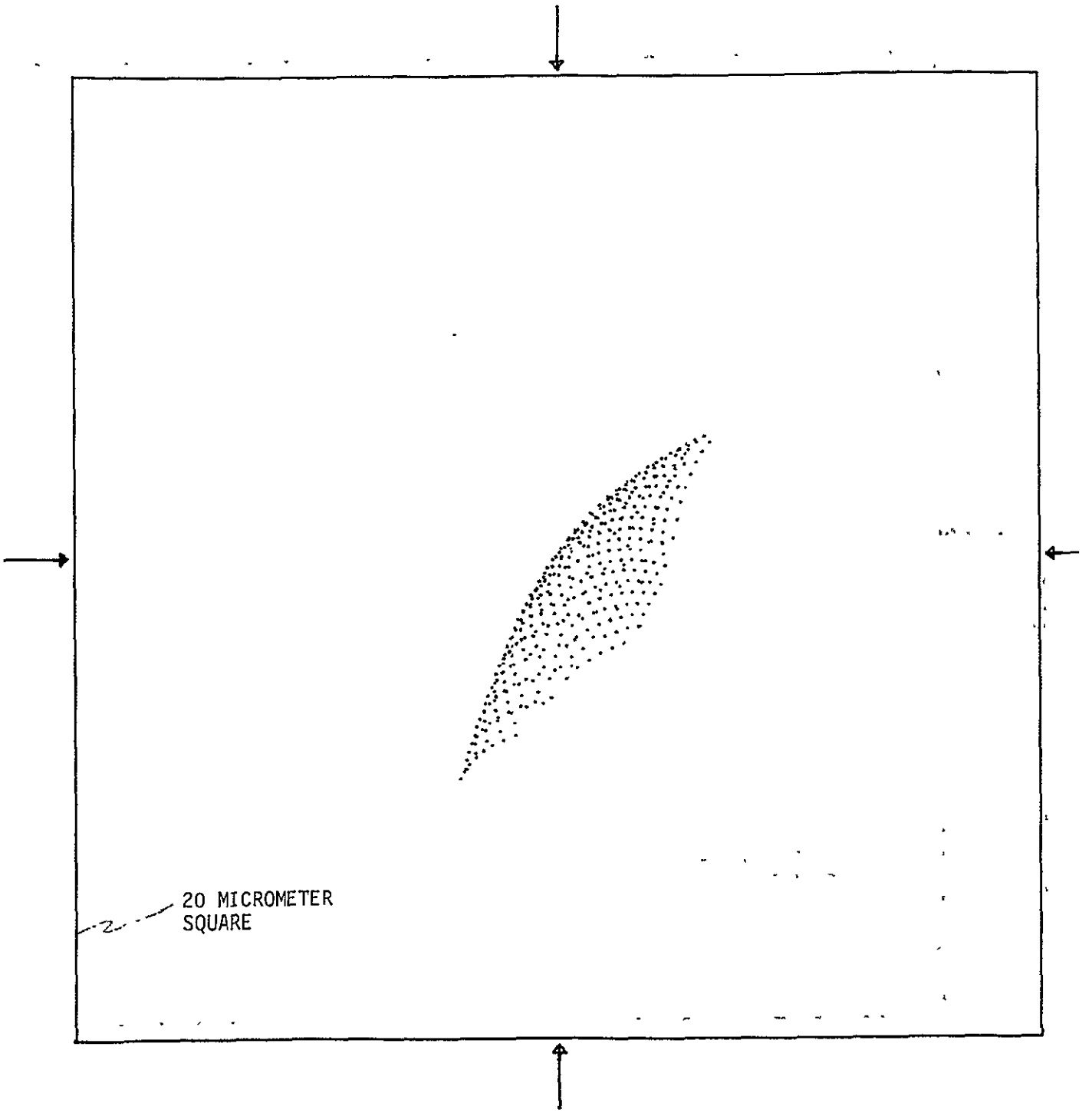

ID LST

FIGURE 1.4-7(f)

HBARX = 0.0 HBARY = 0.750

SCALE= 0.0010

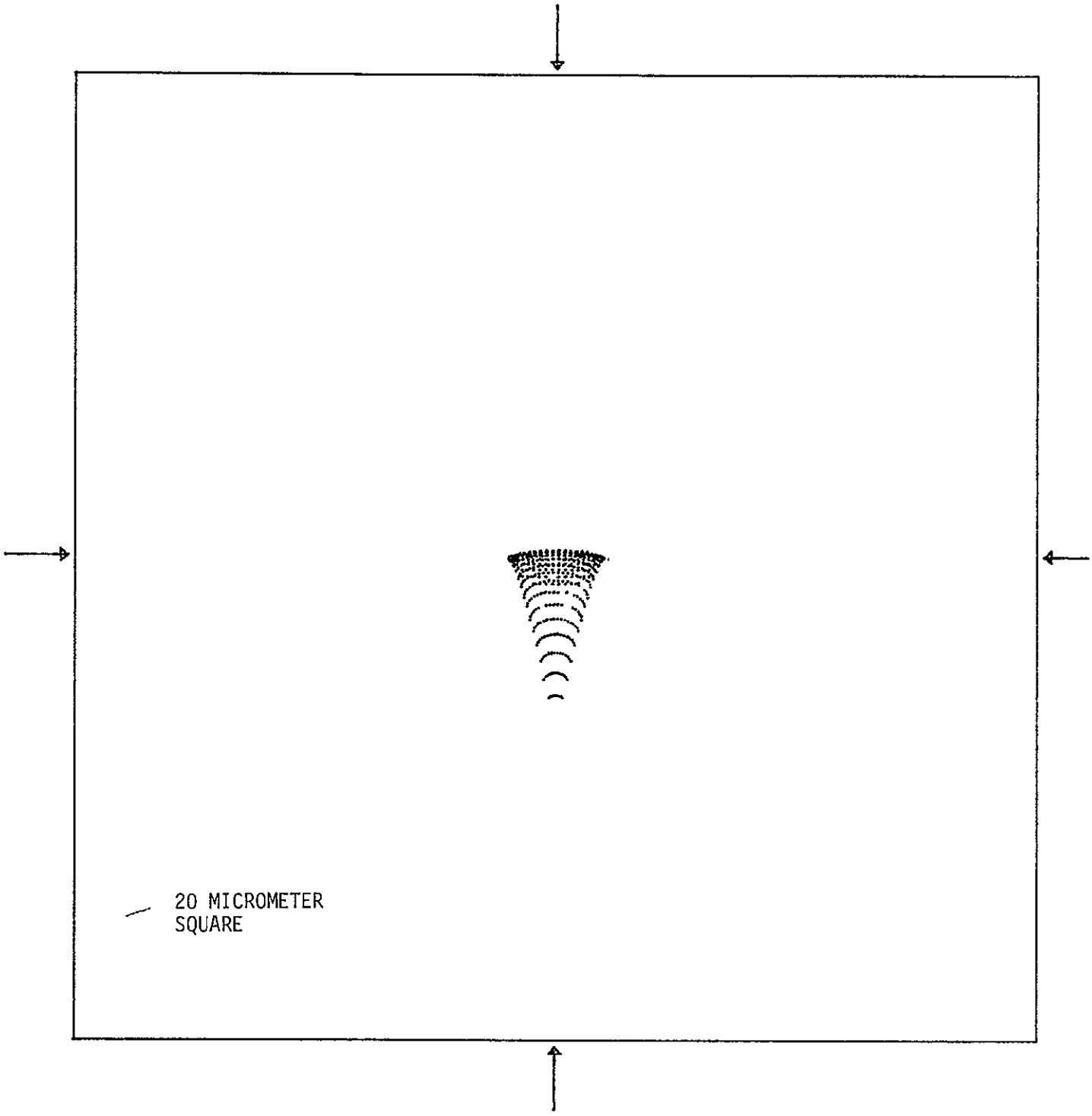


LENS NO. 15 PLOT NO. 1

ID LST
SURFACE NUMBER 5
CLEAR APERTURE 9.0000
CONIC CONSTANT 0.0
CURVATURES CX= 2.0990-04 CY= 1.9550-04
COEFFICIENTS

| | | | | | |
|---|---|---|---|---|---|
| 0.00024 | 0.00014 | 0.00000 | 0.00000 | -0.00000 | 0.00000 |
| 0.00000 | 0.00000 | 0.00000 | 0.00000 | 0.00000 | 0.00000 |
| 0.00000 | 0.00000 | 0.00000 | 0.00000 | 0.00000 | 0.00000 |
| 0.00000 | 0.00000 | 0.00000 | 0.00000 | 0.00000 | 0.00000 |
| 0.00000 | 0.00000 | 0.00000 | 0.00000 | 0.00000 | 0.00000 |
| 0.00000 | 0.00000 | | | | |

CONTOUR INVERVALS
IN MICROMETERS

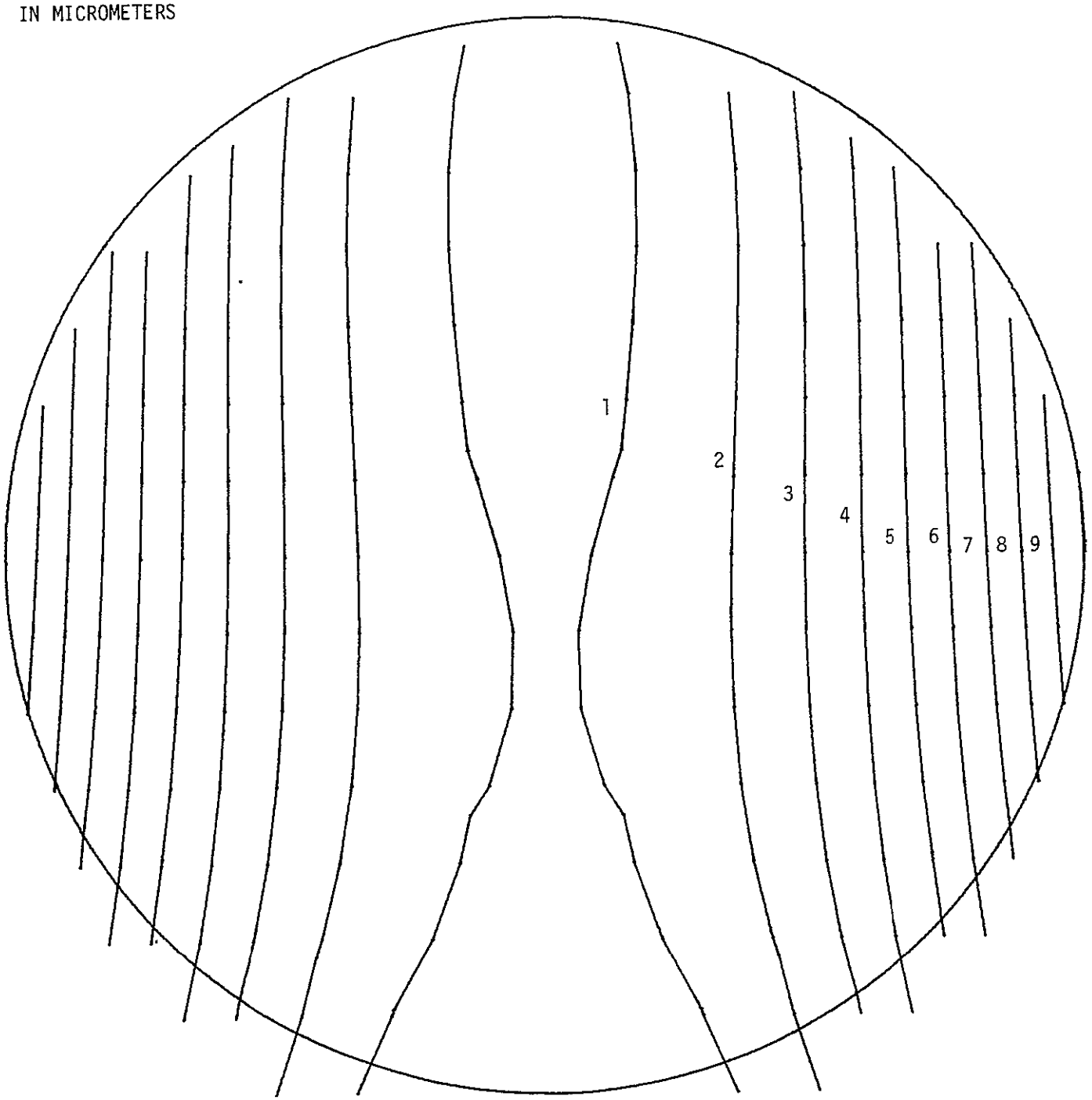


SAG SCALE FACTOR = 0.100000-03

Figure 1.4-9 CONTOURS FOR INTERMEDIATE PICK-OFF MIRROR - CYLINDER REMOVED

U1356 OPTICSGO 14×33×46 75.273 PLOT NO. 1

ID LST
SURFACE NUMBER 5
CLEAR APERTURE 8.0000
CONIC CONSTANT 0.0
CURVATURES CX= 2.8390-04 CY= 1.3550-04
COEFFICIENTS

| | | | | | |
|---|---|---|---|---|---|
| 0.00024 | 0.00014 | 0.00000 | 0.00000 | -0.00000 | 0.00000 |
| 0.00000 | 0.00000 | 0.00000 | 0.00000 | 0.00000 | 0.00000 |
| 0.00000 | 0.00000 | 0.00000 | 0.00000 | 0.00000 | 0.00000 |
| 0.00000 | 0.00000 | 0.00000 | 0.00000 | 0.00000 | 0.00000 |
| 0.00000 | 0.00000 | 0.00000 | 0.00000 | 0.00000 | 0.00000 |
| 0.00000 | 0.00000 | | | | |

CONTOUR INVERVALS
IN MICROMETERS

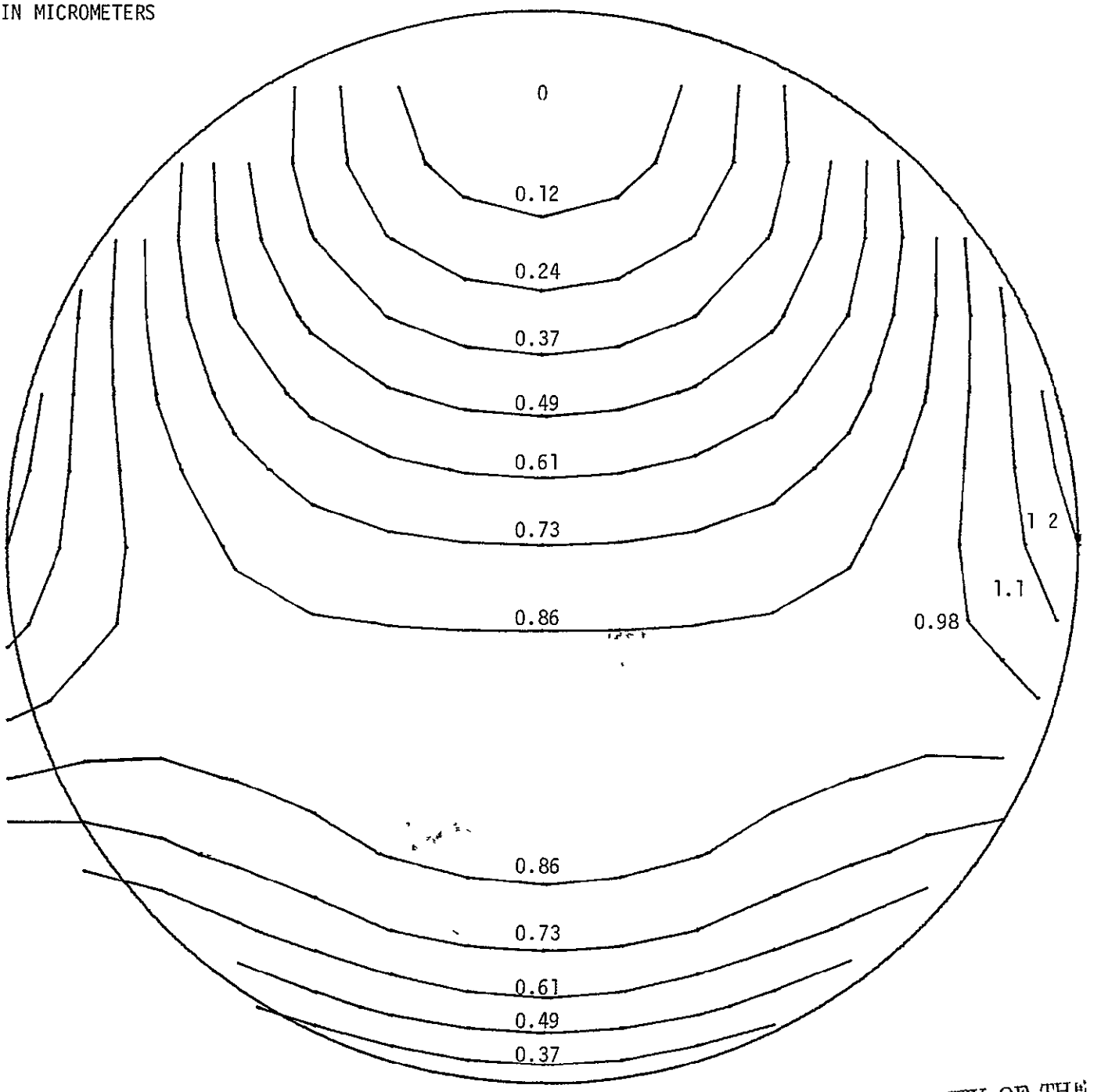


SAG SCALE FACTOR = 0.100000-04

Figure 1.4-10 RAY FANS FOR ON-AXIS PICK-OFF

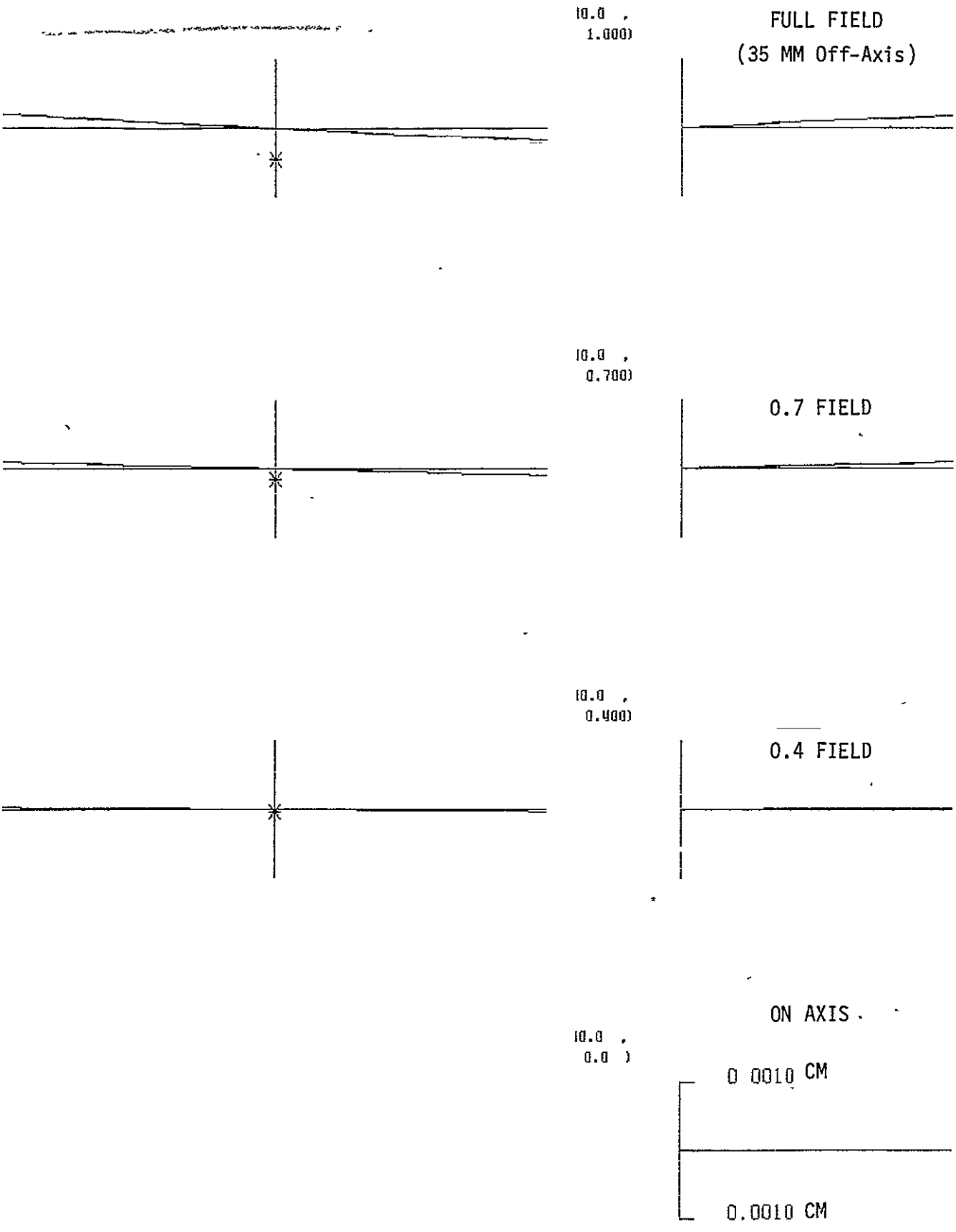

FIGURE 1.4-11

INDEX OF REFRACTION OF MAGNESIUM FLUORIDE

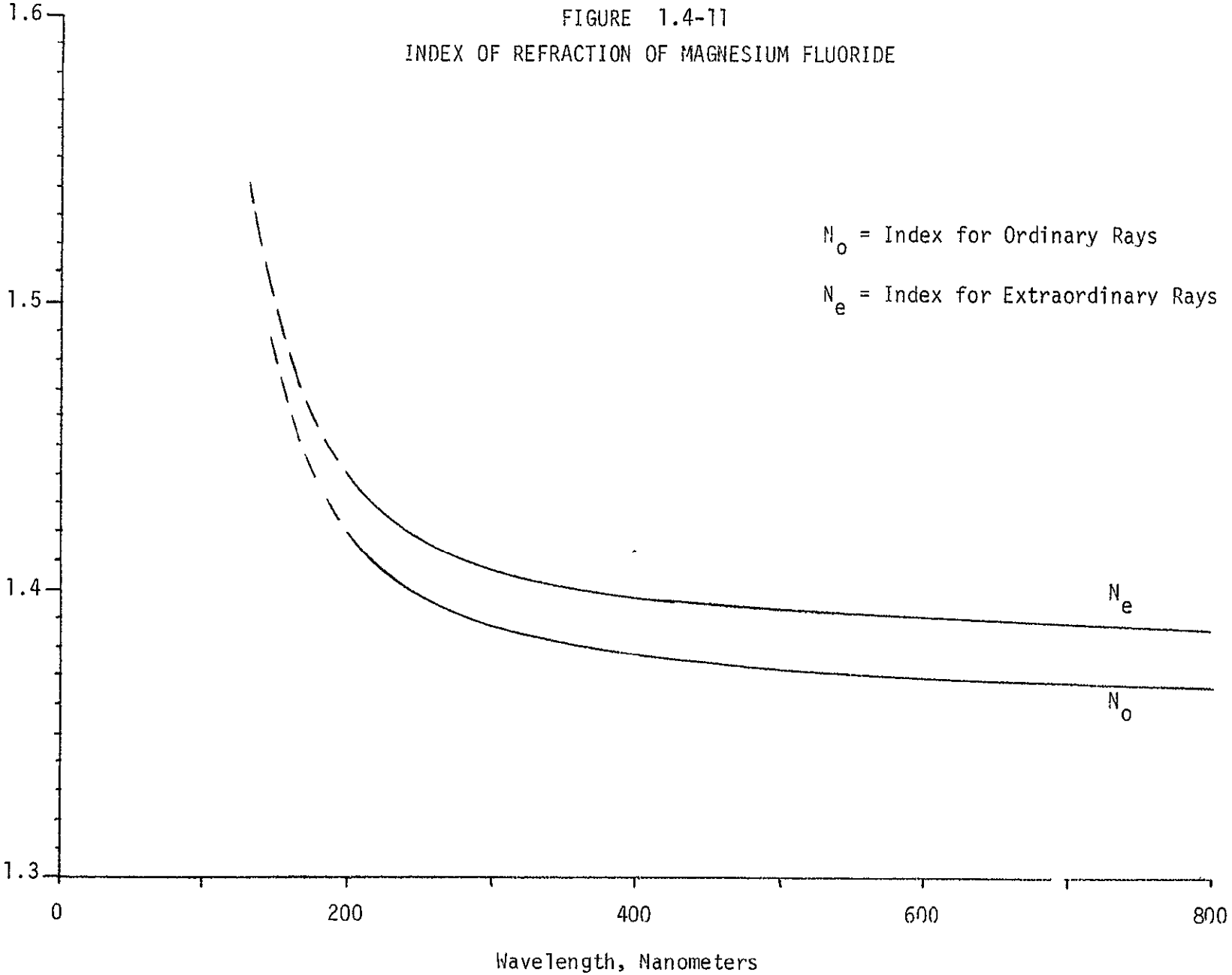

Figure 1.4-12 FACEPLATE FOR ON-AXIS CAMERA

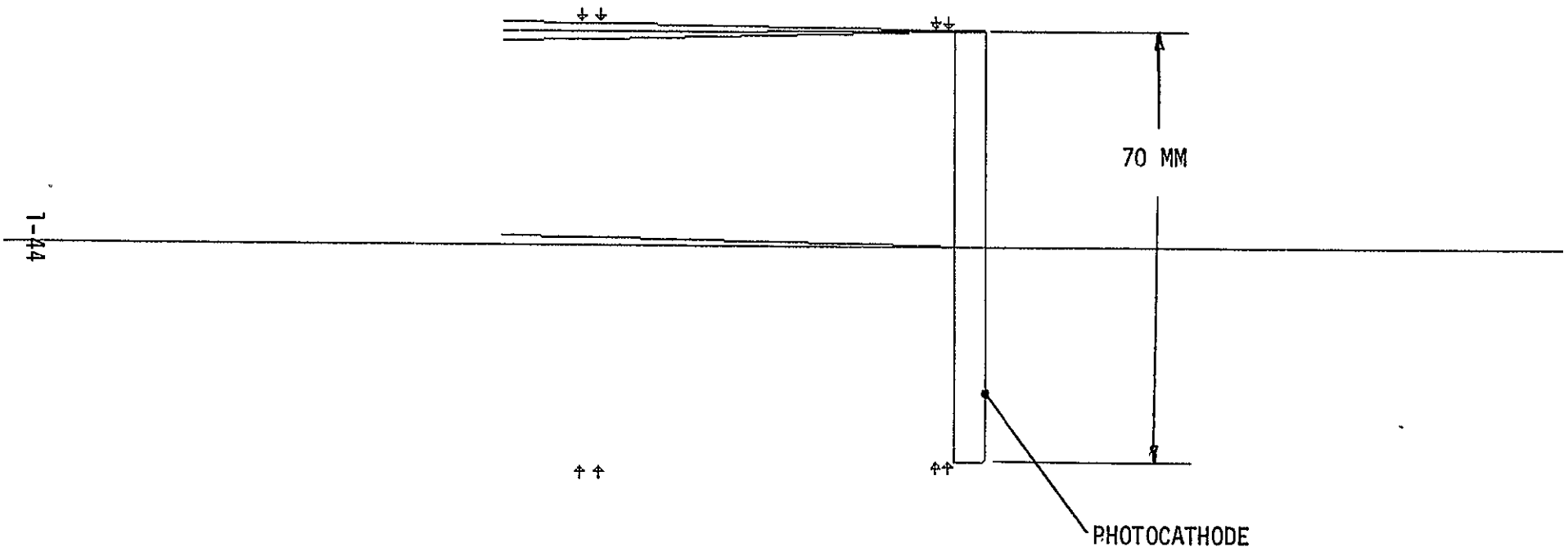

Figure 1.4-13 RAY FANS - ON-AXIS CAMERA PLANE FACEPLATE

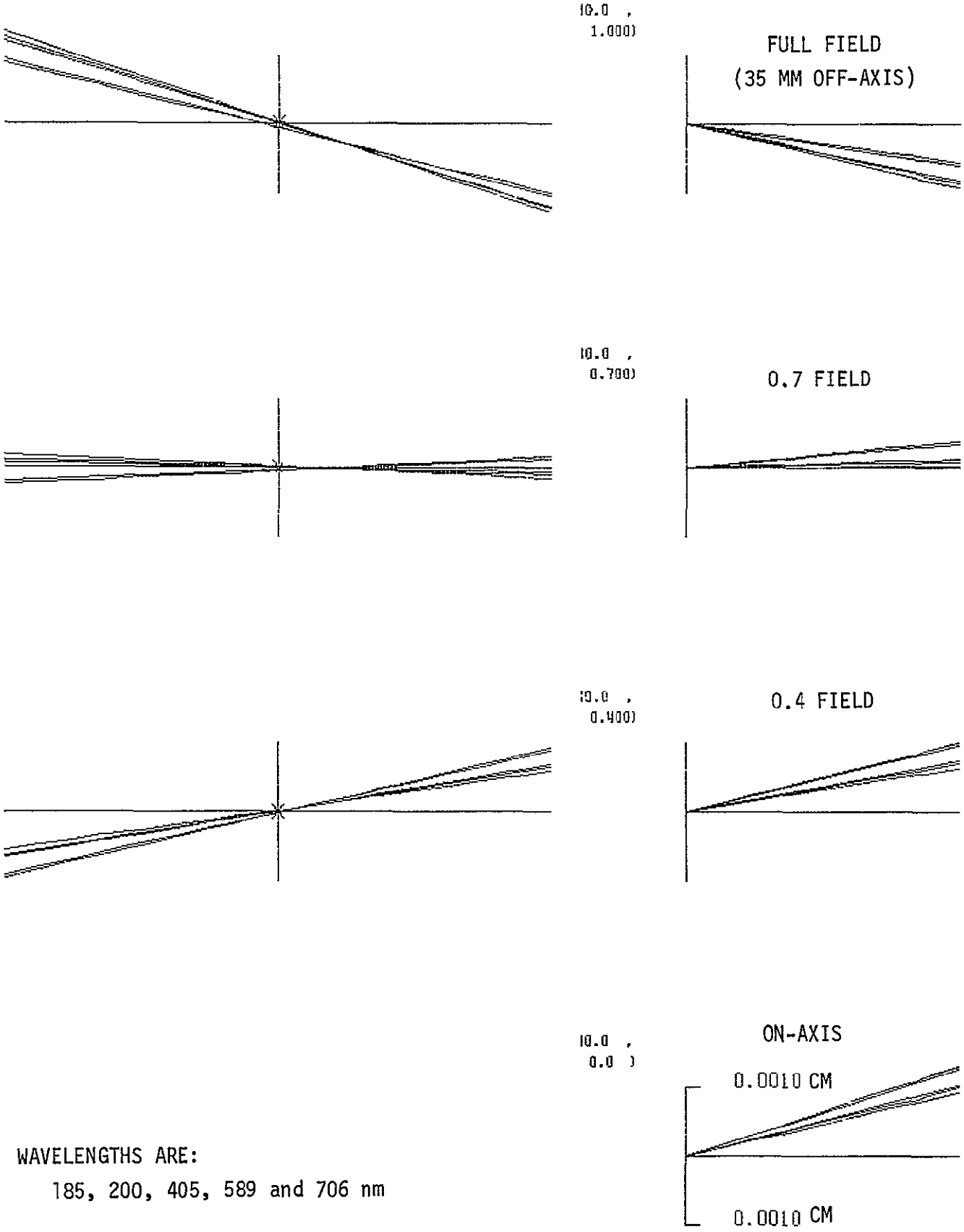


WAVELENGTHS ARE:

185, 200, 405, 589 and 706 nm

Figure 1.4-14 FIELD FLATTENER - ON-AXIS CAMERA

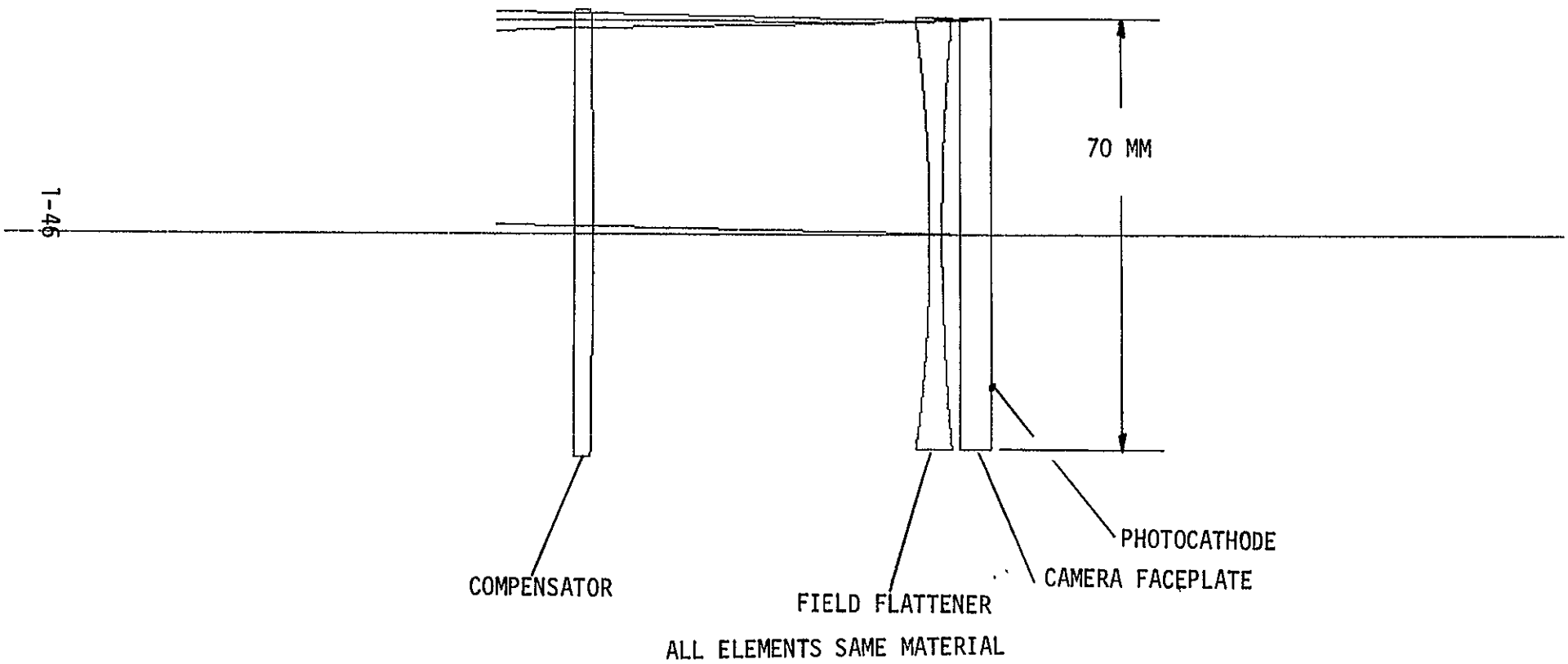

Figure 1.4-15 RAY FANS - ON-AXIS CAMERA WITH FIELD FLATTENER

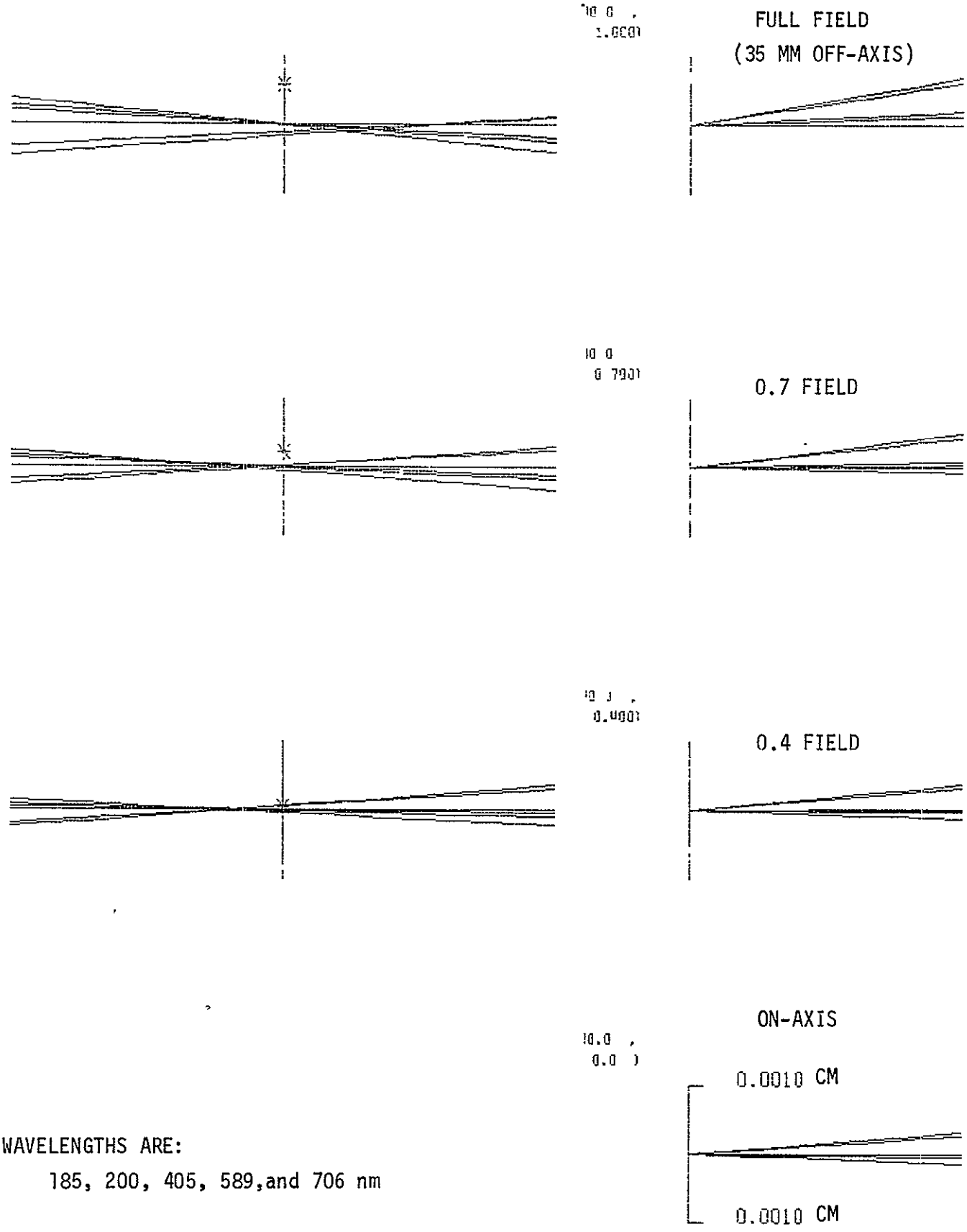


WAVELENGTHS ARE:

185, 200, 405, 589,and 706 nm

plots are given in Figure 1.4-13, which shows the effects of longitudinal chromatic aberration, defocus, and astigmatism. For these ray traces, it was assumed that the detector would be focused at its 7/10 field radius, which is why the ray intercept errors are least at that position. The longitudinal chromatic aberration arises from the system having a different optimum focus for each wavelength because of the varying optical thickness of the faceplate. For narrow band imagery, the filter thickness would be chosen to compensate for the index of refraction at that particular wavelength, and so the focus error would be minimized. For broadband imagery, the transparent material used in place of a filter would add to the chromatic aberration problem. However, even with another 5 mm of magnesium fluoride, the chromatic effect for broadband imagery still would be comparable to the defocus from field curvature, as Figure 1.4-13.

A field flattener design was generated for the on-axis configuration, as shown in Figure 1.4-14. This design requires two elements to prevent a great deal of lateral chromatic aberration from being introduced. The effect of the weak, positive element in front is to make the chief ray displacement at the photocathode equal to zero, thus eliminating lateral dispersion. Both elements are of the same material as the faceplate. The design is such that it can be built into a cell and fit within the focus coils of the camera submodule. The ray trace plots are shown in Figure 1.4-15. When these plots are compared with those of the faceplate alone, Figure 1.4-13, it is evident that although the defocus is reduced, the gain is partially offset by increased longitudinal chromatic aberration resulting from the added optical path length of refractive material. For narrow band imagery, however, the field flattener would give an image in almost perfect focus across the entire detector field.

One disadvantage of the field flattener would be a loss in throughput of about 20% resulting from reflections from the surfaces. Also, from each element, about 1% of the light from a star would be returned to the detector as a highly defocused, ghose image. The energy densities of these ghost images would be much less at the focal plane than the energy densities of the ghost images from the first surface of the faceplate however.

## 1.5 Performance Estimates

Estimated camera performance has been computed in terms of point spread function, encircled energy and modulation transfer function for on-axis and edge-of-field configurations. In predicting the performance of the edge-of-field case, a 0.1 wave rms error at 633 nm was assumed for the mirror, because even though the lens design may show nearly perfect aberration compensation, our experience to data has shown that the limit for manufacturing such a mirror, using computer generated holograms for testing, is about 0.1 wave. A summary of some of our experience with aspherics of this kind is given in Appendix A. Table 1.5-1 summarizes the optical systems analyses.

It was assumed that the camera would be focused to equalize the defocus at the center of the field to the defocus at the corners, giving an intermediate zone of best focus. The curves show results at best focus and the corners and center.

The SECO was modeled using the MTF function shown in Table 1.5-1, with 50% response to a 20 lp/mm square wave.

Table 1.5-1

BASIS OF PERFORMANCE CALCULATIONS

| | |
|---|---|
| OTA | 0.057 WAVES RMS AT 633 NM<br>0.007 ARCSEC RMS IMAGE MOTION |
| PICK-OFF MIRROR | |
| ON-AXIS | PERFECT |
| EDGE-OF-FIELD | 0.1 WAVE RMS AT 633 NM |
| FIELD CURVATURE | 1 MM DEFOCUS AT CENTER AND CORNERS<br>BEST FOCUS IN INTERMEDIATE ZONE |
| SECO | 50% RESPONSE TO 20 LP/MM SQUARE WAVE (39% TO SINE WAVE)<br>MTF ASSUMED: $\frac{1 - EXP\ (-K\nu)}{K\nu}$ |

Figures 1.5-1 and 1.5-6 show the results of the computations. Figures 1.5-1 and 1.5-2 show point spread functions computed at wavelengths of 325 and 633 nm, respectively. Figures 1.5-3 and 1.5-4 are the corresponding encircled energy functions, while Figures 1.5-5 and 1.5-6 are the corresponding modulation transfer functions. These results apply to monochromatic or narrow band imagery. The effects of the chromatic aberrations of the refractive elements will be considered separately.

For reference, Figure 1.5-7 shows the modulation transfer function of the OTA alone (with operating image motion and wavefront error) and the detector alone. It is evident from Figure 1.5-7 that at f/24, the detector characteristics are well matched to those of the OTA.

Table 1.5-2 summarizes the monochromatic performance of the alternate configurations in terms of a performance factor, Q. This represents the effective sampling area at the focal plane to be used when making signal-to noise calculations* by adding in uniformly distributed noise. It is useful in computing the capability of the system to detect faint point sources.

Figures 1.5-1 and 1.5-6 and Table 1.5-2 show that the assumed 0.1 wave rms manufacturing error of the off-axis pick-off mirror would detract significantly from the system performance, especially at 325 nm.

---

*The signal-to-noise ratio calculation is based upon a two-dimensional equivalent spatial frequency passband, $N_{e2}$, defined as

$$N^*_{e2} = \int_0^{2\pi}\int_0^{\infty} T^2(\nu, \phi)\nu \, d\nu \, d\phi$$

where T $(\nu,\phi)$ is the rotationally symmetric system Modulation Transfer Function expressed in polar coordinates $\nu$ and $\phi$. The use of an equivalent passband defined in this manner is analogous to the noise-equivalent-bandwidth used in signal processing noise calculations.

The reciprocal of $N^*_{e2}$ represents the equivalent sampling area:

$$A^*_s = \frac{1}{N^*_{e2}}$$

An image quality factor, Q, is defined for the entire electro-optics train relative to the equivalent passband of a perfect system.

$$Q = \frac{N^*_{e2}\ (\text{real})}{N^*_{e2}\ (\text{perfect})}$$

FIGURE 1.5-1

FOCAL PLANE CAMERA

POINT SPREAD FUNCTIONS AT 325 NM

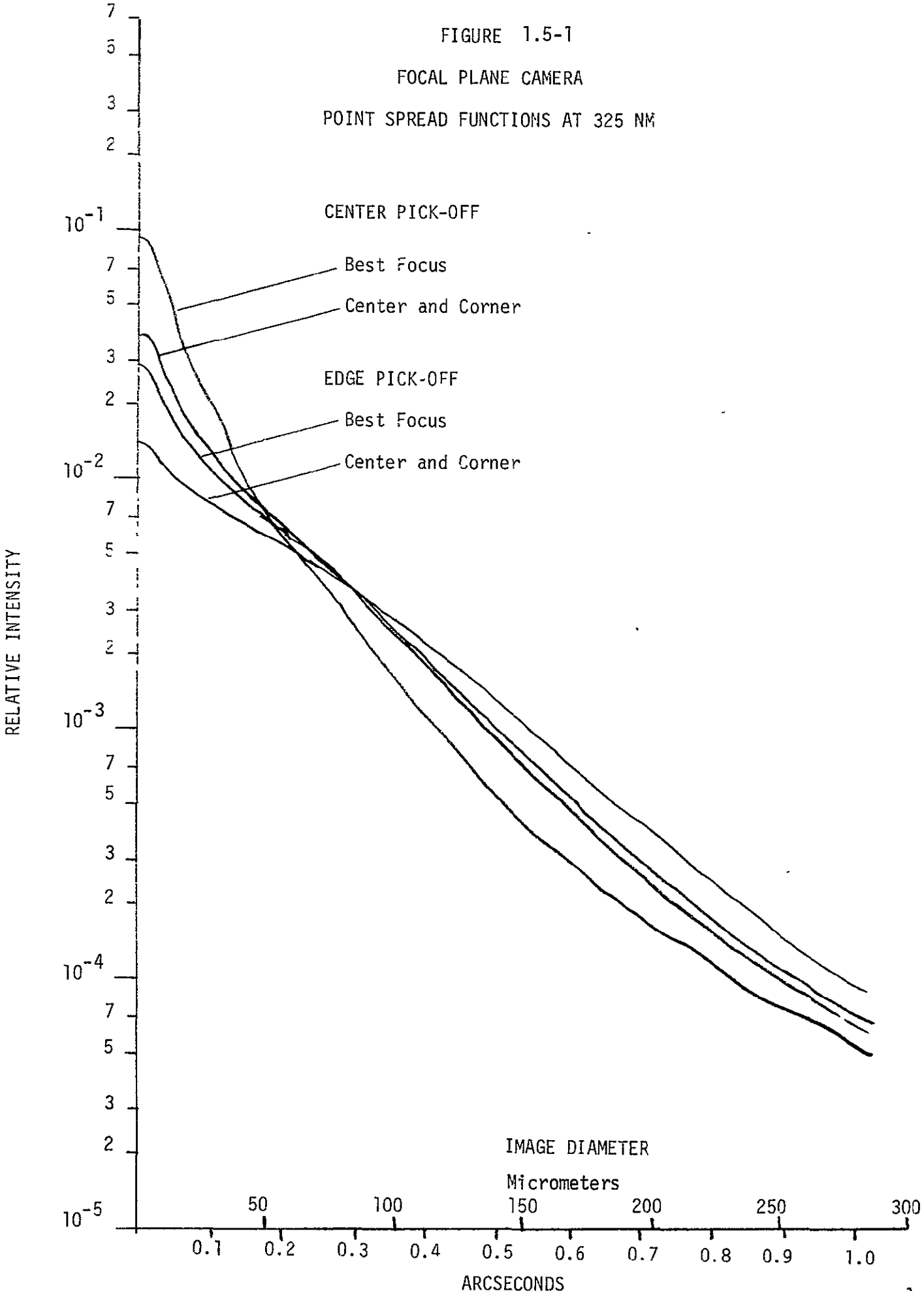

FIGURE 1.5-2
FOCAL PLANE CAMERA

POINT SPREAD FUNCTIONS AT 633 NM

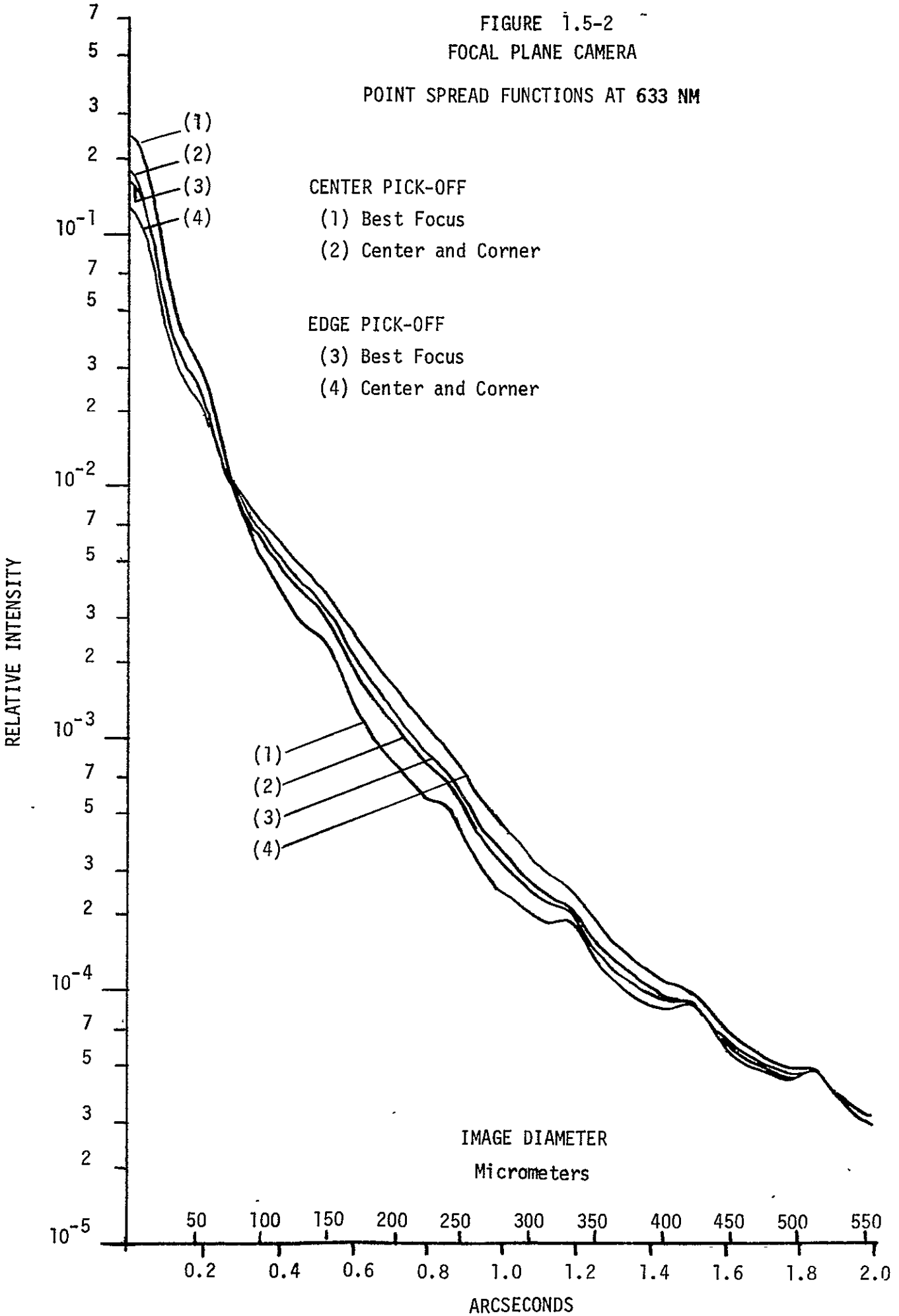

FIGURE 1.5-3

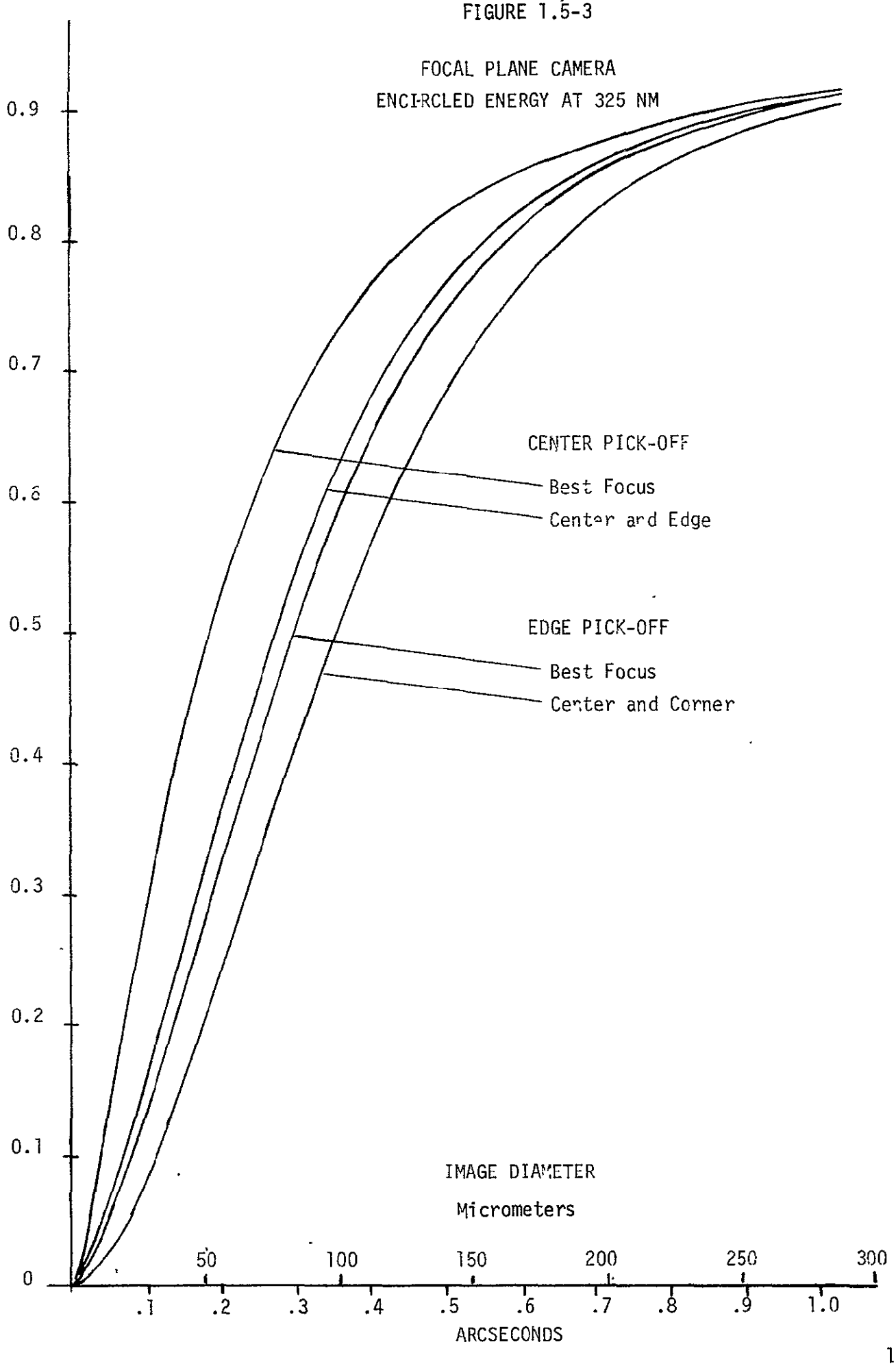
FOCAL PLANE CAMERA
ENCIRCLED ENERGY AT 325 NM
0.9
0.8
0.7
0.6
0.5
0.4
0.3
0.2
0.1
0
CENTER PICK-OFF
Best Focus
Center and Edge
EDGE PICK-OFF
Best Focus
Center and Corner
IMAGE DIAMETER
Micrometers
50
100
150
200
250
300
.1
.2
.3
.4
.5
.6
.7
.8
.9
1.0
ARCSECONDS

FIGURE 1.5-4
FOCAL PLANE CAMERA
ENCIRCLED ENERGY AT 633 NM

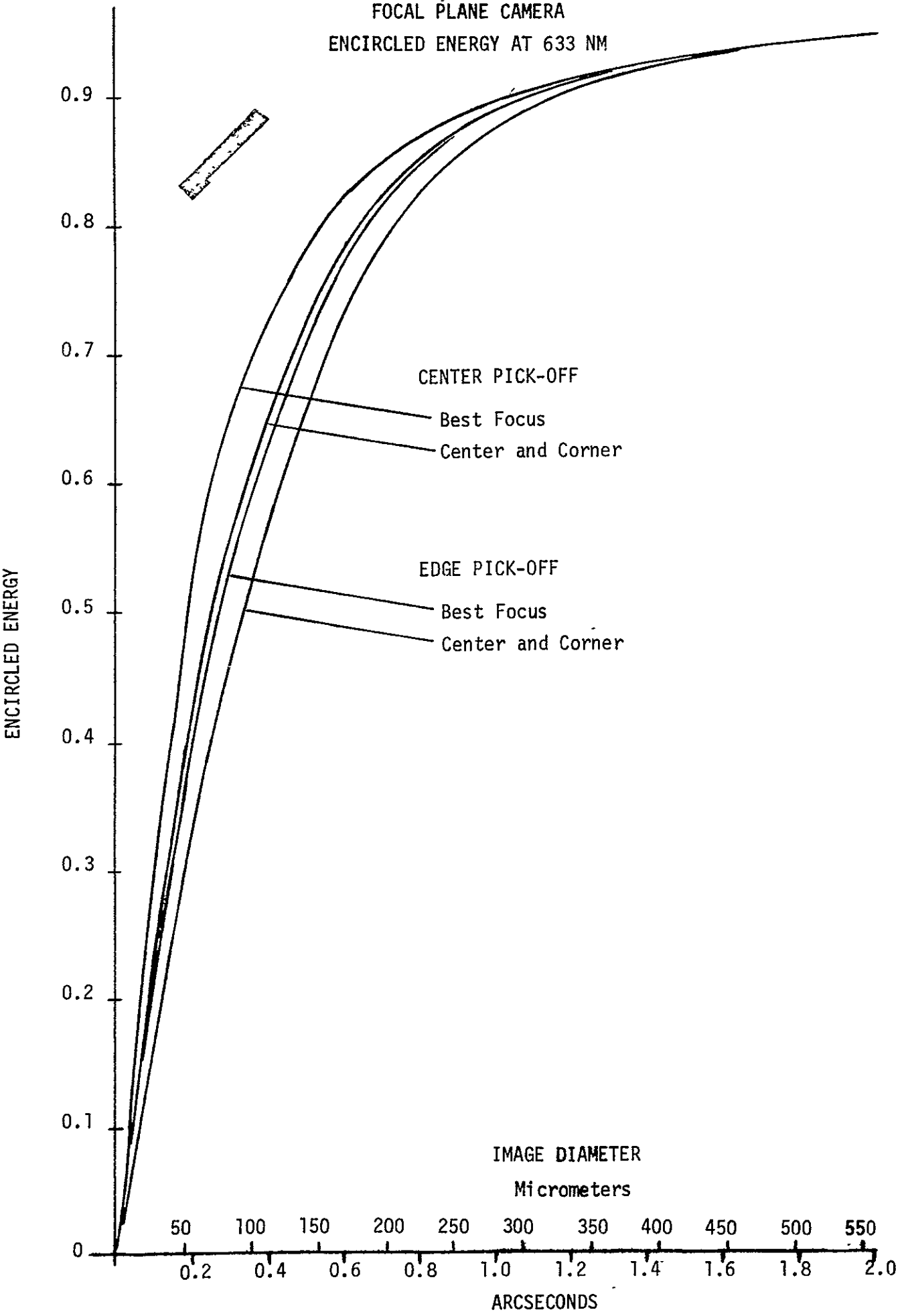

FIGURE 1.5-5

MODULATION TRANSFER FUNCTION AT 325 NM

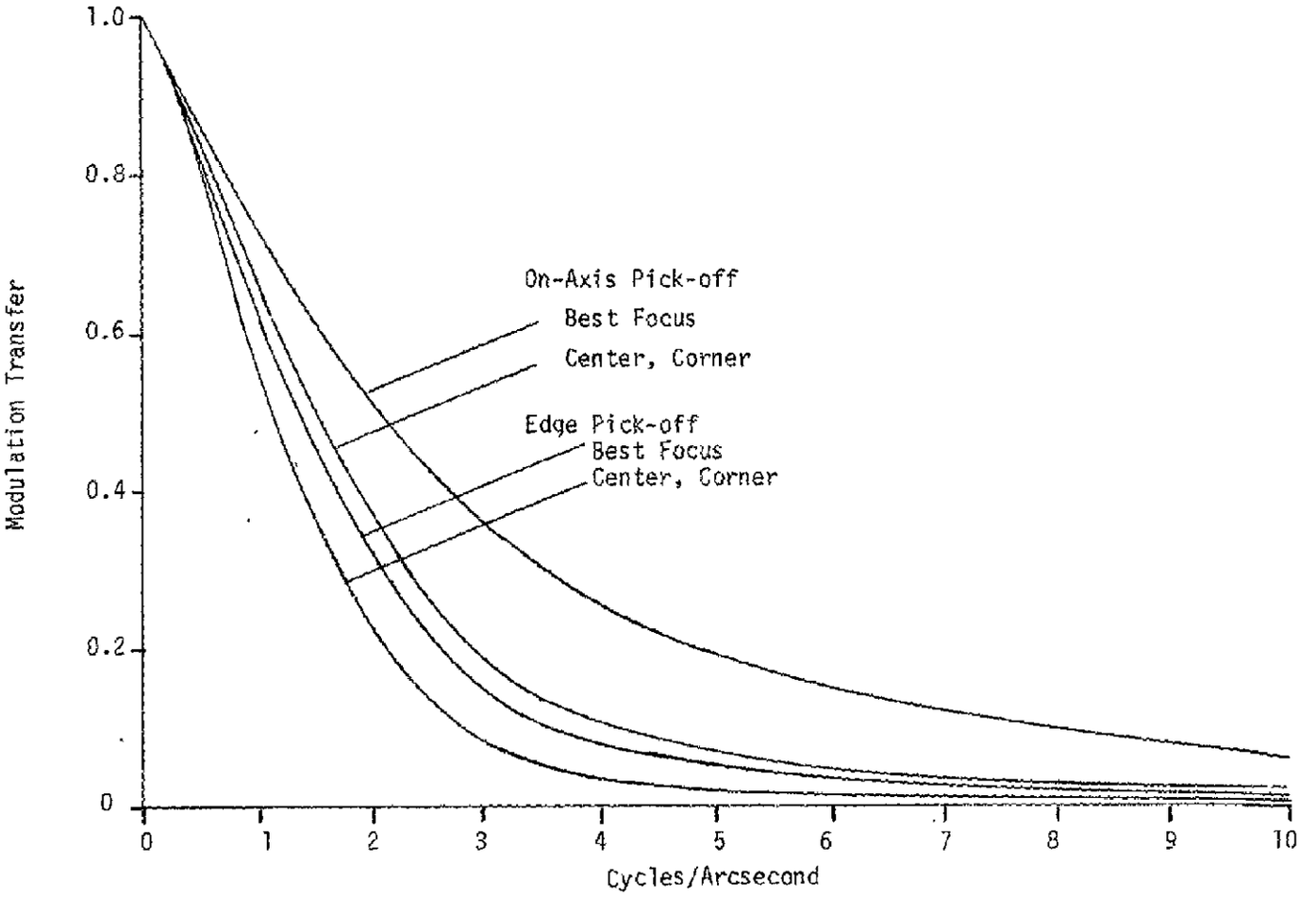

FIGURE 1.5-6

MODULATION TRANSFER FUNCTIONS AT 633 NM

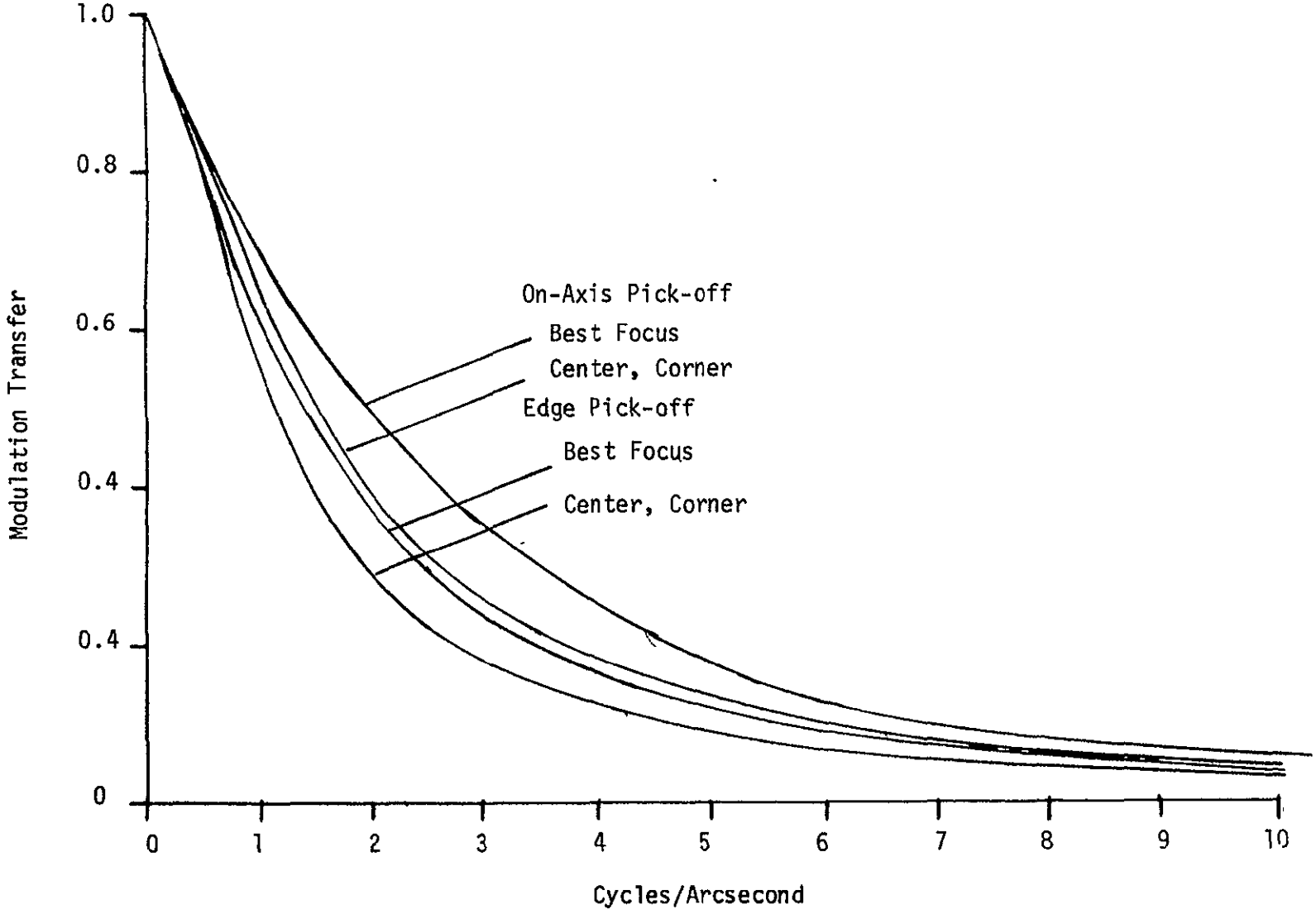

FIGURE 1.5-7

MODULATION TRANSFER FUNCTIONS OF OTA AND SECO

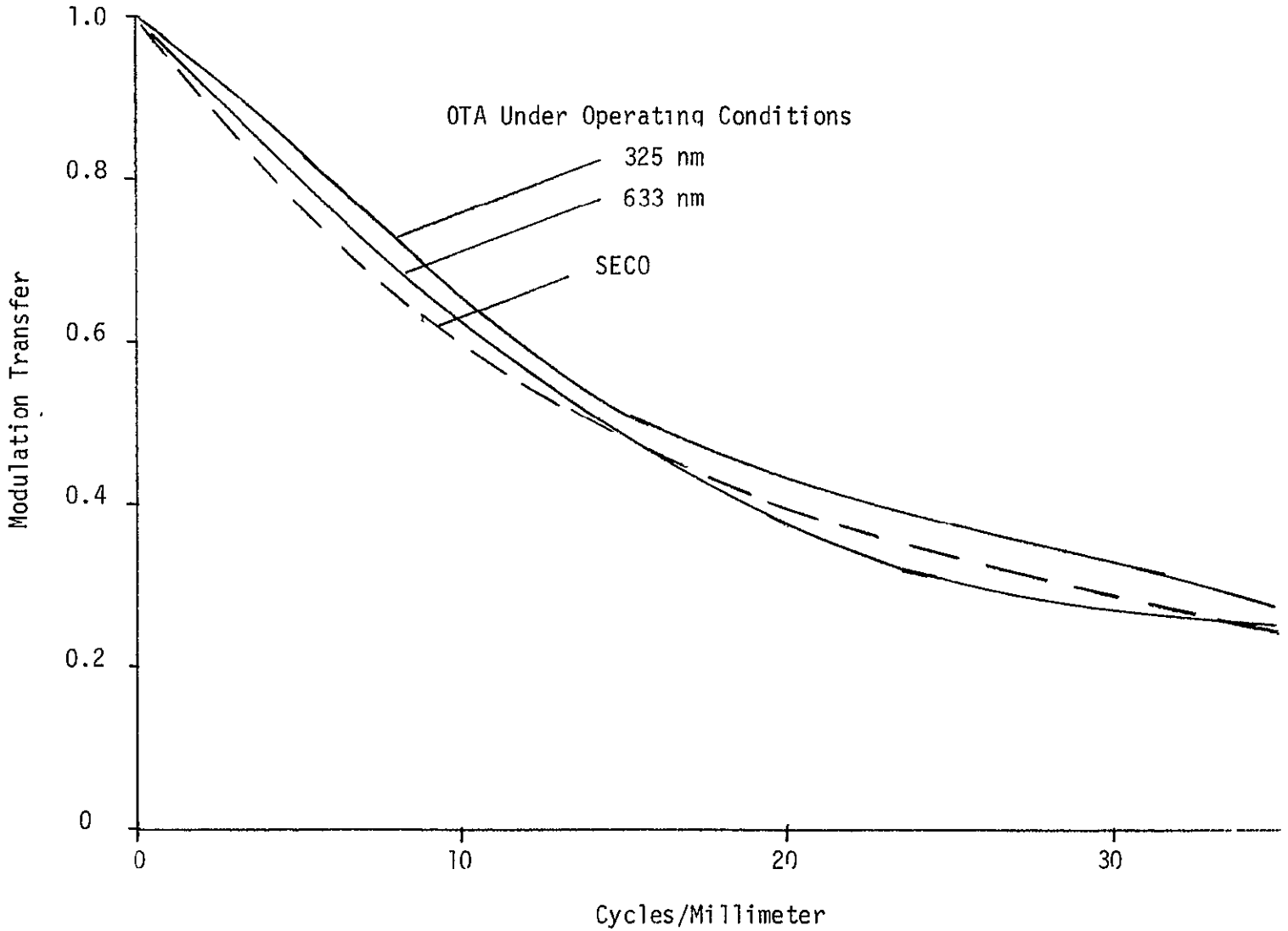

Table 1.5-2

FOCAL PLANE CAMERA PERFORMANCE SUMMARY

$$Q = \frac{\text{NOISE EQUIVALENT SAMPLING AREA FOR PERFECT SYSTEM}}{\text{NOISE EQUIVALENT SAMPLING AREA FOR ACTUAL SYSTEM*}}$$

| | 633 NM | 325 NM |
|---|---|---|
| CENTER PICK-OFF | | |
| IN FOCUS | 0.113 | 0.035 |
| CORNERS AND CENTER | 0.074 | 0.014 |
| EDGE PICK-OFF | | |
| IN FOCUS | 0.065 | 0.011 |
| CORNERS AND CENTER | 0.044 | 0.007 |

* NORMALIZED VOLUME OF THE SQUARE OF THE SYSTEM MTF.

For broadband imagery, the chromatic aberrations introduced by the refractive elements must be considered. For each of the configurations, a 5 mm thick $MgF_2$ faceplate and a 5 mm thick $MgF_2$ filter substrate are assumed. In the case of the edge-of-field configuration, the lateral dispersion of the rays as they enter the faceplate at a 23° angle from normal is much the predominant source of aberration. This would cause an image smeared out in a line. The same is true in the case of the intermediate pick-off configuration, except that the lateral chromatic aberration is not nearly as severe as in the edge-of-field case. In the on-axis case, the aberration is almost purely longitudinal, causing a circular image spread. Table 1.5-3 summarizes the chromatic effects over three bandpasses. The spot sizes for two or more of the indicated bandpasses are determined by adding together the spot sizes for the individual bandpasses. The values given are the sum of the values computed for the lateral and the longitudinal effects.

Note that in Table 1.5-3, the chromatic spot size in the on-axis configuration is larger with the field flattener than without. This is due to the extra glass thickness of the field flattener. Without the field flattener, the defocus spot size is about 20 micrometers at the center and corners of the field, so that with the field flattener there is some gain at some points in the field.

## 1.6 Trade Study

Table 1.6-1 summarizes the configurations studied and the major results. Table 1.7 compares the advantages and disadvantages with the on-axis pick-off configuration and the edge-of-field pick-off configuration. Of the configurations investigated, the on-axis configuration appears to be superior in terms of its simplicity and performance.

Three representative cases were chosen for investigation. Any number of options exist for the placement of the pick-off. Two other options might be of particular interest sometime in the future. In the first, the camera field of view would be centered 15 mm off axis so that the pick-off mirror would obscure the field of two of the axial instruments close to the optical axis, but would leave the other two unobscured. The second option would place the pick-off mirror so that it would block the best part of the field for one axial position, but would leave the other three unobscured. The data presented here should be sufficient to permit valid judgments of the merits of such options at a later time.

Table 1.5-3

EFFECTS OF CHROMATIC DISPERSION IN REFRACTIVE ELEMENTS

| PICK-OFF MIRROR POSITION | SPOT SIZE, MICROMETERS (CHROMATIC EFFECT ONLY) 150-200 NM | 200-350 NM | 350-800 NM |
|---|---|---|---|
| EDGE-OF-FIELD WITH FILTER | 67 | 44 | 18 |
| INTERMEDIATE WITH FILTER | 27 | 18 | 7 |
| ON-AXIS WITH FILTER | 9 | 6 | 2 |
| ON-AXIS WITH FIELD FLATTENER AND FILTER | 16 | 11 | 4 |

Table 1.6-1

FOCAL PLANE CAMERA CONFIGURATION STUDY

| | ON-AXIS PICK-OFF | | INTERMEDIATE | | EDGE-OF-FIELD | |
|---|---|---|---|---|---|---|
| | PRESENT SECO | PM SECO | PRESENT SECO | PM SECO | PRESENT SECO | PM SECO |
| Configuration | OK | Redesign of Focal Plane Structure Required | OK | Ray Interference with PM Assembly | OK | Ray Interference with PM Assembly |
| Maintainability | Replaceable on Orbit | Replaceable on Orbit | Replaceable on Orbit | | Replaceable on Orbit | |
| Focal Plane Vignetting | 60 mm Radius | 63 mm Radius | Off-Axis Vignetted Area for Two Instruments. | | 5 mm Outer Edge-of-Field | |
| Heat Dissipation (Hot Case) | Module Wall 14°C avg. | Module Wall 14°C avg. | Module Wall 14°C avg. | | Module Wall 14°C avg. | |
| Optical Degradation | Minimal | Minimal | < 0.1 Wave RMS Manufacturing Error | | 0.1 Wave RMS Manufacturing Error | |

Table 1.6-2

FOCAL PLANE CAMERA

ON-AXIS VS. EDGE-OF-FIELD PICK-OFF

| | ON-AXIS | EDGE-OF-FIELD |
|---|---|---|
| ADVANTAGES | • PLANE MIRROR.<br>• LIGHT NORMAL TO FACEPLATE<br>• SIMPLE FIELD FLATTENER POSSIBLE<br>• USEABLE WITH PM FOCUS (REDESIGNED STRUCTURE)<br>• BETTER OVERALL PERFORMANCE | • NO INTERFERENCE WITH AXIAL INSTRUMENT FIELD<br>• POTENTIAL FOR LARGER-FORMAT DETECTOR |
| DISADVANTAGES | • SPECTROGRAPH SLITS MUST BE FARTHER OFF-AXIS | • HIGHLY ASPHERIC SURFACE 0.1 WAVE RMS MGF ERROR<br>• LIGHT NOT NORMAL TO FACE-PLATE LATERAL COLOR 75 m MAX<br>• COMPLEX FIELD FLATTENER<br>• POORER OVERALL PERFORMANCE |
| RECOMMENDATION | • ON-AXIS, PROVIDED SIGNIFICANT PROBLEMS IN THE SPECTRO-GRAPH DO NOT ARISE. | |

## 2.0 PRELIMINARY DESIGN

The results and conclusions of the trade study (Section 1) were submitted to the HRC IDT leader, Dr. R. E. Danielson, and to NASA. Subsequent to that submission, direction was received from NASA to proceed with the preliminary design of the focal plane camera in a radial module. Specifically, the focal plane camera was to be designed with an integral on-axis pick-off mirror using the standard SECO, and must be replaceable on orbit. This section details the resulting preliminary design in the technical areas that are critical to instrument feasibility and manufacturability.

### 2.1 Instrument Characteristics

The required instrument characteristics of the focal plane camera are listed in Table 2.1-1. These requirements are extracted from LST Scientific Instrument Requirements for Preliminary Design, Revised 15 April 1975, as amended by Addendum Number 1, 1 August 1975. Supplemental requirements were extracted from the Final Instrument Definition, LST High Resolution Cameras, 20 May 1974.

The focal plane camera is designed to be used in two general scientific areas. First is the area of imaging faint extended and point sources, and second is the area of search and survey work. For the latter area, a serendipitous mode has been considered in the design.

### 2.2 Design Overview

The focal plane camera uses the standard SECO submodule as its detector directly at the ST focal plane. However, the large volume required by the SECO submodule and the associated filter mechanism would preclude access by the other science instruments to that portion of the focal plane possessing high image quality. Therefore, the focal plane camera design incorporates an integral on-axis pick-off mirror to fold the central portion at the focal plane to one side where the SECO submodule is precisely located to avoid observation at the other instruments' entrance apertures.

In order that the camera passes a wide dynamic range and high signal-to-noise ratio at the video output, the photocathode of the SEC detector is cooled to 270°K. The cooling is accomplished by thermo-electric coolers which pump the heat from the detector bottle to the center shell at the detector submodule.

A filter mechanism consisting of four coaxial eight-position wheels is included in the design to provide a capability for up to 28 filters.

Exposure control can be accomplished electronically by gating voltages on/off in the electron imaging section of the detector. This technique is used with image intensifiers range gating applications in which the switching times must be extremely short. For ST, the switching time is relatively long, consistent with a $10^{-2}$ second exposure. The use of electronic exposure control appears to be preferable to the introduction of a precision mechanical shutter with its reliability questions. A capping shutter has been included for detector protection. This capping shutter is also used in the calibration modes.

TABLE 2.1-1

INSTRUMENT CHARACTERISTICS

| | |
|---|---|
| DETECTOR | SEC ORTHICON |
| Photocathode | S-20 |
| Window | $MgF_2$ |
| Cooling | 270°K |
| Data Format | 50 x 50mm (NOM) |
| Resolution | 20 Lp/MM at 50% MTF |
| ACQUISITION | Spacecraft |
| STABILITY | ±.03 Arcsec. |
| CALIBRATION | |
| Internal | Hi Pressure Hydrogen Tungsten Lamp |
| External | Standard Stars |
| FIELD OF VIEW | 3 x 3 Arcmin. |
| Positional Accuracy | 1 Arcsec. |
| ANGULAR RESOLUTION | 0.2 Arcsec. |
| RANGE | 115 - 800 NM |
| EXPOSURE TIME | 10 Msec. - 10 Hours |
| FILTERS | 23 |
| DYNAMIC RANGE | 1.5 $m_v$ to 23 $m_v$/arcsec$^2$ |

The calibration optics are mounted on the capping shutter so that no additional moving parts are required for calibration. Calibration is accomplished by uniformly flooding the photocathode at the detector with light from either a standard star or an internal light source.

The internal light sources also operates as an erase lamp during the prepare mode.

Table 2.2-1 summarizes the salient features of the Itek design.

## 2.3 Details of Focal Plane Camera Design

### 2.3.1 Space Envelope

Figure 2.3.1-1 shows conceptually the envelope requirement of the camera in relation to the existing OTA design. The minimum SI compartment wall radius required for removal of the instrument on-orbit is indicated (84 inches versus present 78-inch minimum). The removal path is shown in phantom. If a radial recess door were located in the SI compartment wall, then the instrument would fit within the present 78-inch radius.

### 2.3.2 Structure

Goals - The goals of the structural design were to provide a package that fits within the available space, to provide stable registration with the focal plane assembly over long periods of time, to dissipate heat from the camera submodule, and to support the pick-off mirror.

Concept - The concept devised to meet these goals was a dual bulkhead system, as illustrated in Figure 2.3.2-1. To explain the concept we begin with the module interface bulkhead. This is a temperature-controlled, invar bulkhead mounted to the focal plane assembly. It provides accurate registration of critical components. The mirror mounting structure is attached to this bulkhead, and the position of the camera submodule is controlled relative to this bulkhead. The idea is to provide for maximum image stability on the detector surface for a long period of time ($\sim$ hours).

Immediately behind the module interface bulkhead is the detector mounting bulkhead. This is made from aluminum and the camera submodule is actually mounted to this bulkhead to provide a good heat conduction path away from the camera submodule. This bulkhead is flexure mounted to the module interface bulkhead to provide registration between the detector and the module interface bulkhead, yet allow for differential thermal expansion without distortion of the module interface bulkhead and without decenter or defocus of the camera submodule. To the detector mounting bulkhead is attached the outer framework and skin of the module, so that heat may be conducted to the skin and then radiated out from the module.

Design Layout - Figure 2.3.2-2 shows the design layout evolved from this concept. The module interface bulkhead is called out in the drawing. The detector mounting bulkhead is attached to the module interface bulkhead by a set of three-axial and three-radial flexures.

TABLE 2.2-1

FOCAL PLANE CAMERA FEATURES

On-axis Pick-off Mirror

50- x 50-Millimeter Field

SEC Orthicon Detector

Photocathode Cooled to 270°K

21 Filters in Three-Wheel Assembly

Capping Shutter

Photocathode Calibration System with No Additional Moving Parts

Calibration with Standard Start

Calibration with Internal Sources

Electronic Exposure Control

Average Power - 97 Watts

Weight - 310 Pounds

FIGURE 2.3.1-1

FOCAL PLANE CAMERA IN OTA

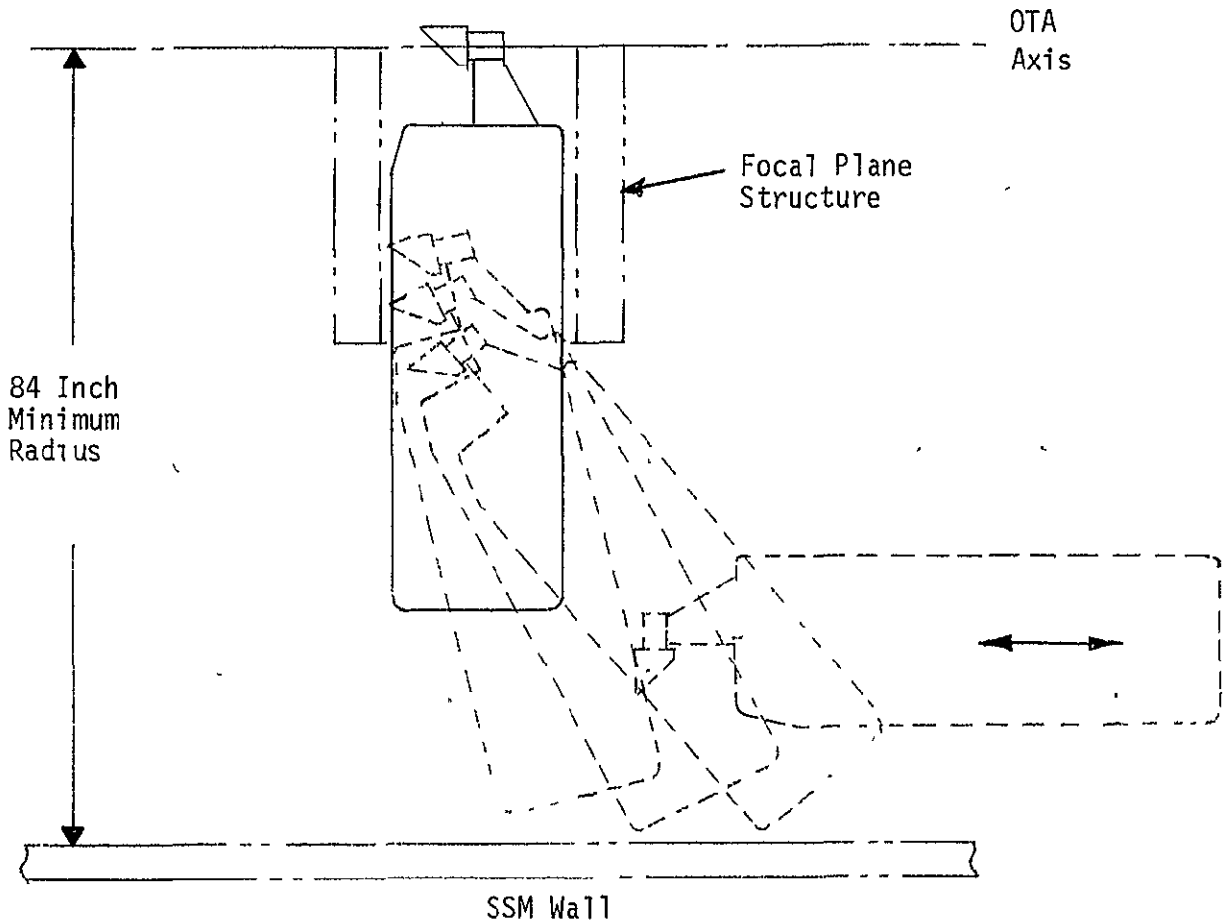

FIGURE 2.3.2-1
STRUCTURE CONCEPT

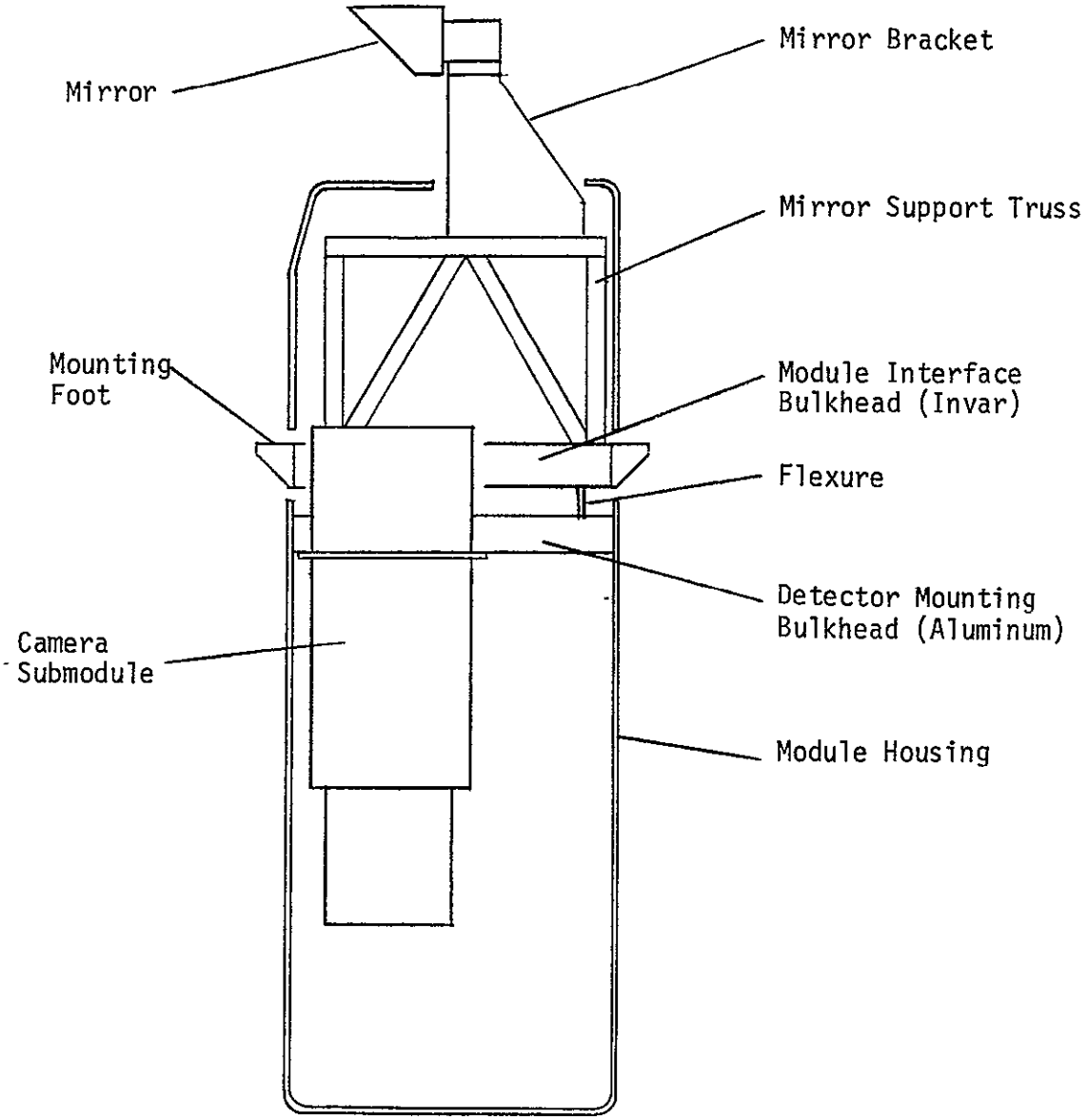

FIGURE 2.3.2.2

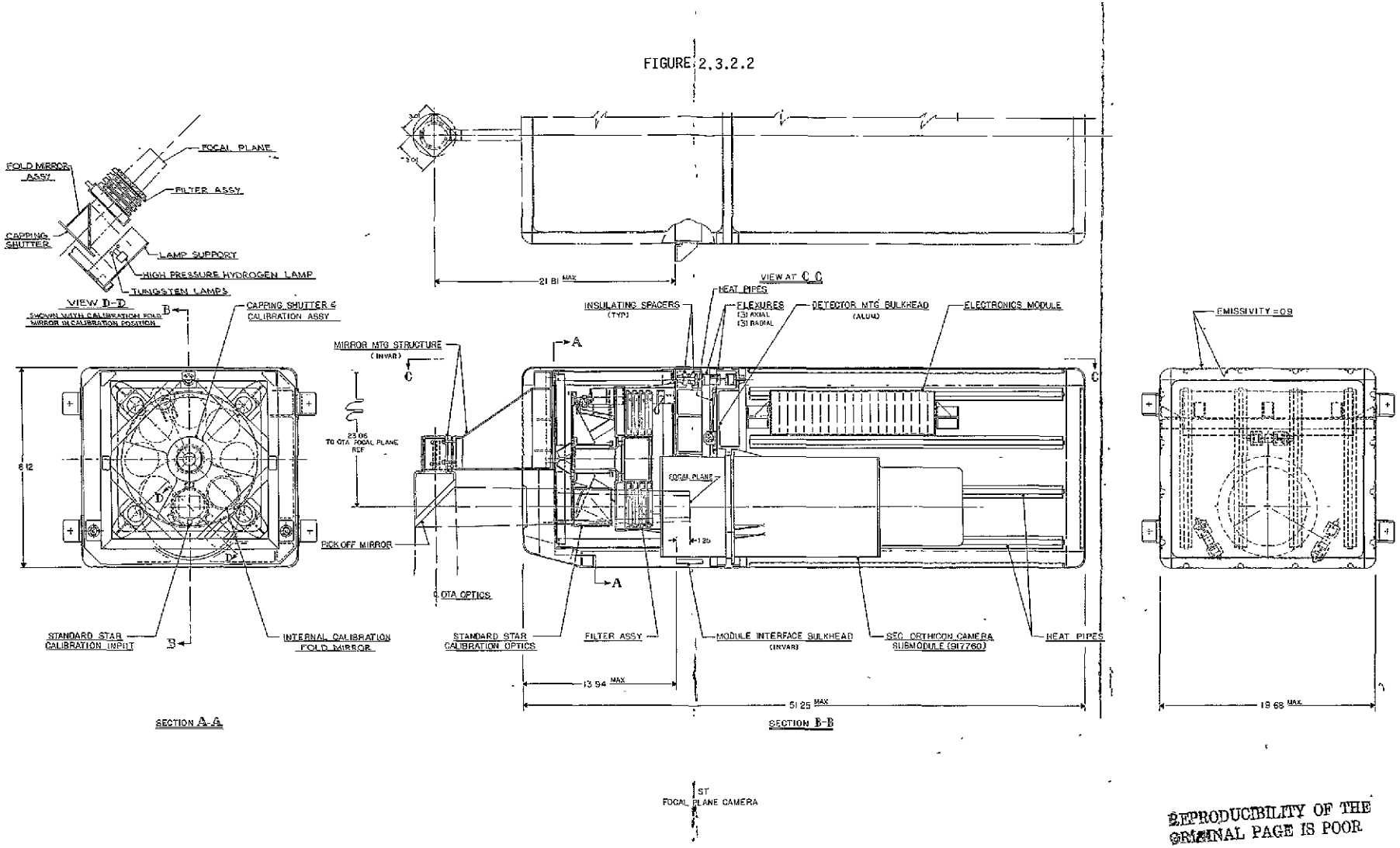




FOLDOUT FRAME 2

FOLDOUT FRAME 1



A31254-1

The axial flexures are aluminum, mounted to the module interface bulkhead through insulating spacers so that the flexures will track the temperature of the detector and the detector mounting bulkhead. The point of attachment at the module interface bulkhead is coplanar with the focal plane of the detector. By this arrangement, focus will be maintained despite temperature changes in the detector and the detector mounting bulkhead.

The radial flexures prevent rotation and decenter of the two bulkheads relative to each other. They are centered around and close to the detector so that the detector will maintain a stable center with respect to the module interface bulkhead. The flexures are invar, with insulating spacers at the detector mounting bulkhead attachment, so that they track the controlled temperature of the module interface bulkhead.

The aluminum frame and skin of the module are attached to the detector mounting bulkhead to provide a good conductive path between the detector and the outside radiating surface of the module. The module skin makes no direct contact with the module interface bulkhead, so that no thermal stresses are put into the module interface bulkhead to distort it or the focal plane assembly to which it is mounted. This is critical because distortion of the module interface bulkhead might cause bending which would move the pick-off mirror cantilevered from the module interface bulkhead, thus causing image motion.

The pick-off mirror is supported from the module interface bulkhead by the mirror mounting structure, which is shown in perspective in Figure 2.3.2-3. It consists of an invar trusswork welded together from angles and annealed. This trusswork provides a mounting stage above the level of the filter wheels and capping shutter. To this stage is attached the mirror support arm, an invar box structure gusseted to the mount points on the truss.

The mirror adjustment means are shown in the layout, Figure 2.3.2-2. Provision is made for rotating the mirror about the OTA axis, tipping it in one direction normal to the OTA axis, and in-out adjustment along the OTA axis. The tipping and in-out motions are controlled by shims.

### 2.3.3 Thermal Control

The thermal control design primarily performs three functions. The module interface bulkhead is controlled to 21°C $\pm$ .5°C. SECO submodule dissipated heat is transferred to the module walls by conduction through the detector mounting bulkhead. Electronics package dissipated heat is transferred to one module wall by conduction.

Thermal control of the module interface bulkhead is provided by thermostatically controlled heaters mounted to it. This bulkhead will have a low emissivity coating and multilayer insulation to minimize heat transfer. The pick-off mirror must also be controlled to 21°C $\pm$5°C. This is accomplished by radiation and conduction from the invar bulkhead and radiation from the inside of the focal plane structure. Thermal isolation from the inside of the module housing is achieved with a low-emissivity coating, such as black nickel ($\alpha$ = .9, $\varepsilon$ = .06), inside the housing in the forward end. Further isolation will be provided by an intermediate shroud with heaters if more detailed analysis shows it to be necessary.

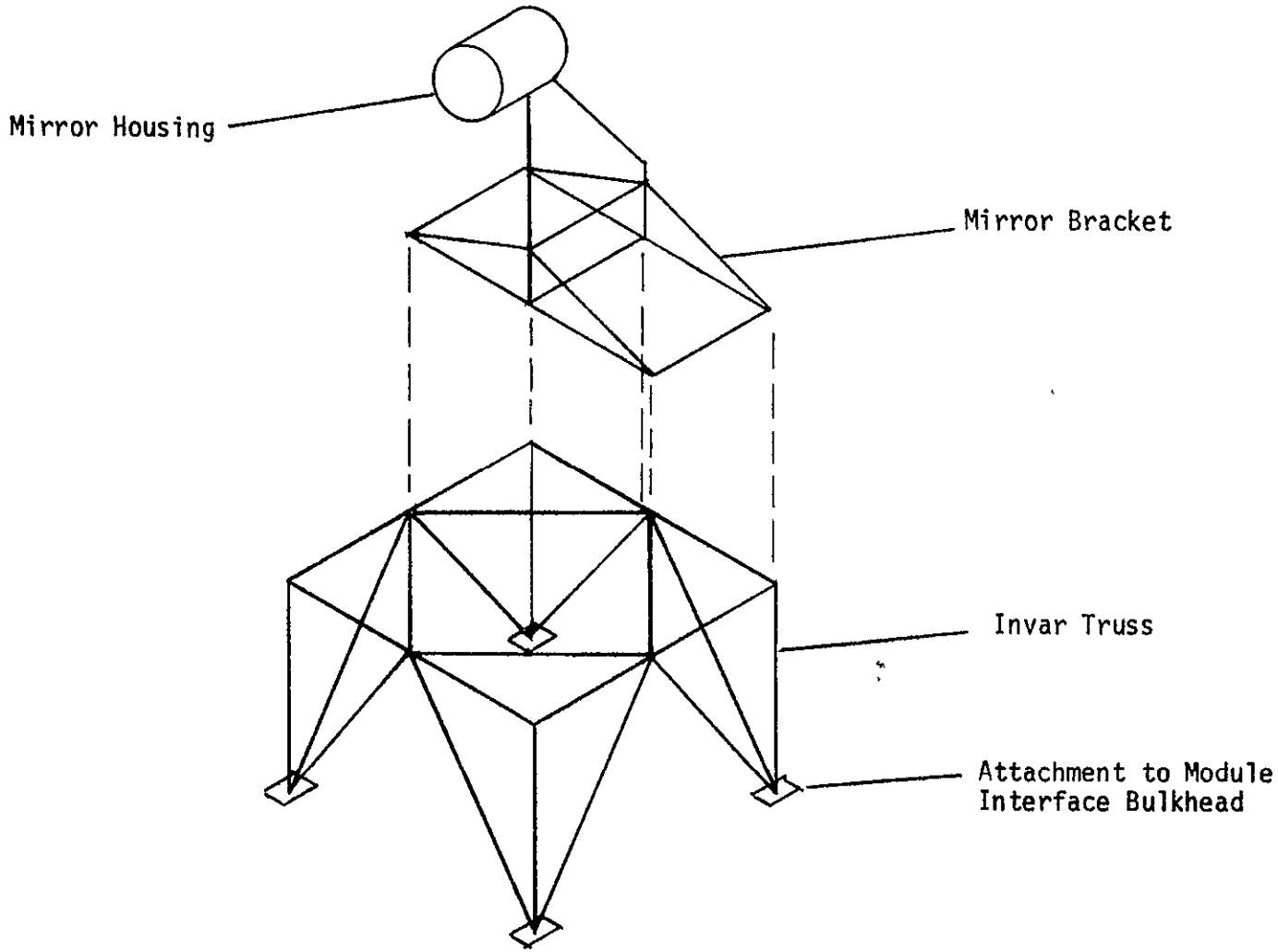


FIGURE 2.3.2-3

MIRROR SUPPORT STRUCTURE

The heat dissipated within the SECO submodule must be transferred to the radial module walls to limit the submodule tmeperature to 30°C. The 30°C limit is imposed to keep SECO cooling power within reasonable limits (see Section 2.4.3). In the hot case, the radial module walls run at an average temperature of 14°C providing insufficient $\Delta T$ for radiative heat transfer. The heat transfer is then accomplished by conduction through the detector mounting bulkhead. Heat pipes on the bulkhead and the module walls are employed to improve the conductivity. The bulkhead heatpipes are arranged circumferentially around the inner and outer edges and radially from the SECO submodule out to the edge as shown in Figure 2.3.3-1.

The module interface bulkhead and the detector mounting bulkhead which experience different average temperatures are thermally isolated from each other. Three aluminum axial flexures are mounted to the module interface bulkhead through insulating spacers so that they will track the temperature changes in the detector. Three invar radial flexures are mounted to the detector mounting bulkhead through insulating spacers so that they will track the temperature of the module interface bulkhead and prevent rotation and decenter of the two bulkheads to each other.

The thermal design of the detector mounting bulkhead must preclude the existence of thermal gradients across the bulkhead. A 1°C gradient across the 12-inch diameter circle that the flexures lie on would effect a decenter on the order of 2 micrometers (0.0072 arcsecond object angle). The circumferential heat pipes on the bulkhead limit such a gradient to a fraction of a degree. Therefore, the thermal decentering is predicted to be 0.001 to 0.002 arcseconds object angle, which is small compared to the 0.007 arcsecond stabilization and negligible compared to the 0.03 arcsecond pointing requirement for the Focal Plane Camera.

The heat from the electronics module is dissipated mostly from one of the side panels. This panel is conductively insulated from the rest of the module by a non-metallic gasket and has a low-emissivity coating on the inside for radiative isolation. As a result, this panel will run at a somewhat lower temperature. This division of the heat dissipation makes the job of the thermoelectric coolers in the camera submodule easier.

Thermal Analysis

A 21 mode thermal model of the radial focal plane camera module was compiled in order to calculate boundary conditions for the image tube. The model contained 138 radiation connections and 26 thermal resistances. It was assumed that the image tube dissipated 42 watts of total thermal power and that the electronics package dissipated 108 watts of power. Panel nodes were tied together with heat pipe conductors in order to more uniformly distribute the heat conducted from the image tube. Heat pipe performance was taken from the Heat Pipe Design Manual of the Dynatherm Corporation. The heat pipe parameters are as follows:

FIGURE 2.3.3-1

HEAT PIPES ON DETECTOR MOUNTING BULKHEAD

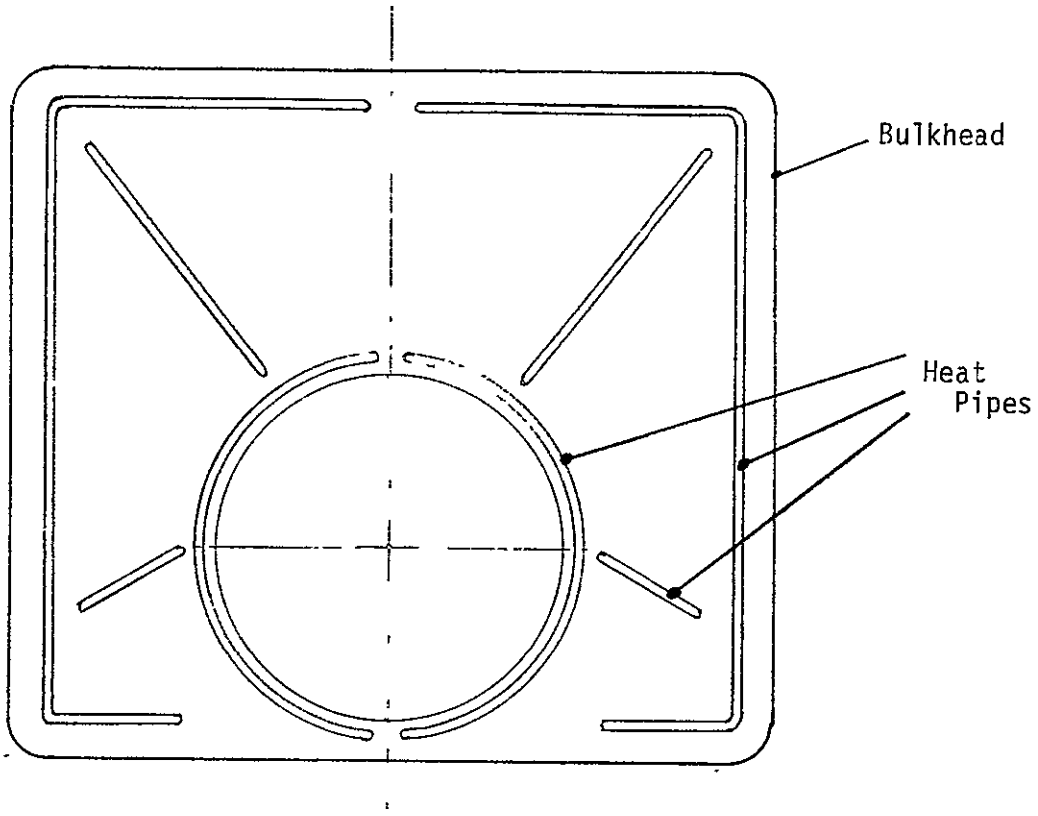

| | | |
|---|---|---|
| Outside Diameter | - | 1/2 inch |
| Length | - | to 40 inches |
| Material | - | aluminum alloy/s.s. wick |
| Working Fluid | - | ammonia |
| Wick | - | slab, circumferential, grooved |
| QL max | - | 100 watt meters |
| Conductance | - | 10 watt/°K |

The model assumed that the electronics package would be conductively tied to a single panel so that its thermal load would be dissipated independently of that of the image tube. This panel is insulated from the rest of the structure by an insulating gasket, assumed to be 1/4 x 1/4 inch rubber for the analysis.

The model was run until it reached steady-state. Figure 2.3.3-2 shows the temperature data resulting from the model. An interpretation of the data shows that the conductive structure temperature for the image tube is 19°C. The module panels which dissipate the heat from the image tube run at 11°C, while the panel which dissipates the heat from the electronics runs at about 38°C in the hot case.

## 2.3.4 Filter Assembly

The filter assembly requires four filter wheels stacked up immediately in front of the camera submodule. Each wheel has eight positions.

Each filter wheel is indexed by a stepper motor, similar to Clifton Indistries Model MSA 15-AS-1 permanent magnet two-phase stepper with 90° rotation per step. Each wheel has a rotary inertia of about 41 lbm $in^2$, or 120,000 gm $cm^2$. The stepper can drive this load through a 200:1 reduction at a rate of 50 pulses/second. One hundred steps are required to move one filter position.

The stepper motor has a winding resistance of 150 ohms. At 28 volts, assuming a 50% duty cycle for the pulses, the motor dissipates an average 2.6 watts. The motor has dual windings for increased reliability.

Figure 2.3.4-1 is a schematic of the drive system for each wheel.

A possible filter complement for the field camera from the HRC FID is shown in Table 2.3.4-1. There are 23 elements in all, up to 7 per wheel. The eighth position on each wheel is open. There is no provision for focusing within the camera, and so all filters must have the same optical path thickness. In general, each filter will have a thickness that will optimize the focus for its particular passband, taking into account the refractive properties of the image tube faceplate.

Figure 2.3.4-2 shows the dynamic disturbances to the ST from operation of a filter wheel.

FIGURE 2.3.3-2

THERMAL MODEL - FOCAL PLANE CAMERA

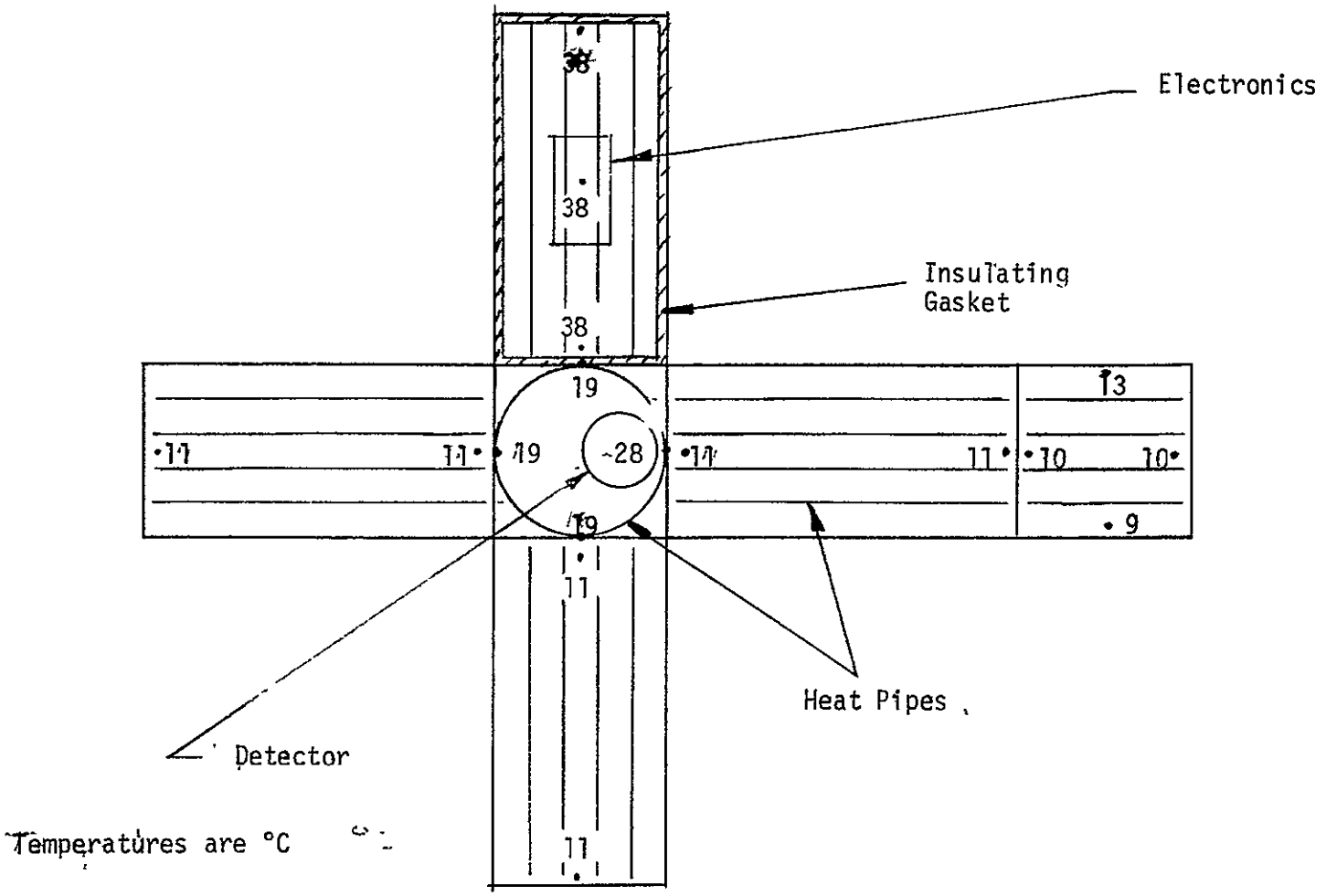

FIGURE 2.3.4-1

F I L T E R  W H E E L

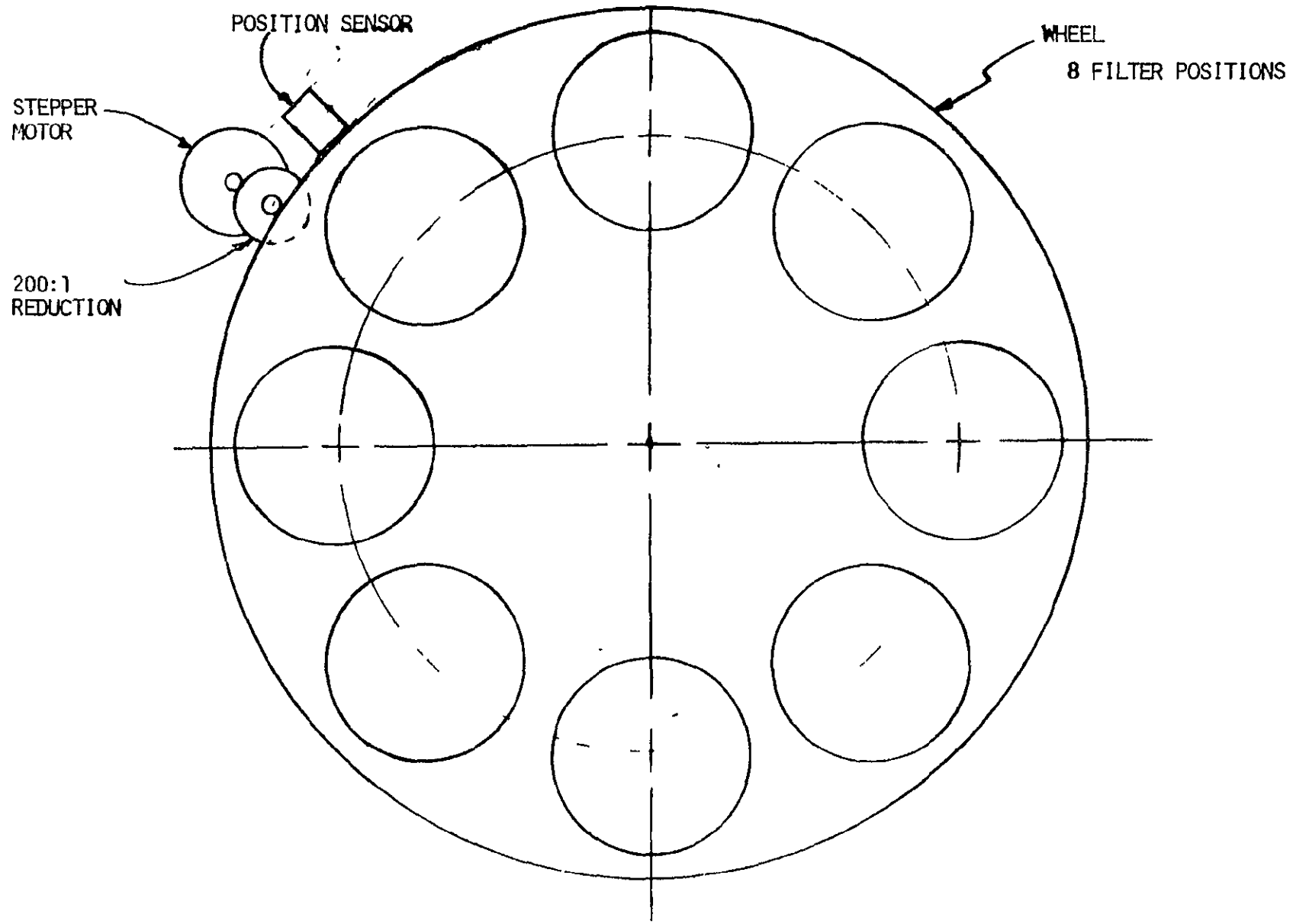

FIGURE 2.3.4-2

# DYNAMIC DISTURBANCES FROM

## FILTER WHEEL

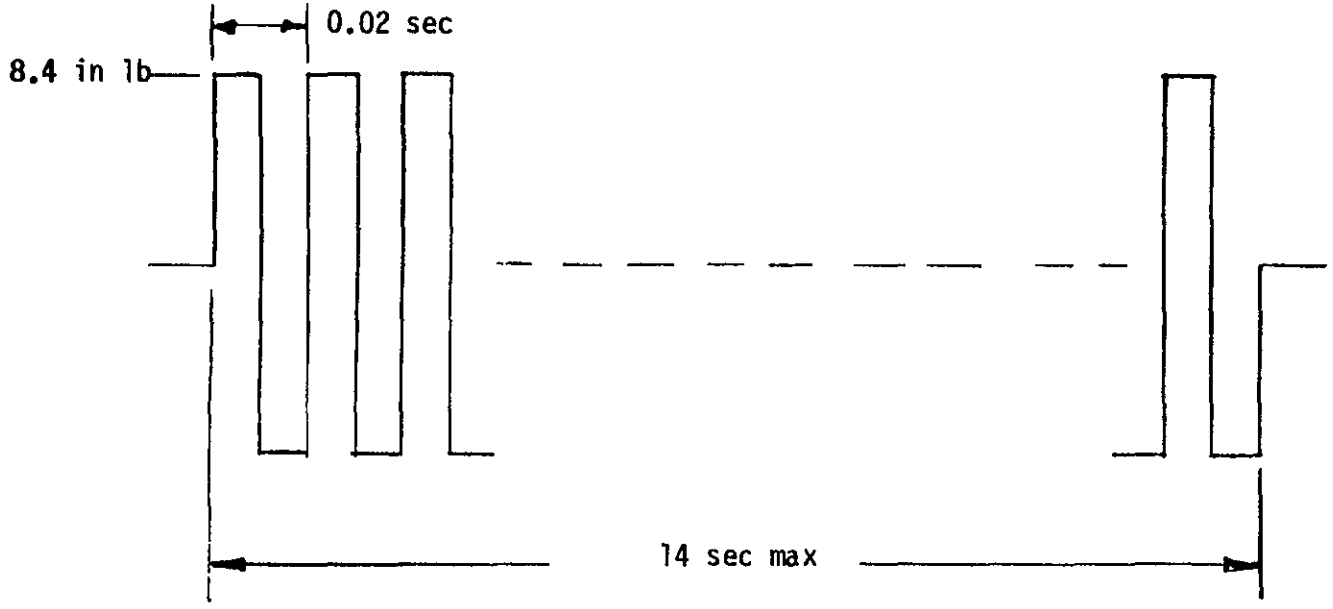

TABLE 2.3.4-1

POSSIBLE FILTER COMPLEMENT

| | FILTER | SPECTRAL RESOLUTION | PEAK TRANSMITTANCE | FILTER TYPE | COMMENTS |
|---|---|---|---|---|---|
| 1. | Transmission Grating | $\lambda/\Delta\lambda = 50$ | | 2500 Å Blaze | Quartz Substrate |
| 2. | Transmission Grating | $\lambda/\Delta\lambda = 40$ | | 3500 Å Blaze | Glass Substrate |
| 3. | U | Standard Filters | | | |
| 4. | B | | | | |
| 5. | V | | | | |
| 6. | R | | | | |
| 7. | I | | | | |
| 8. | 1200 Å | $\lambda/\Delta\lambda = 3\text{-}4$ | 15-25% | Metal-Dielectric-Metal (MDM or MDMDM) | Blocking not Required |
| 9. | 1500 Å | $\lambda/\Delta\lambda = 3\text{-}4$ | 15-25% | | |
| 10. | 1900 Å | $\lambda/\Delta\lambda = 5$ | | | |
| 11. | 2200 Å | $\lambda/\Delta\lambda = 7$ | | | |
| 12. | 2500 Å | $\frac{\lambda}{\Delta\lambda} = 8$ | 30-35% | | |
| 13. | 2800 Å | | | | |
| 14. | 3200 Å | | | | |
| 15. | Neutral Density - 1 | | 10% | | |
| 16. | Neutral Density - 2 | | 1% | | |
| 17. | Glass | | | | |
| 18. | $SiO_2$ | 30 - 50 Å | 40-80% | All Dielectric | Blocking Required ($10^{-4}$ achievable) |
| 19. | 3728 Å | | | | |
| 20. | 4363 Å | | | | |
| 21. | 4860 Å | | | | |
| 22. | 5007 Å | | | | |
| 23. | 6563 Å | | | | |
| 24. | - | | | | |
| 25. | - | | | | |
| 26. | - | | | | |

The disturbance to the body pointing resulting from operation of the wheel was estimated from the characteristic step motions of the wheel, the inertias of the wheel, an assumed inertia of 121 x $10^6$ lbm $in^2$ for the spacecraft, and an assumed body pointing control system gain crossover frequency of 3 radians per second. For disturbances longer than 0.33 second, the reciprocal of the gain crossover frequency, the effects were computed as the step change in velocity of the component inertia and the body inertia.

The assumption of 3 radian/second for the gain crossover frequency was conservative. Normally the filters would not be operated during an exposure. Smaller disturbances would result if the filters were driven at a lower rate.

As shown below, a filter wheel can produce a marginally-significant disturbance to the line-of-sight, but only momentarily. At most, two filter wheels would operate simultaneously: one to return to the open position, the other to advance to the desired filter position.

| COMPONENT | CHARACTERISTIC STEP MOTION | EFFECT ON BODY POINTING (3 RAD/SEC GAIN CROSSOVER FREQ.) |
|---|---|---|
| Filter Wheel | 0.39 rad/sec | 0.009 arcsec |

The vibrational disturbance of operating the filter wheels was estimated by assuming that the stepping frequency was in resonance with the closest vibrational mode of the OTA as determined from the OTA structural analysis. Assuming the resonant build-up was limited by damping, which was 0.5% of critical, the line-of-sight vibrational motion of 0.004 arcsecond was calculated. Vibrations at this frequency would damp out very quickly after the disturbance stopped, even with the low damping assumed. The vibration would damp out to 20% of the maximum amplitude after one second, and 4% after two seconds of settling time.

## 2.3.5 Capping Shutter and Calibration Assemblies

### Capping Shutter

The capping shutter is a pivoted motor-driven blade mounted coaxially with the filter assembly. It is driven by a redundantly wound stepper motor through a 200:1 gear reduction in the same manner as the filter wheels. The shutter blade carries two sets of calibration optics and thus has three positions: 1) open-imaging, 2) open standard star calibration, and 3) closed internal calibration. The shutter blade, with the calibration optics, is counterbalanced so that it pivots about its center of gravity.

### Standard Star Calibration Optics

The standard star calibration optics consists of an inverted, eccentric Cassegrain similar to that proposed in the camera FID, except that the option to rotate the axis of the Cassegrain is not included in the interest of simplicity. The entrance aperture is at the edge of the incoming ray bundle to make the output ray bundle as nearly centered with the camera submodule as possible. The capping shutter to which the calibration optics are mounted serves to block all of the field except at the entrance aperture for the calibration optics. When calibration is to be performed, the capping shutter is moved to position 2 mentioned above. The telescope is pointed so that the rays from the calibration star enter the entrance aperture of the calibration optics. The calibration optics cause the photocathode of the detector to be uniformly flooded with light from one side of the telescope pupil so that shadowing of the secondary mirror will not affect the illumination.

### Standard Star Calibration Exposure Times

To ensure reasonable exposure times, stars selected for calibration should fall in a $1 \leq M_V \leq 5$ range. The Arizona Tonantzintla Catalogue lists in excess of 1000 stars in this magnitude range north of declination -50°. Estimated calibration exposure times (in seconds) for a S/N ratio of 10 are given below.

| | | COLOR TEMPERATURE °K | | | |
|---|---|---|---|---|---|
| | | 1000° | 2000° | 4000° | 8000° |
| $M_V$ | 1 | 1 | 4 | 4 | 2 |
| | 2 | 3 | 9 | 9 | 4 |
| | 3 | 6 | 23 | 22 | 10 |
| | 4 | 16 | 60 | 56 | 25 |
| | 5 | 43 | 156 | 145 | 66 |

Exposure Time - Seconds (S/N = 10)

## Internal Calibration Optics

The internal calibration assembly consists of a fold flat mounted on the shutter blade, calibration sources mounted on the mirror support truss, and reference detectors mounted just forward of the filter wheels. In shutter position 3 above, the capping shutter completely blocks any input from the OTA and positions the fold flat such that the calibration sources illuminate the camera photocathode.

The radiometric calibration of the SEC sensor requires a stable source whose spectral output covers the sensor spectral sensitivity range. The source intensity should be high enough to allow meaningful calibrations at those wavelengths where sensor sensitivity is least. In addition, for the space application, long life, small size and low power are desirable features. The sources selected for the preliminary design are a tungsten lamp and a high pressure hydrogen lamp.

## Tungsten Lamps

Of the various type sources available which emit in the spectral sensitivity band of the SEC sensor S-20 photocathode, the tungsten filament incandescent lamp offers the most desirable characteristics. Generally tungsten filament lamps are stable with respect to long-period drift and have very small, short-period fluctuations. With time, there is a gradual decrease in output that must be accounted for. As tungsten evaporates from the filament, the temperature rises for a constant heating current; the evaporated tungsten coats the inside of the lamp tube causing its transmittance to decrease. Small tungsten bulbs which are adequate for the SEC calibration would normally operate at a color temperature of approximately 2000°K, which limits the ultraviolet spectral emission. The small bulbs have lifetimes in the order of 100,000 hours and can be operated at low voltage and low current (i.e., 5 volts, a few milliamps).

## High Pressure Hydrogen Arc Lamps

A high pressure hydrogen arc lamp will be used to provide ultraviolet spectral calibration. At a pressure of a few TORR, an electrical discharge passing through deuterium (heavy hydrogen) provides a small area source of high radiance in the ultraviolet spectral region (peaking at a wavelength of approximately 2000 Å. The spectral distribution of radiance of a hydrogen lamp exhibits no "spikes" of narrow-band radiation such as are found in other ultraviolet sources. These lamps are typically about 4" long by 1" diameter, and require about 50 volts and from .5 to 1.0 amps to operate. The life of the lamp is usually a few hundred hours. In addition to the operating voltage requirement, a starting voltage of several hundred volts is necessary. As with most arc lamps, stability may cause problems as a calibration source.

Hollow Cathode Lamps

The hollow cathode lamp is an alternate to the hydrogen arc lamp. The source of radiation is usually a hollow or crater-type cathode a few millimeters in diameter. The spectral quality of the output depends upon the gas filling the lamp tube. A neon filled tube provides a spectrum rich in spectral lines from 1200 Å to 3200 Å. A typical hollow cathode lamp requires about 500 volts to start and runs at about 200 volts, 10 milliamps. The lamps are approximately the same size as the hydrogen arc lamps but should offer some improvement in stability and life characteristics. If a rigorous radiometric analysis of the high pressure hydrogen lamp indicates insufficient stability or life for calibration, then the performance of a hollow cathode lamp (such as the one proposed for IUE) should be traded against the high pressure hydrogen lamp.

### 2.3.6 Module Mounting

The module has four mounting feet, as shown in the layout, Figure 2.3.2-2. These feet rest against the mounting surfaces within the OTA Focal Plane Assembly. The details of the mounting are not included in the layout, but the concept is described here.

Two of the four feet have registration holes which center upon pins attached to the Focal Plane Assembly. All four feet have captive screws which are used to screw the module down after it has registered. The captive screws are tightened by means of permanent extensions to the outer end of the module, as shown in Figure 2.3.6-1. The astronaut tightens the four screws successively with a ratchet wrench.

Additional items are required for the installation system. Latches which automatically engage upon insertion of the module hold the module temporarily while the screws are being tightened.

The pick-off mirror is very vulnerable to damage during transport and installation. For this reason, it will be necessary to have a guide rail system for installation. In transport, the mirror will be protected by a cap covering the mirror and its support structure. The cap attaches to the front of the module. The module is installed in the guide rails which serve to guide the module into place without the possibility of the mirror contacting anything along the way. Once the module is installed in the guide rails, but before it is inserted into the Focal Plane Assembly, the cap over the mirror is removed. The module is then moved along the guide rails until the registration pins center it properly and the latches engage. The screws are then tightened. The centering of the module with the registration pins also centers it within the guide rail support so that the module is no longer in contact with the guide rails. Finally, the electrical connections are made via a separate electrical connector on the outer portion of the module.

The design of the protective cap is such that the module cannot be installed with the cap in place.

FIGURE 2.3.6-1

MODULE ATTACHMENT

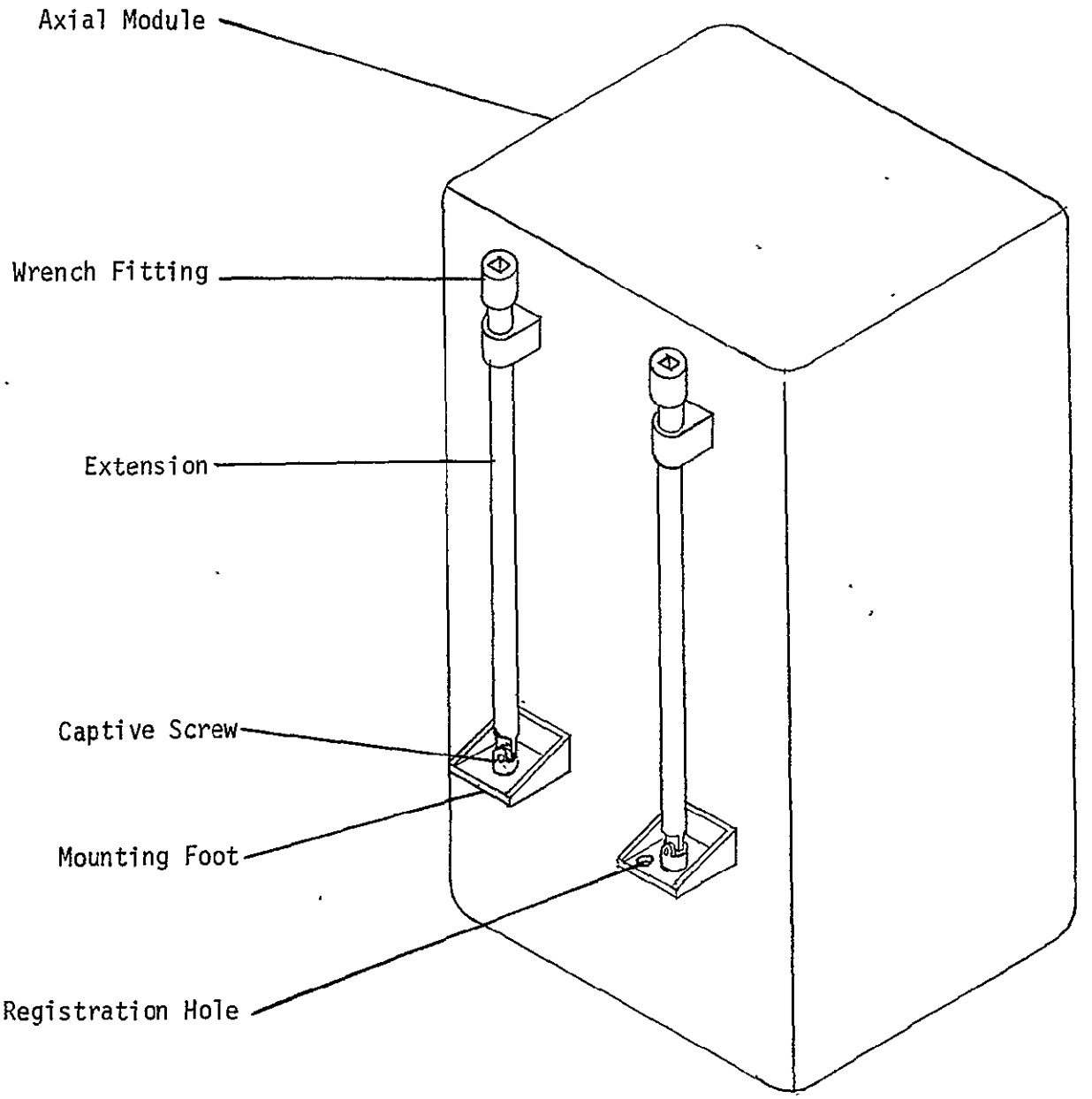

2.3.7 Electrical Subsystem

The electrical subsystem has been developed to the functional block diagram level as shown in Figure 2.3.7-1.

1. SECO Detector Assembly - The functional block diagram of the SECO submodule is shown separately (Figure 2.4.4-1).

2. Aperture Shutter Assembly - The shutter assembly is a three position unit driven by a stepper motor (see Section 2.3.5). The shutter assembly will employ closed position feedback to verify shutter position. The feedback unit will consist of a suitable filtered tungsten lamp (e.g., silicon filter) and indium antimonide photodiodes.

3. Calibration Assembly - The calibration assembly provides three current levels to a calibration lamp. Two current levels provide for calibratec irradiance levels at the detector; the third level provides sufficient irradiance at the detector for pre-exposure in the prepare mode. Two silicon detectors are employed to monitor the output of the calibration source.

4. Filter Mechanism Assembly - The filter mechanism for the field camera consists of three coaxial, eight-position wheels. One position in each wheel will be open.

   Each wheel will be driven by a stepper motor/gear train. One hundred steps will be required between filter positions. The motor will operate at 50 step/second. The maximum time to index from one position to any other will be 14 seconds (assuming unidirectional rotation).

   Each wheel will employ closed loop position feedback to verify filter position. The outer edge of each wheel will contain coded, reflective strips. Four source/detector pairs will be used with each wheel to sense the coded positions.

The Focal Plane Camera also contains the following electronics:

1. Instrument Control Unit - The instrument control unit provides command decoding and unit sequencing for nondetector-specific functions and contains the HRC "INSTRUMENT OFF" status sensors. The unit decodes shutter and filter positions and issues these commands to the appropriate assemblies. It also decodes calibrate commands and/or prepare mode to actuate the calibrate assembly.

   The functions of this unit are relatively simple because the SECO submodule is directly controlled by the SI Data Management System.

2. Power Conditioner Unit - The power conditioner unit consists of two redundant regulators and a power switching unit. The power switching unit, designed free of single point failures, responds to a power command from the DIU and provides the capability to select either regulator and to power the selected regulator from either BUS A or BUS B or both.

FIGURE 2.3.7-1

F/24 FOCAL PLANE CAMERA

FUNCTIONAL DIAGRAM

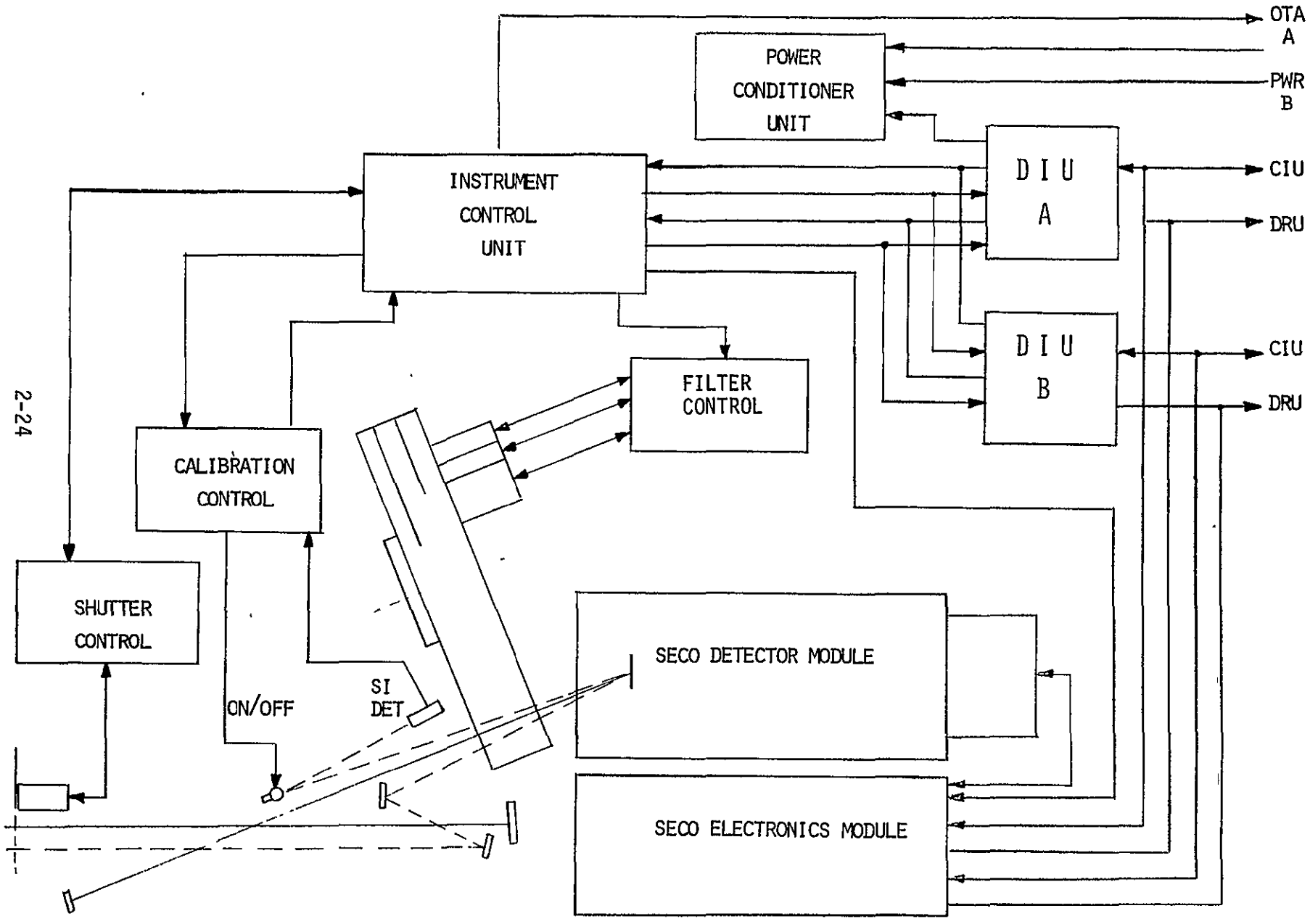

3. Redundant Digital Interface Units (DIU's) - The Focal Plane Camera interfaces with the SI Data Management System via redundant DIU's.

2.3.8 Command and Data Lists

Table 2.3.8-1 gives the command list for the Focal Plane Camera and the number of bits comprising each command. The commands are input according to a standard command format.

The power select command determines which of the two redundant power regulators and power busses are used.

The mode select command sets the camera in one of the following modes:

ACTIVATE STANDBY
ACTIVATE PREPARE SEQUENCE
ACTIVATE CALIBRATION SEQUENCE/WAIT FOR READ
ACTIVATE CALIBRATION SEQUENCE/FOLLOWED BY READ
ACTIVATE EXPOSE SEQUENCE/WAIT FOR READ
ACTIVATE EXPOSE SEQUENCE/FOLLOWED BY READ
ACTIVATE READ SEQUENCE

The shutter and filter commands cause those devices to advance to the command position.

The SECO submodule commands determine the state of the SECO Camera submodule and are listed in Table 2.3.8-2.

TABLE 2.3.8-1
COMMAND LIST (20 Command Bytes)

| COMMAND | BITS |
|---|---|
| POWER SELECT | 3 |
| MODE SELECT | 5 |
| SHUTTER | 7 |
| FILTER | 9 |
| EXPOSURE TIME | 24 |
| SECO CAMERA SUBMODULE STATES | 96 |
| SPARE | 16 |
| TOTAL | 160 |

TABLE 2.3.8-2

SECO CAMERA SUBMODULE STATE LIST

(12 Bytes)

| | BITS |
|---|---|
| SPARE | 6 |
| FOCUS CURRENT | 10 |
| ALIGNMENT X | 4 |
| ALIGNMENT Y | 4 |
| DEFLECTION GAIN X | 8 |
| DEFLECTION OFFSET X | 8 |
| DEFLECTION GAIN Y | 8 |
| DEFLECTION OFFSET Y | 8 |
| TARGET | 4 |
| FILAMENT | 4 |
| GRID 1 | 8 |
| GRID 3 | 8 |
| GRID 4 | 8 |
| PHOTOCATHODE | 8 |
| TOTAL | 96 |

Table 2.3.8-3 gives the diagnostic data list for the field camera and the number of bits. The data output follows a standard format. First the command list is echoed. Then status monitor samples are read out, followed by calibration reference samples. The 15 (8-bit) status monitor samples include 6 temperatures, 6 voltages, filter position, shutter position, and a spare. An additional 500 bits are available for on-board merging of engineering data from other ST sources.

TABLE 2.3.8-3

DATA LIST (51 Data Bytes)

| | BITS |
|---|---|
| COMMAND LIST ECHO | 144 |
| STATUS MONITOR SAMPLES (8 Bits Each) | 120 |
| CALIBRATION REFERENCE SAMPLES (12 Bits Each) | 120 |
| SPARE | 16 |
| END-OF-TRANSFER CODE | 8 |
| TOTAL | 408 |

Science data is output over a separate science channel to the ST Data Management System. At this time, the focal plane camera science data rate is TBD but probably will be a minimum of 200 KBPS and a maximum of 1 MBPS.

## 2.3.9 Power

Figure 2.3.9-1 shows the power profile for the field camera, including time for warmup, target preparation, exposure and readout. The makeup of the total power is as follows:

| | |
|---|---|
| Camera Submodule | 42 watts |
| Two Digital Interface Units | 12 watts |
| Capping Shutter Control | 5 watts |
| Calibration | 25 watts |
| Filter Control | 5 watts |
| Instrument Control Unit | 10 watts |
| Thermal Control | 5 watts |

The power conditioner unit is assumed to have an efficiency of 75%. Its regulation applies to everything except the thermal control power. The maximum power, including the power consumed in the power conditioner unit is 137 watts. The average operating power is 97 watts.

## 2.3.10 Weight

Table 2.3.10-1 gives the estimated weight of the module.

TABLE 2.3.10-1
WEIGHT OF FOCAL PLANE CAMERA

| | | |
|---|---|---|
| Camera Submodule | 125.0 | lb. |
| Module Interface Bulkhead | 20.0 | |
| Detector Mounting Bulkhead | 10.6 | |
| Filter and Shutter Structure | 3.4 | |
| Filter Wheel Assembly | 13.0 | |
| Capping Shutter and Calibration Assembly | 5.0 | |
| Mirror and Mirror Mounting Structure | 14.6 | |
| Module Frame | 8.5 | |
| Module Skin | 13.6 | |
| Heat Pipes and Connectors | 37.6 | |
| Electronics Box | 10.0 | |
| Installation Devices | 4.0 | |
| Electrical Connector | 1.0 | |
| | 266.0 | |
| Contingency - 15% | 40.0 | |
| Total | 306.0 | |

FIGURE 2.3.9-1

FOCAL PLANE CAMERA POWER PROFILE

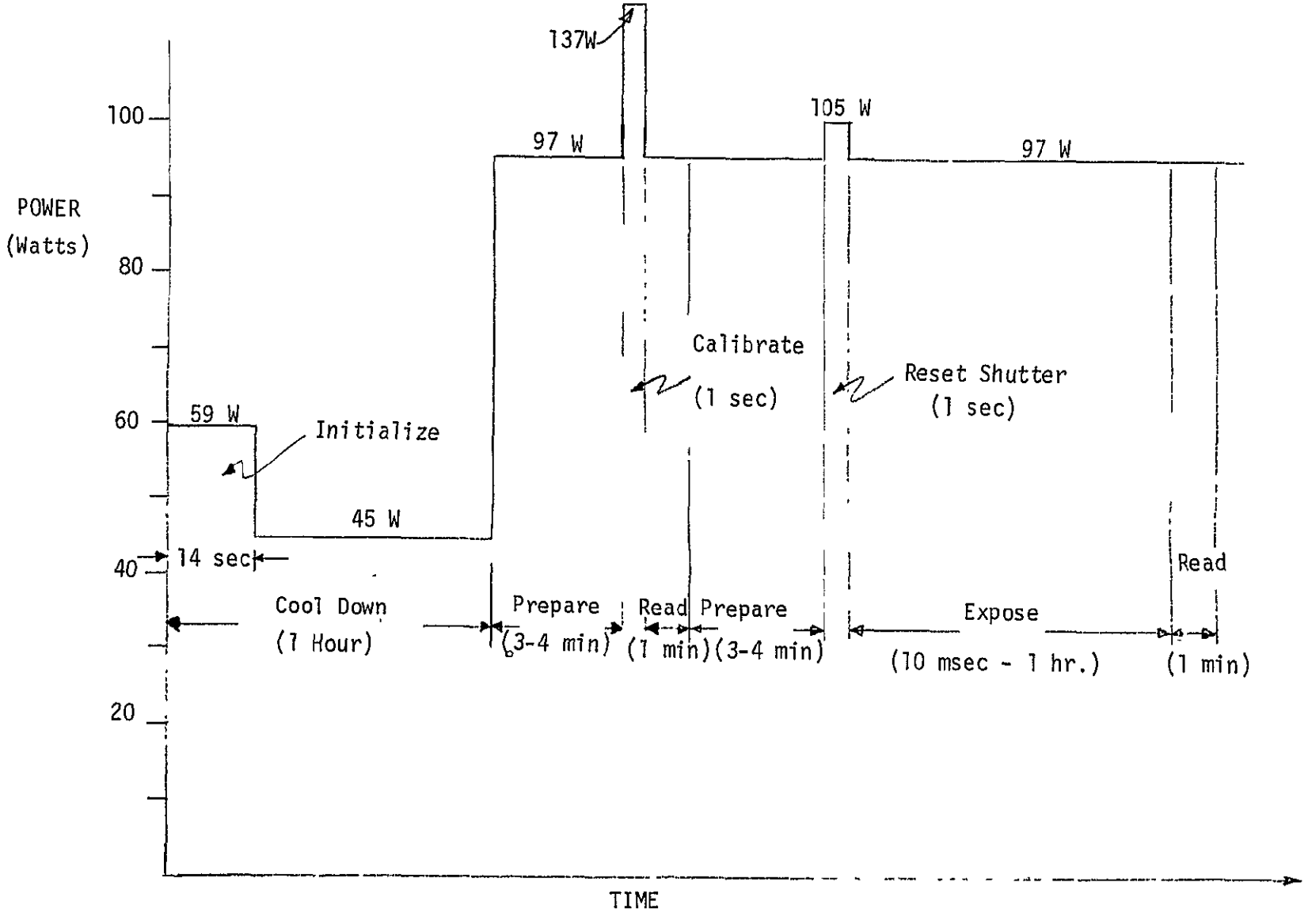

## 2.4 SECO Submodule Design

This section summarizes the design of the SEC orthicon camera submodule and gives the results of supporting analysis. The image tube used is as defined in the HRC FID. Coil packages similar to the ones used in the Princeton experimental study are shown in the design. The cooling of the photocathode is accomplished by thermoelectric coolers within the submodule. Heat from the submodule is dissipated radiatively from the submodule wall. Electronics requiring very close proximity to the components of the submodule are located within the submodule itself, while other electronics associated with the submodule are located in an adjacent electronics box to minimize the heat dissipated from the submodule. The peak power used is 80 watts, as in the SI Requirements document. The weight of the submodule is estimated to be 125 pounds. Table 2.4-1 summarizes the features of the design.

TABLE 2.4-1

SEC ORTHICON CAMERA SUBMODULE DESIGN

| |
|---|
| Image Tube Defined in FID |
| Coil Packages as in Princeton Study |
| Thermoelectric Cooling of Photocathode |
| Radiative Heat Dissipation |
| Electronics Within Submodule and in Adjacent Box |
| 80 Watts Peak Power |
| 125 Pounds Weight |

### 2.4.1 Submodule Layout

The SEC Orthicon Camera submodule uses the image tube defined in the HRC FID, and focus, deflection, and alignment coils with the dimensions of those used in the developmental work at Princeton University. Figure 2.4.1-1 shows the layout of the submodule design.

The most significant design problem in the packaging of the submodule is the cooling of the photocathode and the dissipation of the heat from the coils and the coolers. The following is an explanation of the layout drawing, working from the inside out. The image tube is potted into a beryllium oxide sleeve with a conductive contact to the faceplate to be cooled. The beryllium oxide sleeve has conductance of about 140 BTU/HR/FT/°F, nearly that of copper, but is electrically non-conductive so that it will not affect the deflection field by eddy currents. This sleeve is gold-coated on the outside to minimize radiation to it from the coils, and is separated from the coils by a gap. The forward end of the sleeve is attached to the outside housing by means of a non-metallic, low-conductivity end cap with a labyrinth form to maximize the heat conduction resistance. At the rear end, the sleeve is spaced away from the coils by three small devices built into the inside of the coil mandrel.

# SEC ORTHICON CAMERA

# SUBMODULE LAYOUT

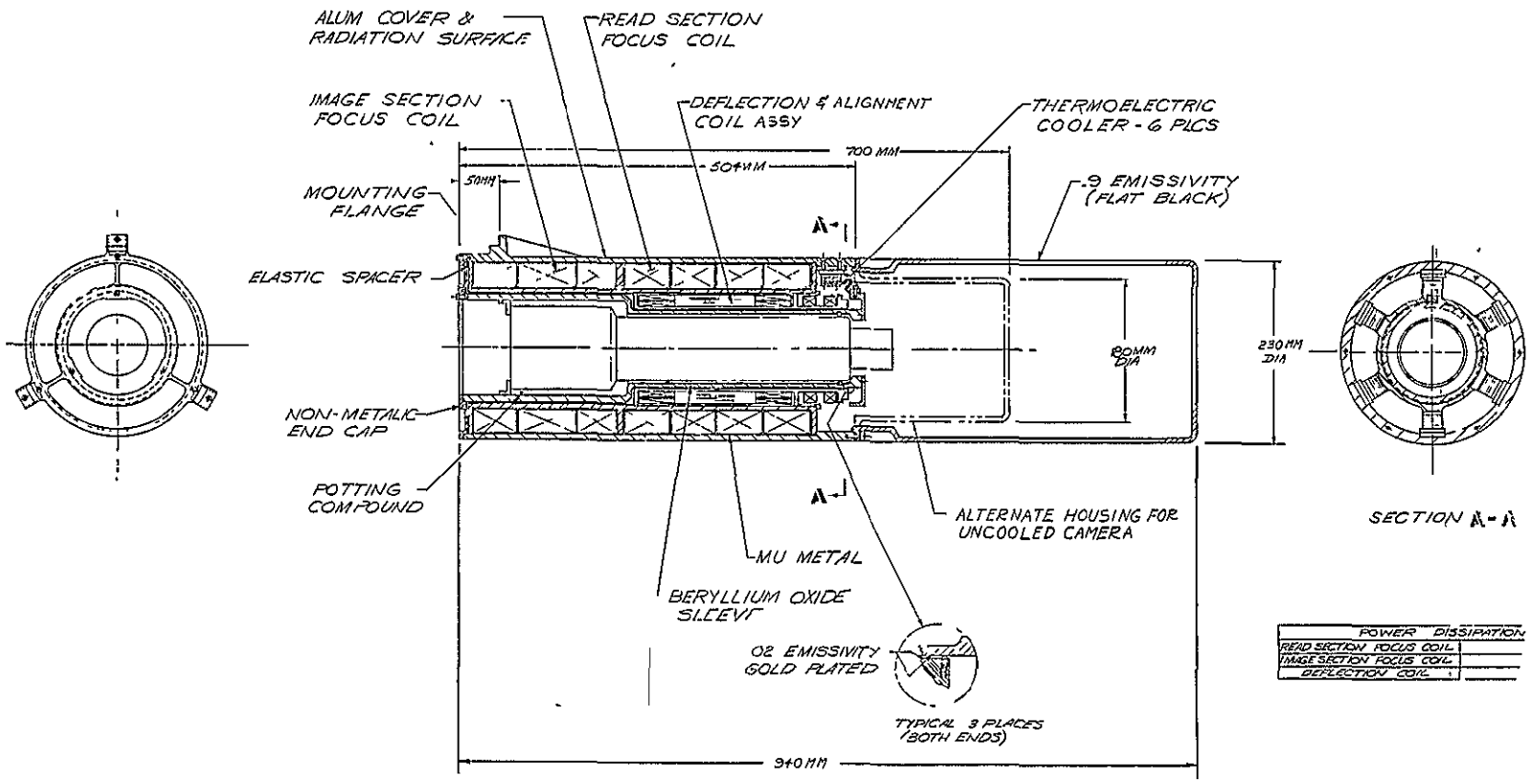


FIGURE 2.4.1-1

The aft end of the sleeve is thermally connected to six thermoelectric coolers by flexible copper straps made up of many layers of thin copper sheet. These straps permit relative thermal expansion between the inner sleeve and the submodule cover without introducing undue strain into the coolers. There are six coolers, similar to Cambion 801-1003 two-stage device.

The outside cover is the support for the coils on their mandrels. It is made of aluminum and is thick enough (0.25 inch) to provide good conductive heat dissipation to the outside. A large aft cover provides extra radiating surface to ensure adequate heat dissipation capability. In applications not using coolers, an alternate rear cover, just large enough to house necessary connectors and preamplifier electronics, can be used.

Mounting of the camera submodule is via three feet projecting from the outside cover near the forward end.

The coil packages used in the layout were based upon the coils made by Penn Tran Corp. for the Princeton study. The Penn Tran focus coil assembly has a length of 18 inches, an inside diameter of 5.5 inches, and an outside diameter of 8.5 inches, plus a 0.031 inch thick mu-metal shield.

The alignment and deflection coil assembly is 10.5 inches long, with an inside diameter of 3.437 inches, and an outside diameter of 5.0 inches. In the layout, the diameters of this coil were enlarged to 4.0 inches inside and 5.6 inches outside in order to accommodate the thermally-conductive sleeve between the coils and the image tube. A section of the focus coil mandrel inside diameter was assumed to be bored out to act as a retainer for the 5.6 inch outside diameter of the deflection and alignment coil assembly.

The weight of the camera submodule is estimated to be about 125 pounds, including 70 pounds for the coils and image tube, 26 pounds for the outer shell, 8 pounds for the conductive sleeve, and 21 pounds for coolers, electronics, cabling, fasteners and fittings, etc.

### 2.4.2 Submodule Thermal Design

The thermal design requirement from the FID is a photocathode temperature of -3°C. The photocathode cooling is accomplished with three pairs of thermoelectric two-stage coolers. Each pair of coolers is capable of maintaining the photocathode at -3°C under worst case conditions with a 50% duty cycle. Temperature sensors near the photocathode provide the error signal to the cooler controller. Cooler switching rates will be controlled to maintain EMI within acceptable limits. Table 2.4.2-1 summarizes the thermal design.

### 2.4.3 Thermal Design Analysis

The temperatures resulting from a 90 node thermal model analysis are shown in the thermal map of Figure 2.4.3-1. In the analysis, the thermal electric hot junction went to 28°C. The temperature differential across the cooler (cold to hot junction) was 41°C. From the cooler characteristic of Figure 2.4.3-2 , each cooler is capable of pumping 3 watts of thermal power. The energy balance map of the tube requires a cold junction heat flow of 1.7 watts. The hot junction heat flow, on the average, is 8 watts. Thus the assumed thermoelectric dissipation of 10 watts is reasonable. The predicted photocathode temperature is -3°C which satisfies the design requirement.

TABLE 2.4.2-1

SECO SUBMODULE THERMAL DESIGN

1. $T_{photocathode}$ Requirement: -3°C
2. $T_{instrument}$ Comp Wall Max: -12°C
3. Six Dual Stage Cascaded Thermoelectric Devices for Temperature Control
4. BeO Conducting Sleeve
5. Strain Isolating Cu Strap From Cold Junction to Conducting Sleeve
6. Gold Plated Tube to Suppress Radiant Leaks
7. Low Conductance Supports
8. Bipolar Controller Electronics (Remote)
9. $Q_{focus\ coils\ during\ integration}$ 12W
   $Q_{cold\ junction}$ 2W
   $Q_{hot\ junction}$ 10W
10. $T_{radiating\ sleeve}$ 27°C
    $T_{photocathode}$ - 3°C
    $T_{cold\ junction}$ -13°C
    $\Delta T_{thermoelectric}$ 41°C
    $T_{ambient\ module}$ 30°C

FIGURE 2.4.3-1

# TEMPERATURE MAP OF COOLED SEC SUBMODULE

TEMPERATURES IN °C

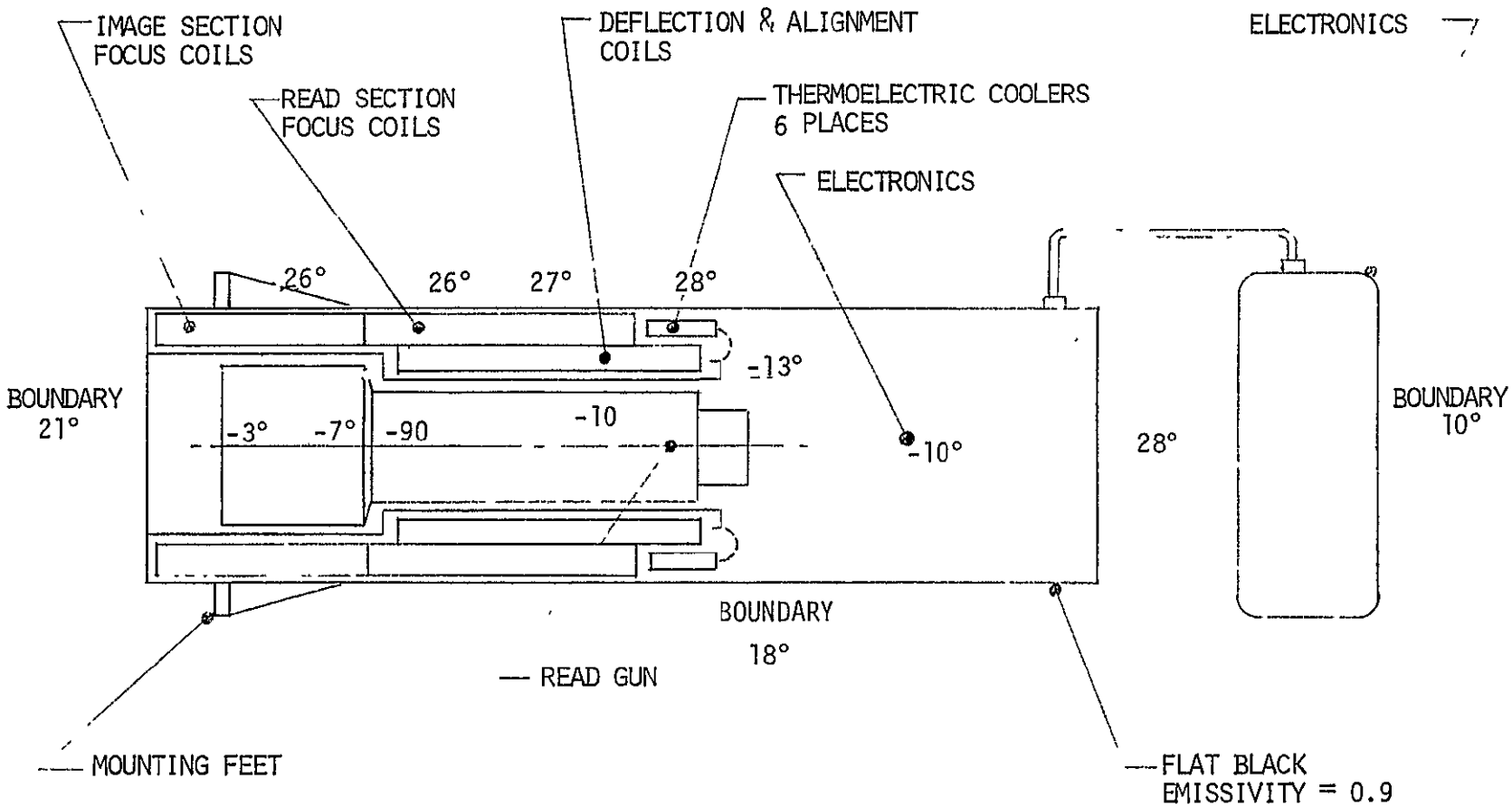

FIGURE 2.4.3-2
COOLING CAPACITY OF SECO COOLERS
(CAMBION 801-1003)

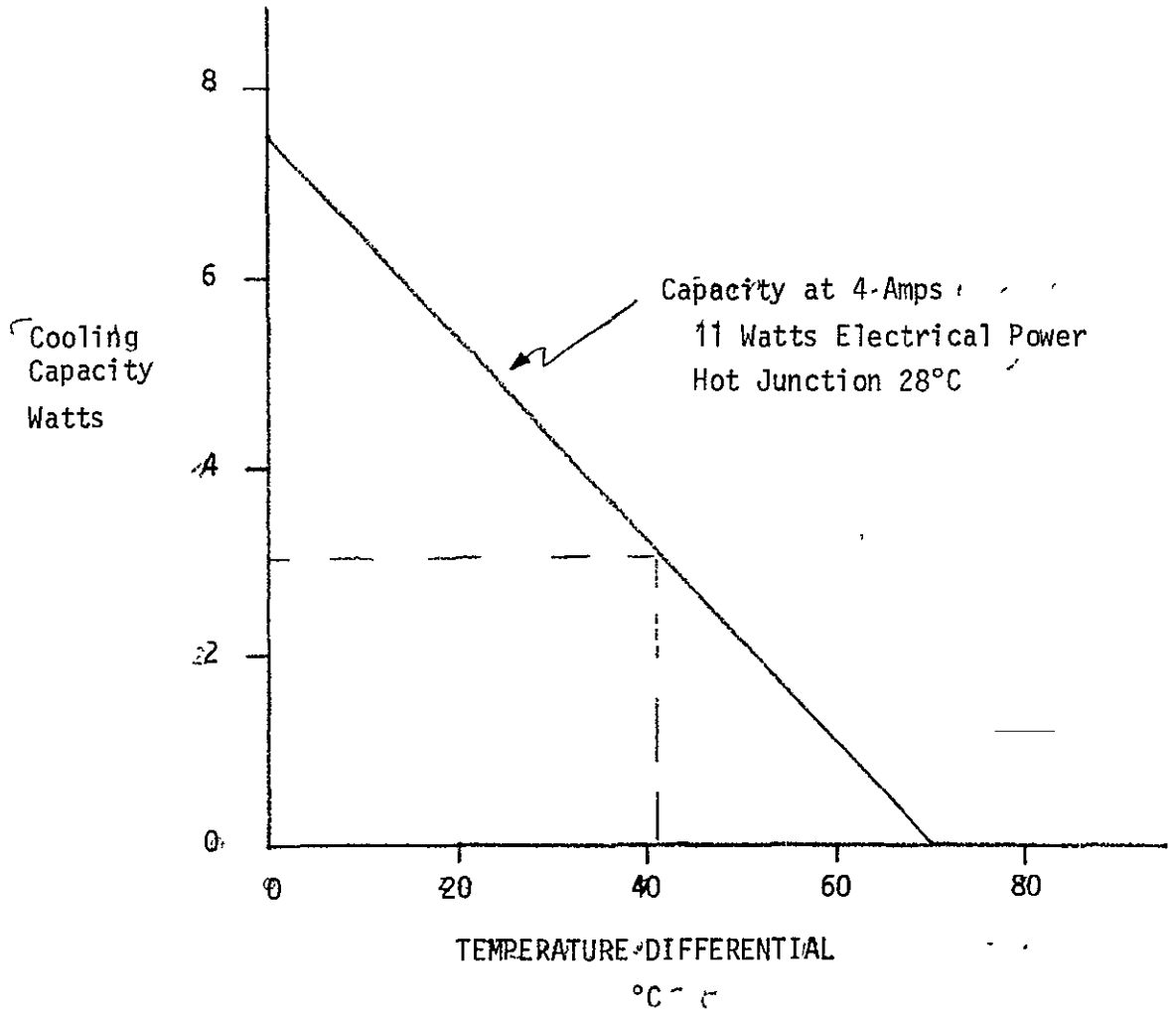

### 2.4.4 Standardized SECO Submodule Block Diagram

A preliminary block diagram of a standardized SECO submodule is shown in Figure 2.4.4-1 . As indicated in the diagram, the SECO submodule has been designed as a self-contained camera. All requisite functions (power regulation, high voltage supplies, photocathode cooling unit, video electronics, focus and deflection electronics, and computer compatible command interface) are included.

The redundant digital interface units are the standard SI DIU's. The DIU's interface directly with the CIU and DRU outside the instrument data handling system. Additional contacts will be provided on the DIU cards such that, at the SI contractor's option, the DIU's may be interfaced internal to the Science Instrument.

The remainder of the functional blocks are relatively self-explanatory. Focus regulator currents, alignment voltages, target voltage, photocathode voltage, and grid voltages are remotely programmable. Deflection system gain and offset are also remotely programmable.

The control and scan generator, in addition to providing deflection control, contains built-in (remotely modifiable) prepare, expose and read sequences. Nominal cycle times* are as follows:

| | |
|---|---|
| Prepare (1 expose, 4-5 reads) | 3-4 minutes |
| Expose | 10 MS - 10 hours |
| Read | 1 minute |

The video output is nominally 1 Mbit/second serial, 10 bit quantization.

## 2.5 Performance

### 2.5.1 Optical Quality

The camera performance is determined by the OTA and the SECO. The on-axis pick-off mirror has a negligible degrading effect on performance in terms of image quality. The OTA/SECO response in terms of point spread function is given in Figures 1.4-15, 1.5-1 through 1.5-5. The applicable curves are those labeled "on-axis pick-off". A flat faceplate with no field flattener is assumed. The camera is focused at an intermediate field point so that the center of the field and the corners are equally out of focus.

The performance curves are for monochromatic imaging at two wavelengths. For broadband imagery, the degradation resulting from longitudinal color aberration of the filter and faceplate can be assessed with the aid of Table 1.5-3. The SECO pixel size, for reference, is 25 micrometers.

* Assumes KCl Target

FIGURE 2.4.4-1

# STANDARDIZED SECO MODULE BLOCK DIAGRAM

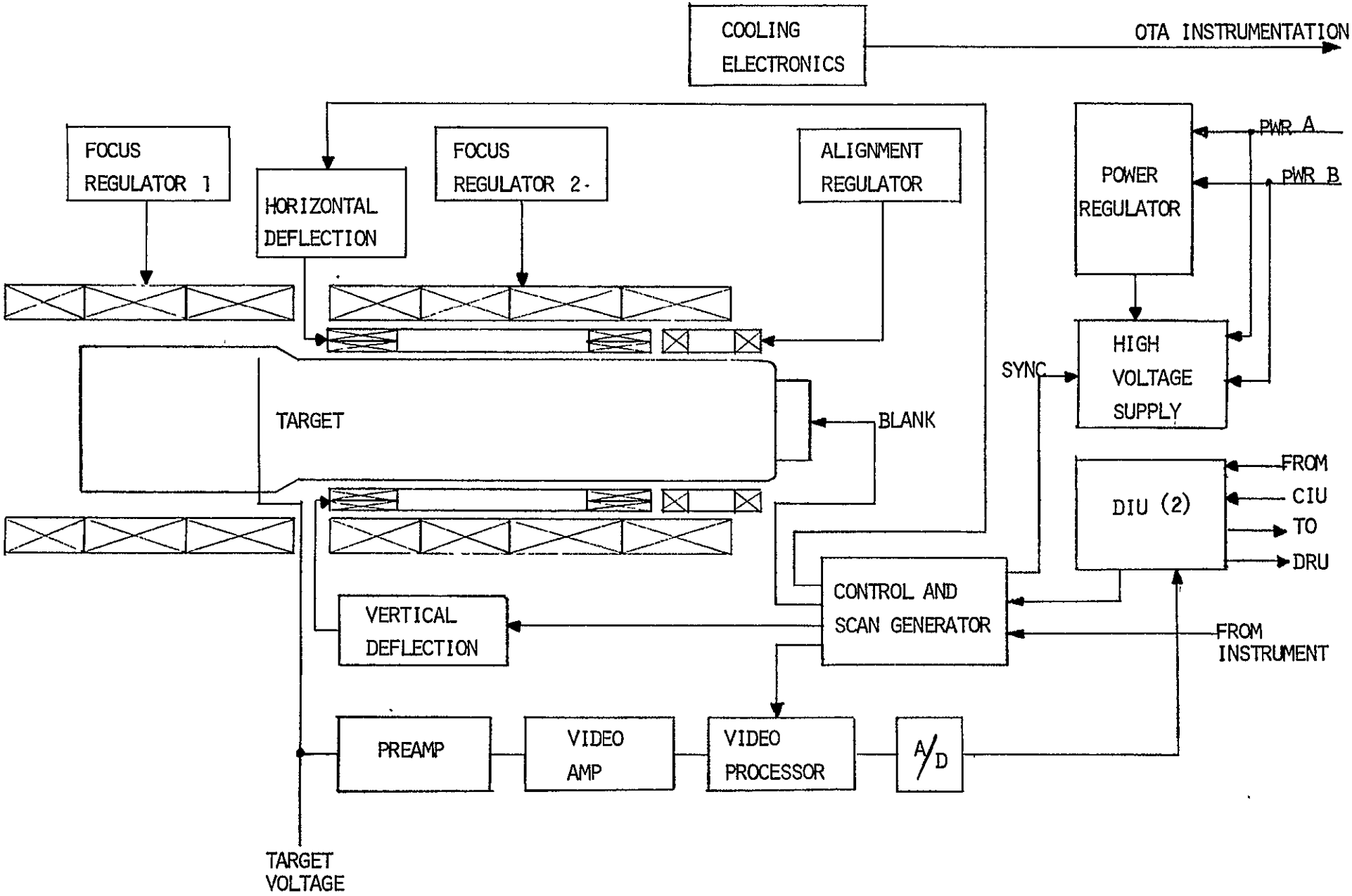

## 2.5.2 Computer Program for Detector Performance Analysis

### 2.5.2.1 General Description

A computerized model of the operation of an imaging system incorporating an electronic focal plane has been developed. The purpose of the computerized model is to perform parametric trade-offs to obtain data on which to base the selection of a high resolution camera configuration for the ST. A flow chart for use of the program is given in Figure 2.5.2.1-1. The program accepts four blocks of input data. They are the descriptive parameters of 1) the scene, 2) the optics, 3) the electronic image detector, and 4) system operation. The program uses the input to produce data for plots of integration time required to attain a given signal-to-noise ratio versus star equivalent black body temperatures for a range of star visual magnitudes and optical system f/numbers. The program is built as a group of modules and can be manipulated to accept additional input parameters, to obtain plots of different variables, or to extend generally its capabilities.

A potentially important use of the program is parametric characterization of a particular system which, when coupled with measured parameter values and uncertainties, can be used in estimating such properties as photometric uncertainty and in showing clearly the parameters limiting the system performance.

### 2.5.2.2 Assumptions/Capabilities

The computerized model is based on an analysis that is directed at point source detection. Since imagery is used to determine the presence and location of stars, galaxies, and other small faint objects, the program uses relationships developed for the detection of point sources against an extended continuous background. The expression for the signal-to-noise ratio is written for a photoelectron flux that assumes a Poisson distribution in time at the photocathode. The sources of noise considered are signal noise, background noise, thermonic noise within the detector and preamplifier noise.

The signal-to-noise ratio calculation is based upon a two-dimensional equivalent spatial frequency passband, $N_{e2}$, defined as

$$N^*_{e2} = \int_0^{2\pi} \int_0^{\infty} T^2(\nu, \phi)\nu \, d\nu \, d\phi$$

where $T(\nu,\phi)$ is the rotationally symmetric system Modulation Transfer Function expressed in polar coordinates $\nu$ and $\phi$. The use of an equivalent passband defined in this manner is analogous to the noise-equivalent-bandwidth used in signal processing noise calculations.

The reciprocal of $N^*_{e2}$ represents the equivalent sampling area:

$$A^*_s = \frac{1}{N^*_{e2}}$$

FIGURE 2.5.2.1-1

COMPUTER PROGRAM

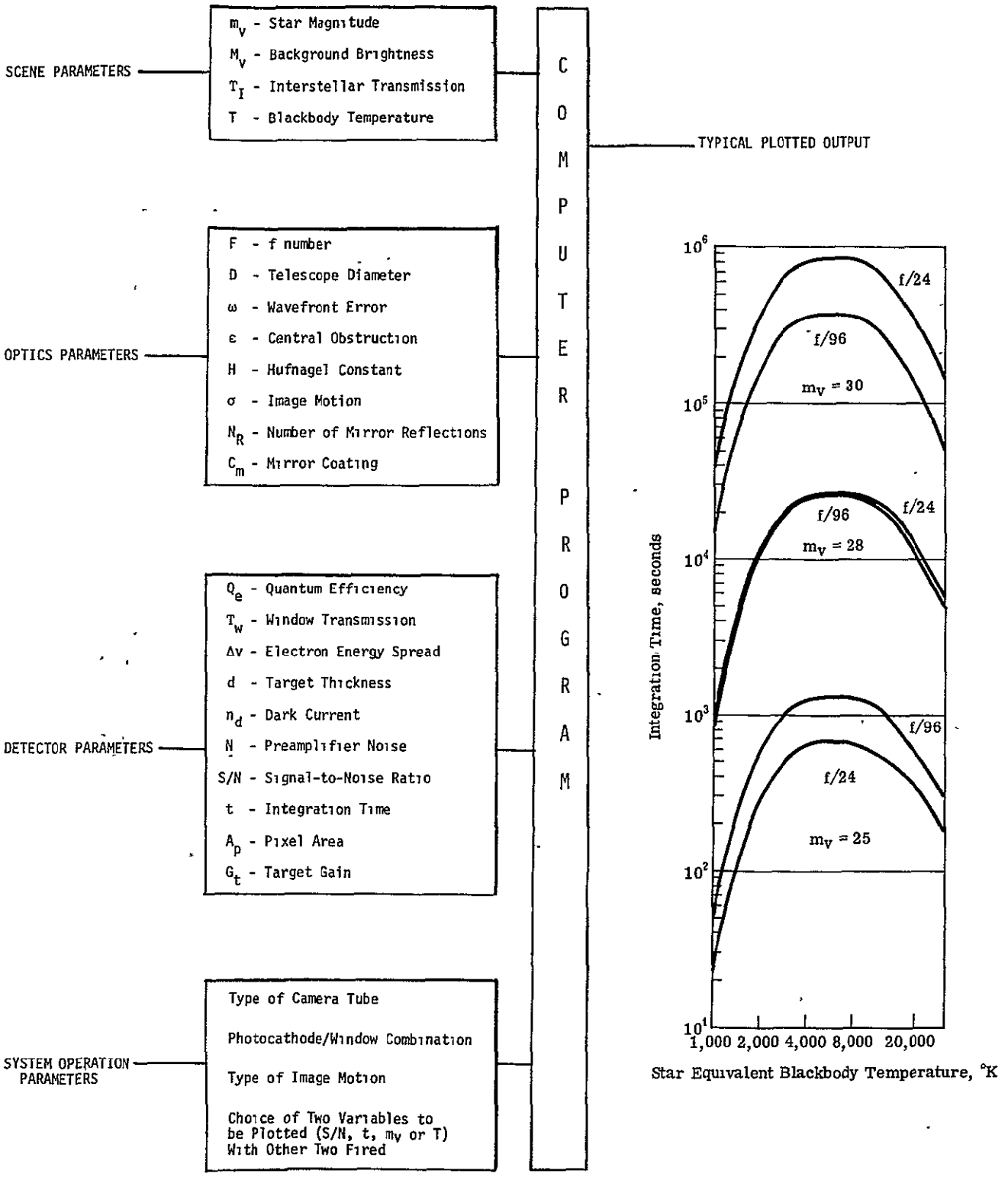

An image quality factor, Q, is defined for the entire electro-optics train relative to the equivalent passband of a perfect system:

$$Q = \frac{N^*_{e2}\ (\text{real})}{N^*_{e2}\ (\text{perfect})}\ ,$$

Q can be used as a basis of comparison of SI systems with different parameters.

The program is capable of evaluating configurations utilizing SIT, SEC, and silicon target vidicons. Data on a variety of photocathode and window materials has been incorporated in the program so that their combinations can readily be evaluated.

The MTF of the system, needed to calculate the equivalent sampling area, is determined by cascading the component MTF's. The MTF's due to 1) diffraction, 2) central obscuration, 3) wavefront error, 4) the electron optics, 5) tracking jitter, and 6) the storage target are considered. The first four of these are functions of wavelength, and spectral variations must be accounted for in arriving at the MTF's. Diffraction and central obscuration were handled by estimating an effective wavelength based on the combination of photocathode and source temperature considered. Wavefront error was calculated for various wavelengths and a weighted average computed using the spectral response and source distribution as weighting functions. The electron optics MTF was calculated using a similar procedure to compute a spectrally weighted electron velocity distribution.

A detailed description of the program mathematics is given in the Concept Design Report for the Phase B Study, 1 April 1974, Itek 74-8237-2 (NASA Contract NAS8-29949), P2-43 ff. The work is based, in part, upon the results of the "Large Space Telescope Image Quality Analyses" report, 4 December 1973, Itek 72-9486-1a (NASA Contract NASx-2313).

The program has been used to examine the sensitivity of HRC configurations to point objects and particularly the variability of sensitivity with the choice of tube and relay.

### 2.5.2.3 Exposure Times for an S20/$MgF_2$ SECO

Figure 2.5.2.3-1 shows the integration time required to achieve a signal-to-noise ratio of 10 for broadband imagery of stars of various magnitudes and temperatures, for both S-20 and S-25 photocathodes.

The performance is shown at two focal ratios, F/24 and F/96, for a telescope with a 30% obscuration, 1/20 wave RMS wavefront error at 633 nm, and 0.005 arcsecond RMS image motion. The analysis, therefore, does not apply strictly to the F/24 camera, but serves to show qualitatively, the tradeoffs between several factors. The curves were generated for preamplifier noise in the readout of 400 electrons, which is consistent to one $M_v$ 23 star per square arcsecond.

FIGURE 2.5.2.3-1

# PHOTOCATHODE COMPARISONS FOR THE SEC SUBMODULE

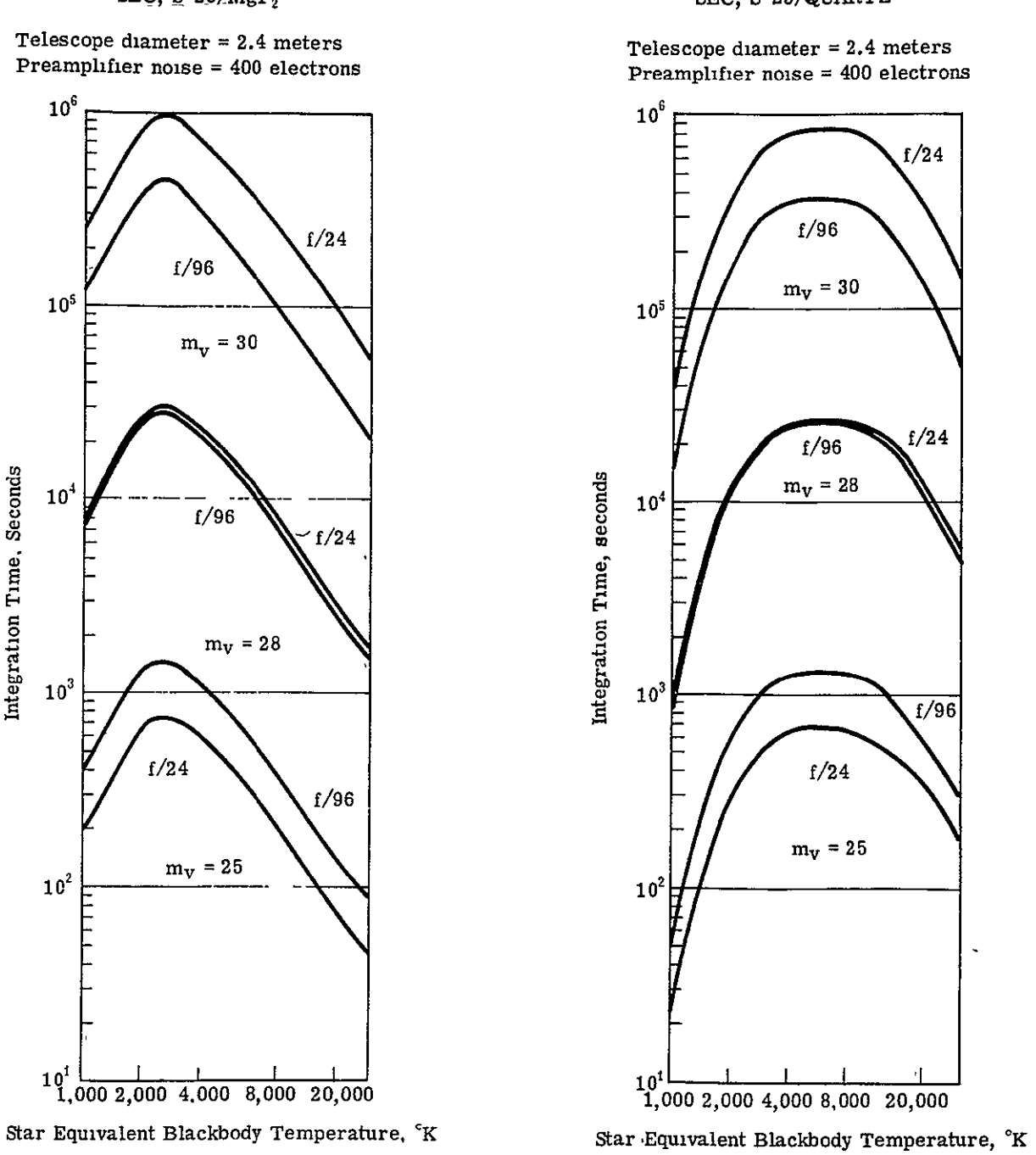

The difference in the spectral response between the two different photocathode/window combinations is evident. The rapid reduction of time at the low temperature end is the result of the curves being generated at constant visual magnitude and the relatively greater sensitivity to red of the photocathodes over the eye.

The reversal in position of the F/24 and F/96 curves from $M_V$ 30 to $M_V$ 25 is the result of the change in the relationship between the sky background intensity and the intensity from the star, the F/96 image being spread across more pixel elements of the detector.

The curves from Figure 2.5.2.3-1 were regenerated with the preamplifier noise reduced to 200 electrons, which might be achieved by developmental work. The results are shown in Figure 2.5.2.3-2. For exposure times on the order of one hour ($3.6 \times 10^3$ seconds), the required exposure time for the same signal-to-noise ratio is cut about in half. This indicates that the gain from reduced preamplifier noise would be significant, increasingly so for shorter and shorter exposure times.

FIGURE 2.5.2.3-2

# EFFECTS OF PREAMPLIFIER NOISE REDUCTION

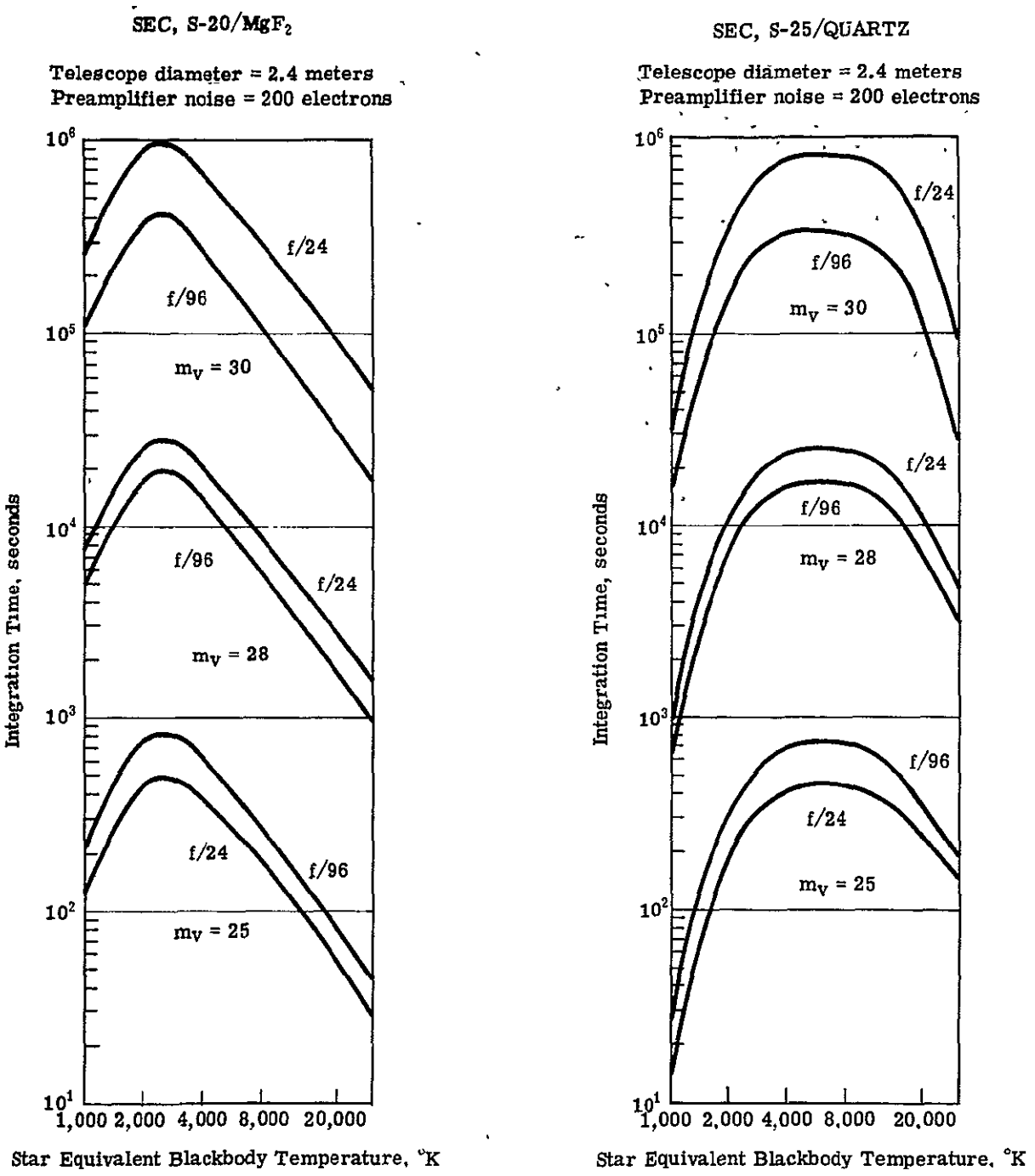

## 2.6 Design Verification

The present protoflite approach to hardware development delays the availability of complete instrument verification to the F.P.A. level of SI testing. To improve the system performance predictions we have inserted into the verification plan, testing and analyses at the breadboard level of all functioning subsystems. Specifically, qual level tests will be conducted on the electronic camera and the filter assembly, including its supporting electronics. Analytical and physical models of the thermal control system will be verified at the SI and F.P.A. assembly level with complete environmental tests. Structural testing is not planned in the development phase since it is expected that the design safety factors utilized negate this requirement. Our recommendation for the optical system is to verify the design with an SR&T effort but since this may not come about we have planned to completely breadboard and test the optical components of the reimaging optics.

Per the GSFC ST/SI plan, we are providing a fully debugged and checked out SI unit to GSFC. We plan to conduct a partial acceptance type test in a simulated environment on the instrument prior to shipment in test facilities available at Itek. Final acceptance and qualification will be at GSFC with all instruments operating in concert, mounted in the E.M.F.P.A., and tested with an optical simulator and an SSM simulator supplied by GSFC.

Table 2.6-1 summarizes the camera design verification plan.

TABLE 2.6-1

DESIGN VERIFICATION PLAN

| SUBASSEMBLY LEVEL | BREADBOARD/ENG. MODEL | FLIGHT MODEL |
|---|---|---|
| . Electronic Camera (SEC or CCD) | Qual Level Tests (SE) | Performance Tests (A) |
| . Imaging Optics | Performance Tests (A) | Performance Tests (A) |
| . Filter Assembly | Qual Level Tests (SE) | Performance Tests (A) |
| . Thermal Controls | Thermal Model Tested (SE) in Simulated Environment | - - - - - |
| SYSTEM | - - - - - | Performance Test (A)<br>Pre-Acceptance Test (SE) |
| SI/FPA | | |
| . Thermal/Struct Models | Comp. Env. Test (SE) | |
| . Flight Instruments | | Comp. Accept/Qual Test (SE) |

SE = Simulated Environment

A = Ambient

## 2.7 Support Equipment Requirements

Support equipment is required at the various subassembly levels in the factory build-up and test process for the camera systems. With the projected procurement of the electronic camera with the instrument, a complete test set including an SI interface assembly, T&C console and the optics bench and target simulators is required. Conduct of subsystem tests will require a thermal vacuum test facility to evaluate the camera and thermal controls performance in a simulated space environment. At the system level tests, an F.P.A. interface simulator which provides optical targets for the camera system is required. This simulator and the SI will be installed in a thermal-vacuum facility and operated from an SSM simulator/T&C console which:

a. Provides commands and controls to the SI

b. Records, stores and presents the output of the camera system for evaluation of instrument performance and diagnosis of internal failures

This assembly can later be upgraded for delivery to GSFC, on the integration site for on-site trouble-shooting and instrument calibration.

Table 2.7-1 summarizes the support equipment requirements.

TABLE 2.7-1

SUPPORT EQUIPMENT REQUIREMENTS

| SUB-ASSEMBLY LEVEL | REQUIREMENTS |
|---|---|
| Electronic Camera | Test and Checkout Bench Console |
| | Optical Bench and SI Interface Assembly |
| | Target Simulator |
| Imaging Optics | Optical Bench and Test Optics |
| Filter Assembly | Test and Checkout Bench Console |
| | Environmental Test Facility |
| Thermal Model | Environmental Test Facility |
| System | SSM Simulator/Test and Checkout Console |
| | FPA Interface Simulator |
| | Environmental Test Facility |

Figure 2.7-1 shows a simple test fixture that could be used as part of the FPA interface simulator in verifying the performance of the camera. It uses a simple set of optics adjustable on slides to simulate the OTA image one point at a time. A star can be simulated at any point in the field by adjusting each of the five adjustments to precomputed values for that particular field point. In the simplest form, the optics would be refractive, and the full spectral range of the cameras would be tested quasi-monochromatically, using the camera filters and computing the focus adjustment for the simulator optics separately for each center wavelength.

The fixture contains registration fittings for the instrument module that are identical to those on the OTA.

FIGURE 2.7-1

TEST FIXTURE FOR FOCAL PLANE CAMERAS

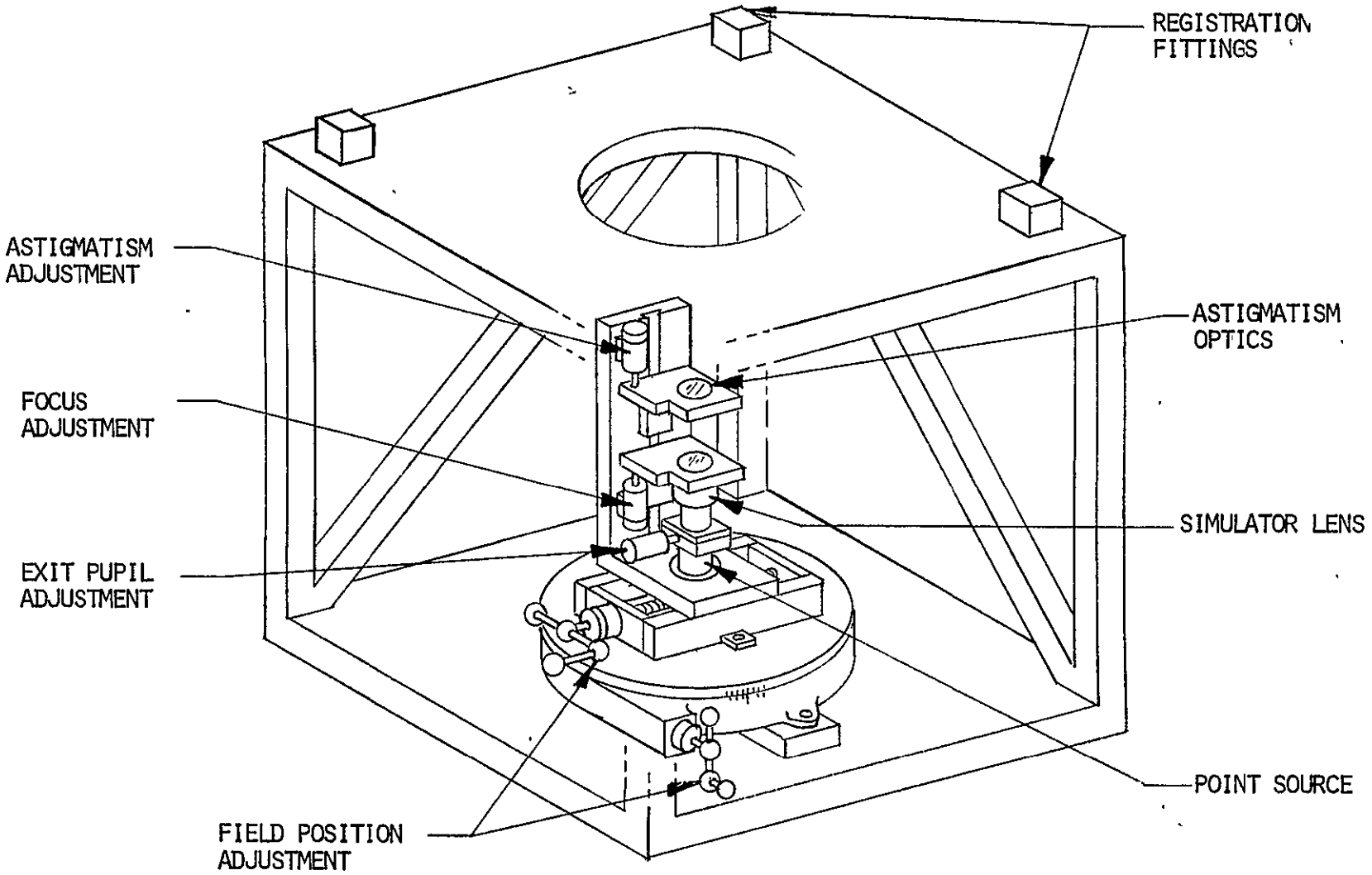

# APPENDIX A

## Itek Experience With Aspheric Optics

Itek has produced several systems with aspheric optics which involved the use of computer generated holograms in testing. One of these was a 27-inch eccentric aperture cassegrain which had a primary mirror with 368 waves of asphericity. This mirror was actually manufactured using a rather complicated null lens, but it later was tested for comparison using a CGH-Maksutov sphere combination.

Another system was a 10-inch, 4-mirror unobstructed aperture system having no axis of symmetry. The asphericity of the elements ranged from 100 waves to 350 waves. All elements were made using CGH's.

In a third system, a 2-inch secondary mirror for a Ritchey-Chretien Cassegrain was made using a CGH hindle sphere test. In this test, the CGH made up the 2.5 wave difference between the desired figure and a true hyperboloid.

Table A-1 summarizes the Itek experience.

TABLE A-1

ITEK EXPERIENCE WITH ASPHERIC OPTICS

| SYSTEM | MANUFACTURING TESTING | ASPHERICITY |
|---|---|---|
| 27 Inch Eccentric Aperture Cassegrain | Null Lens CGM Maksutov Comparison | 368λ |
| 10 Inch 4-Mirror Unobstructed Aperture System | CGH | 100λ - 350λ |
| 2 Inch Hyperboloid Secondary Mirror | CGH Hindle Test | 2.5λ |

## A-1 CGH Maksutov Test of an Eccentric Cassegrain Primary

A major obstacle in using aspheric surfaces in optical systems has been the difficulty involved in accurately testing them. A common method of testing an aspheric optical element is to make a second optical system (null lens or null mirror) which converts the wavefront produced by the element under test into either a spherical or plane wavefront. This wavefront is interferometrically compared with a known reference wavefront. In the testing of steep aspherics, the null optics are often very expensive to produce accurately.

It has been shown that null lenses can be replaced with computer generated holograms (CGH). Unfortunately, the CGH required to test steep aspherics are also difficult to produce. However, instead of testing steep aspherics using either a very expensive null lens or a very complicated CGH, often the

test can be performed using the combination of a relatively inexpensive null lens and a relatively simple CGH. A study was conducted at Itek whose purpose was to use the combined null lens-CGH method to test the primary mirror of an eccentric cassegrain system which had a departure of approximately 455 waves (at 5145 Å) and a maximum slope of approximately 1,500 waves per radius. The test set-up is shown in Figure A-1.

The null optics was a Maksutov sphere which reduced the departure and slope of the aspheric wavefront from 910 waves to 45 waves and 3,000 to 70 waves per radius, respectively. A hologram was then used to remove the remaining asphericity. These results were compared to the test results obtained testing the primary with an expensive null lens.

When the aspheric wavefront from the mirror under test illuminates the hologram, several wavefronts are produced, one of which would be a perfect plane wave if both the hologram and mirror under test were perfect. The hologram acts just like a conventional null lens. A spatial filter passes only this plane wavefront and the plane reference wavefront. Thus, if the piece under test were perfect (and also if the CGH were perfect), two collimated beams would be interfering in the interferogram plane shown and straight fringes would be obtained. That is, a null test is being performed.

The interferometer was ray traced to obtain the data needed to produce the CGH. It is important that the entire interferometric setup shown be ray traced since elements such as the diverger may introduce little aberration when used with spherical wavefronts but a large amount of aberration when used with aspheric wavefronts as in this test.

A computer program was written to calculate the instructions necessary to make a laser beam recorder (LBR) plot the desired CGH. The master CGH is shown in Figure A-2.

The LBR plot (CGH) was then photo-reduced 8 x and placed in the interferometer.

An analysis made of the errors in the CGH Maksutov test showed that the errors in the test would produce less than a 1/8 wave peak-to-peak uncertainty in the measurement of the aspheric surface. The results obtained using the CGH Maksutov test were compared with earlier results obtained testing the same surface using a rather sophisticated null lens, and it was found that the two tests gave the same aspheric surface to well within the 1/8 wave peak-to-peak estimated error. The peak-to-peak surface error measured using the null lens was 0.46 wave (6328Å), while for the CGH Maksutov test it was 0.39 wave (5145 Å). The RMS surface error was measured to be 0.06 wave (6328 Å) using the null lens, while the CGH Maksutov test gave 0.07 wave (5145 Å). The study demonstrated how complicated null optics can be replaced with relatively simple null optics and a CGH. Figure A-3 shows the comparative test results.

## A-2 Predicted Manufacturing Errors

Itek has undergone very thorough evaluation of the process for making the computer-generated holograms used in the test null optics. The plotter used to make the hologram master is the limiting factor in the test optics. With the present plotter, the testing can be accomplished accurately to 1/8 wave P-P at the surface for mirrors with the degree of asphericity of the first mirror of the relay.

Theoretically, the figure error can be reduced indefinitely to the point at which the repeatibility of the figure measurement becomes the limiting factor. Itek experience to date indicates that figuring of the camera fold mirror can be accomplished to within 1/4 to 1/6 wave peak-to-peak at the surface with a reasonable effort.

These predicted manufacturing errors can be converted to RMS wavefront error by the 20% rule-of-thumb (40% of the surface error), as below:

| | RMS WAVEFRONT ERROR (6328 Å) |
|---|---|
| Computer Generated Hologram | |
| 1/8 Wave P-P Surface With Present Plotter | 0.05 |
| Figuring - 1/4 to 1/6 Wave P-P Surface | 0.007 - 0.10 |
| | 0.08 - 0.11 |

FIGURE A-1

# CGH MAKSUTOV TEST OF AN ECCENTRIC CASSEGRAIN PRIMARY

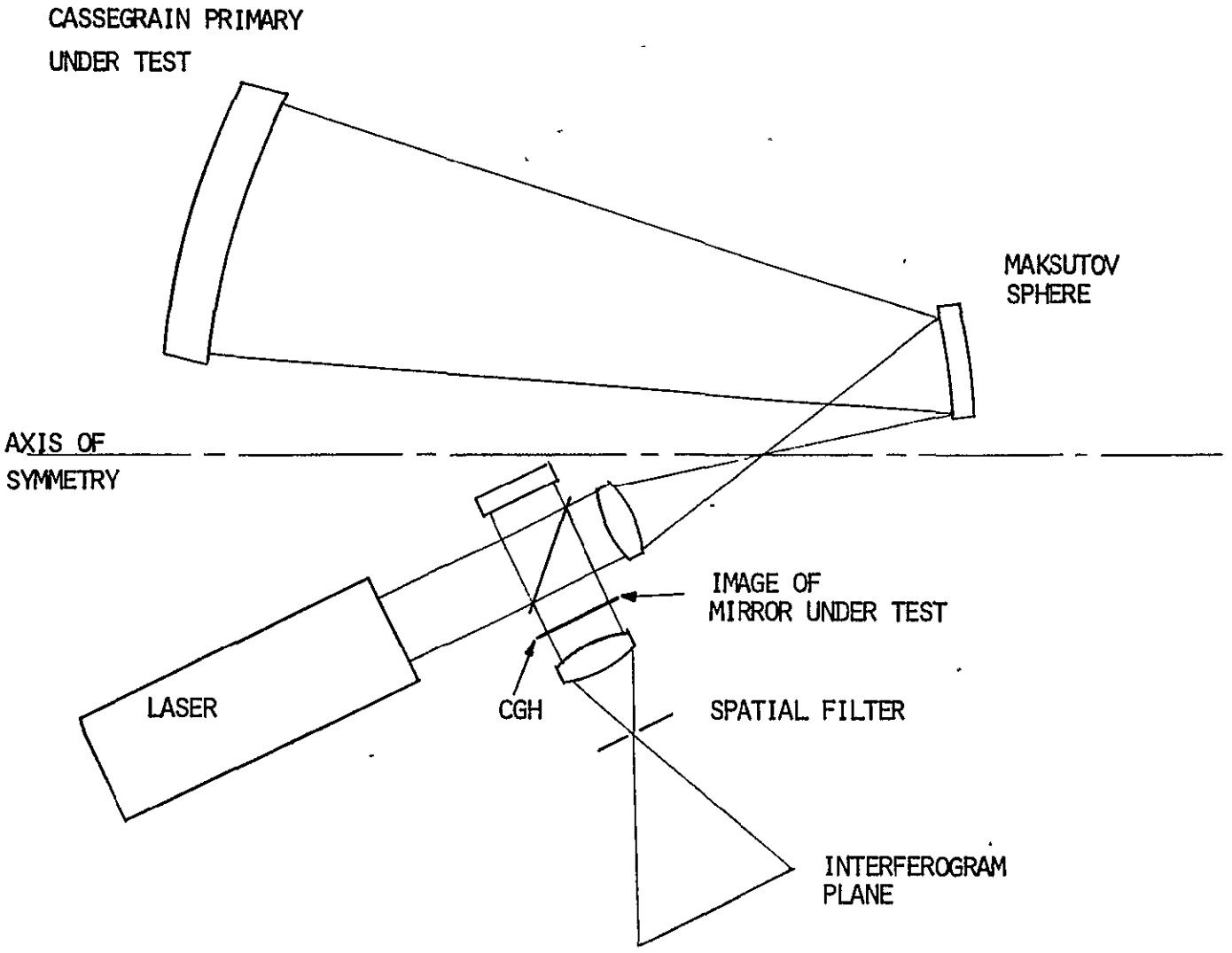

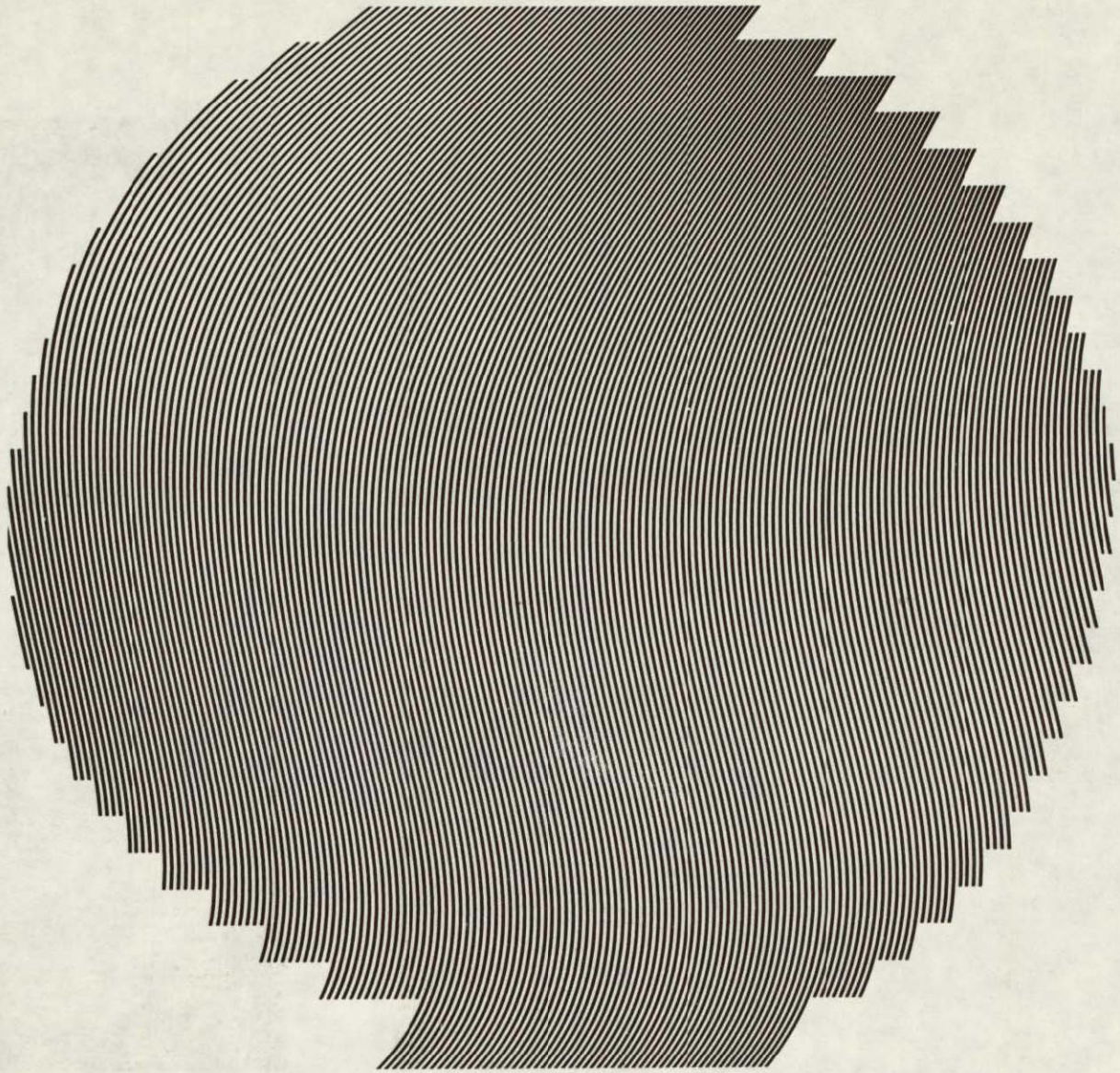

FIGURE A-2

MASTER CGH FROM PLOTTER

(a) Results obtained using Maksutov test without CGH

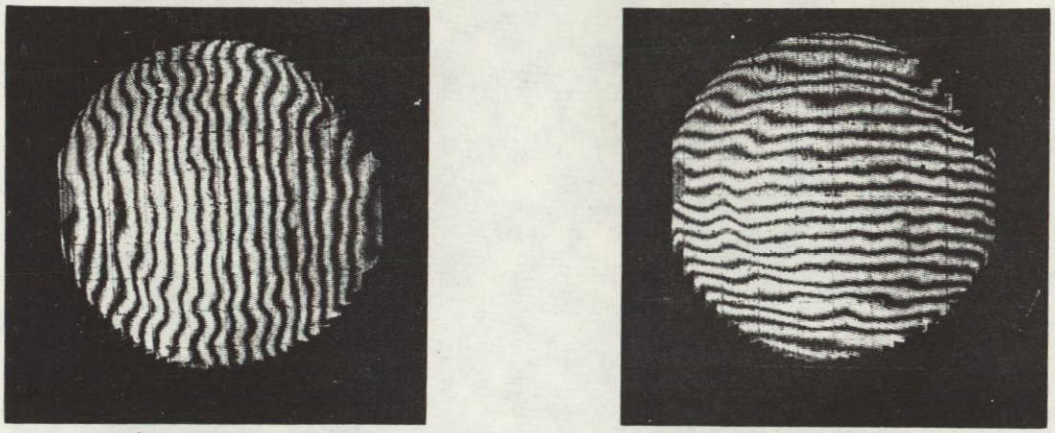

(b) Results of CGH Maksutov test ($\lambda$ = 5145 Å)

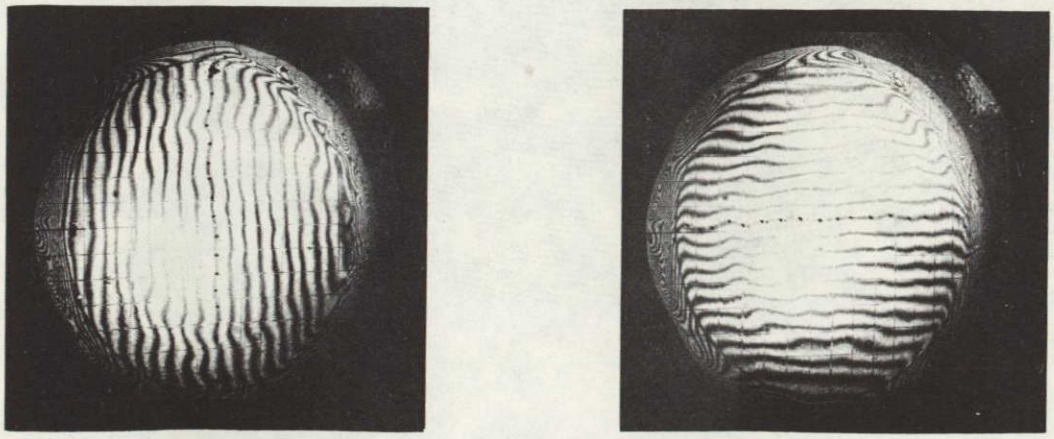

(c) Results obtained using null lens ($\lambda$ = 6328 Å)

FIGURE A-3

TEST RESULTS